# Design, Manufacturing and Development of Hybrid Manufacturing System for Rapid Investment Casting

by

**Piyush Arora**

A thesis submitted in partial fulfillment of the requirements for the degree of

Master of Science

Department of Mechanical Engineering
University of Alberta

**ABSTRACT**

Direct rapid investment casting integrates additive manufacturing (AM) technology into conventional investment casting. This approach addresses the challenges of high lead time and cost but is effective only on a small scale (up to a cube of 0.3 m side). It utilizes thermoplastics such as Acrylonitrile Butadiene Styrene (ABS) as a sacrificial pattern material, but after burnout, thermoplastics can lead to defects such as shell cracking and residual ash. The layer-by-layer printing process in AM introduces stair-stepping defects, significantly impacting surface quality. Additionally, the conventional investment shell fabrication method, involving submerging the pattern in a ceramic tank, results in uncontrolled shell thickness, leading to shell cracking due to the formation of local hotspots while pouring molten metal.

A novel hybrid additive-subtractive manufacturing chain is proposed to address these issues. This approach incorporates 3D printing for large-scale pattern fabrication and post-processing to improve surface quality and dimensional precision. Another additive module fabricates the investment shell around the processed pattern. This methodology eliminates the need for complex tooling in conventional investment casting, resulting in saving lead time and costs.

A three-axis cartesian large-scale hybrid manufacturing system was designed and manufactured in-house to validate the proposed hybrid chain. This system is capable of producing metal castings up to one cubic meter in size and incorporates additive and subtractive modules selected based on literature review. Fused Granulated Fabrication-Additive Manufacturing (FGF-AM), a large-scale extrusion technology was employed in the study for printing sacrificial patterns using wax, a material preferred in foundries for producing defect-free metal castings. The methodology involved the development of a systematic approach to optimize and validate critical printing parameters using a

design of experiments (DoE). An in-situ CNC machining facility was integrated to address stair-stepping issues, improving surface quality and dimensional tolerance to meet investment casting (IC) standards. After post-processing patterns, the subsequent step involved fabricating the investment shell using Direct Ink Writing additive manufacturing (DIW-AM), employing a large-scale extrusion process with red earthenware clay as the feedstock material. Influential printing parameters were optimized using DoE to achieve fully dense investment shells.

The utilization of the hybrid system yielded positive outcomes where FGF-AM achieved an optimal throughput of 0.5 kg/hour, and in-situ machining ensured an average dimensional accuracy of ±40 μm, precision of ±170 μm, and a surface roughness of 3 ± 0.5 μm Ra, all within the prescribed investment casting (IC) norms. Additionally, the sacrificial pattern printed at optimal parameters exhibited 0.5% porosity, affirming the print quality and the system's capability to generate dense patterns. The Direct Ink Writing (DIW) technique for printing investment shells attained the maximum mass flow rate of 2.2 kg/hr. It achieved objects with a relative density of 99.5% under optimal printing parameters.

The system's capability and conformity to investment casting standards were demonstrated through case studies, which included the fabrication of an ASME wax slip-on flange and several intricate clay artifacts. The research findings suggest that the developed system exhibits substantial potential for industrial scalability, delivering 10–20 times higher productivity than alternative 3D printing methods and reducing the total cycle time for investment casting applications by 50–60%.

## PREFACE

This thesis is an original work by Piyush Arora. It adheres to the University of Alberta thesis guidelines. One conference and one journal paper related to this thesis have been attended and submitted, as listed below.

1. **Piyush Arora**, Shirin Dehgahi, David S Nobes, Pierre Mertiny, Ahmed Jawad Qureshi, “Production of Rapid Investment Casting wax pattern through Fused Granulated Fabrication Additive Manufacturing process”, ASTM International Conference on Advanced Manufacturing – ICAM 2023, October 29 – November 3, 2023.
2. **Piyush Arora**, Shirin Dehgahi, Sajid Ullah Butt, David S Nobes, Ahmed Jawad Qureshi, “Fabrication of sacrificial wax pattern through large-scale fused granulated fabrication (FGF-AM) hybrid manufacturing system”, Progress in Additive Manufacturing (under-review).

**ACKNOWLEDGEMENTS**

Firstly, I would like to thank god for providing me with this opportunity to work on such a wonderful project where I gained a lot of knowledge and executed it to finish this thesis.

A special thanks to my supervisors Dr. Ahmed Jawad Qureshi – Associate Professor, and Dr. David S. Nobes – Professor, in Department of Mechanical Engineering - University of Alberta, for their constant support and guidance. This thesis would not be possible without their belief in me. Thanks to Dr. Sajid Ullah Butt, Research Associate, and Dr. Shirin Dehgahi, Postdoctoral Fellow at the University of Alberta, for being my mentors and friends. I cannot imagine this work being successful without their valuable feedback and help at each and every step of this research. I would also like to thank my colleagues Mr. Nathan Wieczorek, Mr. Anish Abraham Philip, Mr. Adam Lim, and Mr. Remy Samson from the ADAM'S Lab for providing valuable advice throughout this thesis.

This project would not be possible without the help of the Alberta Innovates, Additive Design and Manufacturing Systems Lab (ADAM'S Lab), and the Department of Mechanical Engineering at the University of Alberta.

Finally, I am forever indebted to my beloved parents, Mr. Rajeev Arora and Mrs. Mona Arora, for their unconditional love, support, and encouragement which have been crucial in this journey and succeeding of the program. Apart from my own efforts, this thesis is a result of the constant guidance and motivation from all my family members.

Thank You

**Table of Contents**

**List of Tables**

**List of Figures**

**List of Equations**

## LIST OF ABBREVIATIONS

| | |
|---|---|
| IC | Investment Casting |
| AM | Additive Manufacturing |
| RIC | Rapid Investment Casting |
| HIC | Hybrid Investment Casting |
| FDM | Fused Deposition Modeling |
| ABS | Acrylonitrile Butadiene Styrene |
| PLA | Polylactic Acid |
| CTE | Coefficient of thermal expansion |
| HMS | Hybrid Manufacturing System |
| FGF – AM | Fused Granulated Fabrication – Additive Manufacturing |
| DIW – AM | Direct Ink Writing – Additive Manufacturing |
| CAD | Computer Aided Design |
| SLA | Stereolithography |

# Chapter 1 Background and Motivation

The first chapter gives a contextual background on casting processes, emphasizing investment casting (IC). It motivates the project by addressing limitations in the traditional IC process and proposing an innovative hybrid manufacturing chain. This chain focuses on the additive-subtractive framework, eliminates complex tooling, saving cycle time and costs. The chapter concludes with an overview of the thesis structure, summarizing each chapter and providing a visual layout to clarify the project's contributions.

## 1.1 Casting manufacturing process

Casting is a widely used manufacturing process in industries like transportation and construction [1–4], which involves pouring molten metal into a mold to achieve the desired shape. The global metal casting market reached $151.6 billion in 2022 and is projected to grow to $236.7 billion by 2028 [5].

### 1.1.1 Advantages of Casting Process

Casting offers several advantages over other conventional metal manufacturing processes, such as:

- **Dimensional precision and surface finish:** Casting is renowned for achieving exceptional dimensional tolerances within the range of ± 0.1 – 2.5 mm and surface roughness spanning from 1.6 – 50 μm Ra, eliminating the need for post-processing [6].
- **Material versatility:** Casting supports a broad array of materials, including metals, alloys, and plastics, providing adaptability to cater to diverse applications [7].

- **Size variability:** Casting accommodates various sizes, from microscale components to large structures weighing over 300 tonnes [8].
- **Material properties:** Components produced through casting exhibit favorable mechanical properties, including high strength, durability, and heat resistance [9].
- **Reduced waste:** The ability to reuse excess material contributes to waste reduction, aligning with sustainable manufacturing practices [10].

### 1.1.2 Types of Casting Process

Various casting methods are used in the industry based on material, production volumes, and size. Figure 1-1 illustrates standard metal casting techniques, detailing the manufacturing process and applications. The thesis focuses on an investment casting process, detailed in later sections.

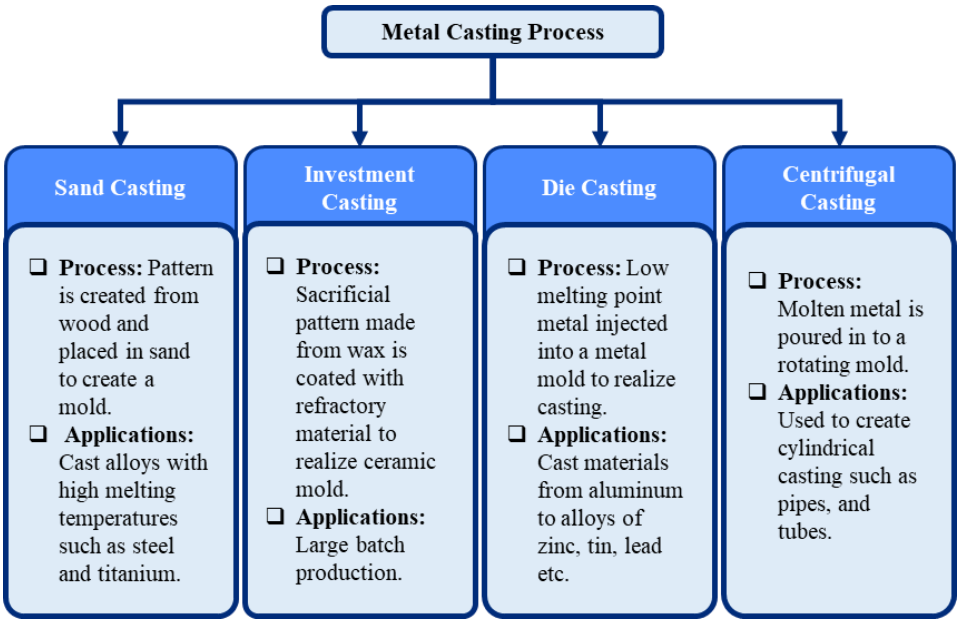


Figure 1-1. Types of metal casting processes

## 1.2 Investment casting process

Investment casting has become highly notable due to its capacity to produce intricate, near-net, and geometrically complex metallic components at an industrial scale. Industries like automotive, aerospace, defense, power, oil and gas, food processing, and customized commercial products, such as medical implants, have substantially relied on IC processes [11,12]. As of 2022, the global market share for IC surpassed a valuation of 16 billion US dollars and is projected to exceed the 20-billion-dollar threshold by 2028 [13].

Investment casting follows a series of steps, as shown in Figure 1-2, beginning with NC/CNC machining for the master mold production, injecting the molten wax into the mold, cooling, and solidifying to create a sacrificial pattern. This pattern is then coated in a ceramic slurry and dried. The ceramic investment shell is heated in dewaxing to melt out the sacrificial pattern, creating a cavity mirroring the final product shape. The shell is then sintered for strength and thermal shock resistance. Molten metal is poured into the shell, forming a casting replicating the original pattern. After solidification, the shell is broken or removed in the knock-out stage, revealing the cast metal object.

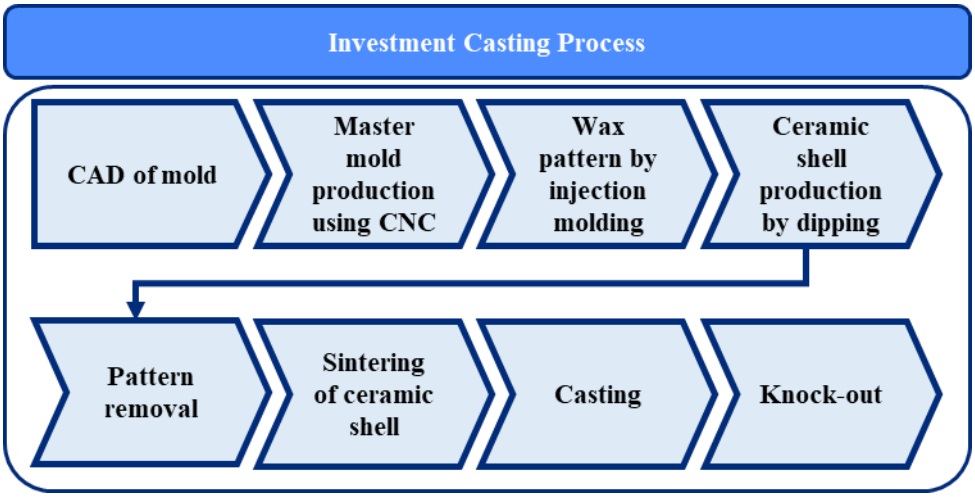


Figure 1-2. Processes involved in investment casting technique

### 1.2.1 Advantages of Investment Casting

In addition to the discussed advantages of the casting process in sub-section 1.1.1, the IC process offers the following distinct benefits compared to other casting techniques:

**Intricate design:** IC is particularly well-suited for producing castings featuring intricate details, undercuts, thin walls, and complex geometries that are challenging with alternative casting techniques [14].

**Large-Batch production:** IC can efficiently produce multiple identical or similar castings, fulfilling high-volume demand and contributing to economies of scale.

**Near-Net shape:** The process excels in achieving near-net shape components, minimizing the need for extensive post-processing. This results in cost savings and reduces overall cycle time [15].

**Versatile applications:** The lost wax technique employed in IC extends its application to the casting of components with a diverse size range, including but not limited to turbine blades [16], bone implants [17], dentures [18], and jewelry [19].

### 1.2.2 Limitations of Investment Casting

The IC framework unfolds as a sequential operation, with the most prominent bottleneck in the initial stage being master mold production. This process relies on complex tooling of metals like Aluminum. As depicted in Figure 1-3, the conventional IC methodology approximately requires an extensive time of upto 21 weeks, of which mold production alone consumes almost 14 weeks [15]. Depending on size and complexity, it also entails significant costs ranging from tens to hundreds of thousands of dollars. Consequently, the economic viability of the IC process is most evident in large-batch production scenarios [15,20]. Furthermore, any deviations or adaptations to the sacrificial pattern in use mandate the creation of an entirely new master mold, causing inevitable capital outlays and delays in the production process [21,22]. Hard tooling also restricts the ability to produce complex features such as non-linear geometries or complicated interiors in the master mold [23].

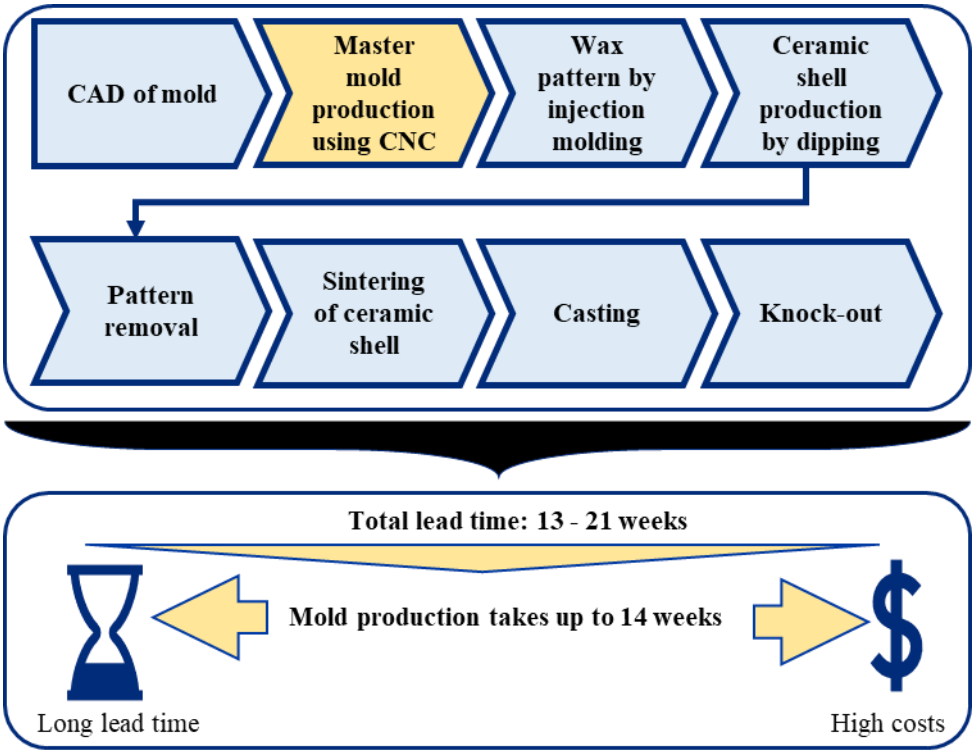


Figure 1-3. Limitations in conventional investment casting process

In the investment shell fabrication stage, the sacrificial pattern is submerged into a large tank filled with ceramic slurry. The dipping process, reliant on operator skill, can result in uneven shell thickness, leading to the development of local hotspots during molten metal pouring. This unevenness may contribute to casting defects, such as shell cracking [15]. Additionally, the ceramic slurry has a specific setting time, and once set in the tank, it becomes unusable, leading to material wastage and increased production costs [24]. Moreover, the slurry may contain hazardous constituents such as silica dust, necessitating proper handling and disposal [25]. Addressing these drawbacks can be explored by modifying the conventional manufacturing chain through an additive manufacturing (AM) technique known as rapid investment casting (RIC).

### 1.3 Additive Manufacturing

Additive Manufacturing (AM) [26–29], also known as 3D printing, involves the layer-by-layer construction of a three-dimensional object based on a digital 3D CAD model. Various material feedstocks, such as powder grains, slurry, resin, and filament, are fused, deposited, or solidified to build a tangible object progressively. This technology includes a diverse range of printing technologies and materials, leading to its widespread adoption in industries such as aerospace [30], healthcare [31], automotive [32], and consumer goods [33]. Introduced four decades ago [34], AM has experienced rapid growth, with a projected compound annual growth rate of 20.8% from 2022 to 2030, reaching a market capitalization of US $76.16 billion, as indicated by forecasts from Grand View Research [35]. This technique autonomously produces objects, ranging from nanoscale [36] to multi-story houses [37]. AM surpasses conventional manufacturing processes by providing superior geometric design flexibility, minimizing material waste, reducing tooling costs, and expediting prototyping and production processes [12].

### 1.4 Rapid Investment Casting (RIC)

Acknowledging the challenges in IC, Cheah et al. [15] introduced various manufacturing chains integrating additive manufacturing (AM) technologies to reduce lead times and costs. The infusion of AM techniques within the conventional IC framework is designated as rapid investment casting (RIC) [12,38,39] or hybrid investment casting (HIC) [21]. In a comparative study, Lee et al. [40] revealed a substantial 89% reduction in time and a 60% reduction in costs for pattern fabrication achieved through the FDM process.

### 1.4.1 Different Rapid Investment Casting Methods

RIC is classified into direct and indirect methods based on integrating 3D printing into the investment casting manufacturing chain. In direct RIC, 3D printing creates sacrificial patterns or ceramic molds, while indirect RIC involves 3D printing a soft or hard mold to produce sacrificial patterns. The timeline outlined in Figure 1-4 shows that direct RIC is faster than the indirect method due to fewer steps. This conclusion aligns with the study conducted by Chua et al. [20]. The indirect method offers the advantage of producing multiple patterns with a single mold, but direct RIC is preferred for intricate pattern designs to avoid mold damage during pattern removal [11,15]. Therefore, this thesis focuses on the direct RIC method.

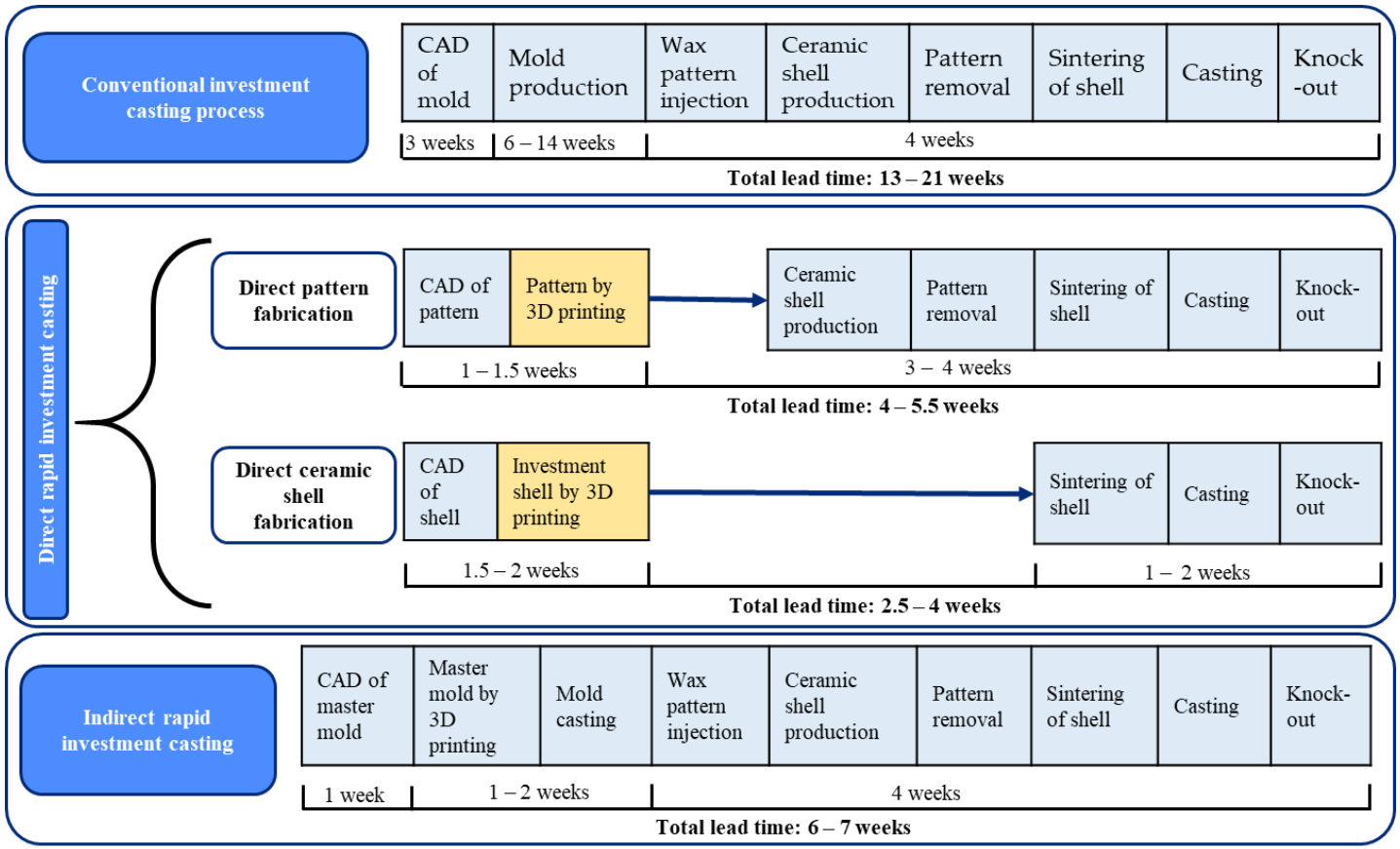


Figure 1-4. Types of rapid investment casting process along with timeline comparison

### 1.4.2 Direct rapid investment casting

The direct Rapid Investment Casting (RIC) method comprises two approaches, as shown in Figure 1-4. The first involves pattern fabrication using 3D printing with the required post-processing, followed by the conventional IC method. In the second approach, the shell is directly fabricated using 3D printing, bypassing the need for a sacrificial pattern. However, the shell cannot be post-processed due to machining limitations resulting in poor dimensional precision and surface quality of the metal cast. Additionally, producing complex-shaped hollow shells without sufficient bottom support leads to potential sagging and impacts geometric integrity.

Innovatively integrating the printing of sacrificial patterns and investment shells might address the mentioned challenges. The concept involves utilizing printed patterns to provide the necessary support for printing investment shells. Once completed, the printed pattern can be burned out to create an investment shell. Challenges in implementing this novel proposed manufacturing chain are discussed in the next section.

## 1.5 Challenges in implementing the proposed manufacturing chain

This section explores challenges in implementing the conceptualized manufacturing chain. Addressing these challenges is crucial to affirm the proposed chain's feasibility.

### 1.5.1 Dimensional precision and surface quality of the 3D printed pattern

As mentioned earlier, the IC process is renowned for its precision castings that rely directly on high-quality sacrificial patterns. Industry standards require specific criteria for surface quality (16 to 20 μm Ra) and dimension (±0.05 to ±0.254 mm) [40]. However, patterns printed through standard AM techniques have lower surface quality

and dimensional accuracy due to the stair-stepping, as shown in Figure 1-5 [41]. One of the proposed solutions is to reduce the layer height [42], but it extends printing time. An alternative approach involves vapor bath smoothing of FDM-fabricated ABS patterns, significantly reducing surface roughness (from 14.40 µm to 0.37 µm) [43]. Another approach is to enhance the surface finish by creating a hybrid manufacturing framework that combines subtractive manufacturing with the existing additive module, like Amanullah et al. [44] integrated abrasive milling operations with a desktop FDM printer. Their research shows a significant improvement, with up to 99% enhancement in dimensional accuracy and 91.3% in surface roughness (Ra) for machined PLA specimens.

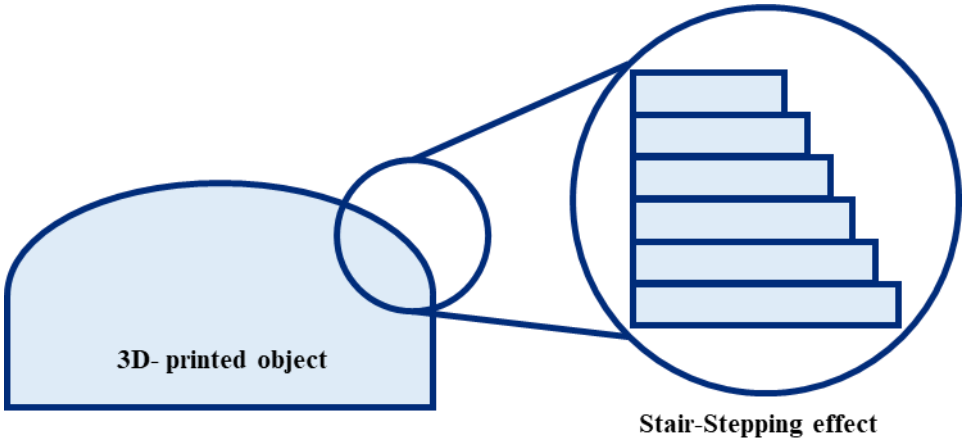


Figure 1-5. Stair-Stepping effect observed in the 3D-printed objects

### 1.5.2 Material used for fabricating sacrificial pattern

Besides addressing strict criteria for dimensional accuracy and surface quality, researchers encounter a significant challenge of shell cracking during the pattern removal phase due to its material [45]. Thermoplastics used in 3D printing possess high CTE, which induces thermal stresses during pattern burnout, potentially causing cracking if these stresses exceed the shell's modulus of rupture [46]. To address this,

quasi-hollow patterns can be designed to collapse inward during melting due to a substantial cavity [15,47]. Adopting low-density patterns is a cost-effective solution that reduces printing time [22]. According to Ćwikła et al. [48], a honeycomb pattern with 40-50% infill and 2-3 layers of shell thickness, produced through FDM, results in durable patterns.

While hollow thermoplastic patterns demonstrate promise in reducing the likelihood of shell cracking, foundries prefer wax as the pattern material due to its distinct advantages, including substantially lower CTE and complete burnout during the casting process [14]. However, some AM techniques for direct RIC applications cannot directly use wax due to constraints related to its physical state, type, and the printer's layer-building mechanisms. These limitations necessitate the exploration of innovative solutions to enhance RIC processes.

### 1.6 Objective of the thesis project

The primary aim of this thesis project is to reduce lead time and costs in the conventional investment casting process by reconfiguring the traditional manufacturing chain through a hybrid manufacturing system, as shown in Figure 1-6. The overarching objective comprises three milestones. Task 1 shifts focus from using complex tooling for the master mold to directly fabricating large-scale sacrificial patterns using an additive manufacturing process. This approach enhances design flexibility through layer-by-layer printing, ensures the sacrificial printing material is printable, and meets minimum investment casting requirements.

Task 2 aims to improve the quality of 3D-printed patterns by incorporating in-situ CNC machining with the additive module, ensuring adherence to IC standards for surface finish and dimensional precision.

Task 3 proposes using 3D printing to create the investment shell directly around the processed pattern, avoiding the traditional immersion in ceramic slurry. The chosen shell material must be printable and meet the specified requirements for the investment casting process.

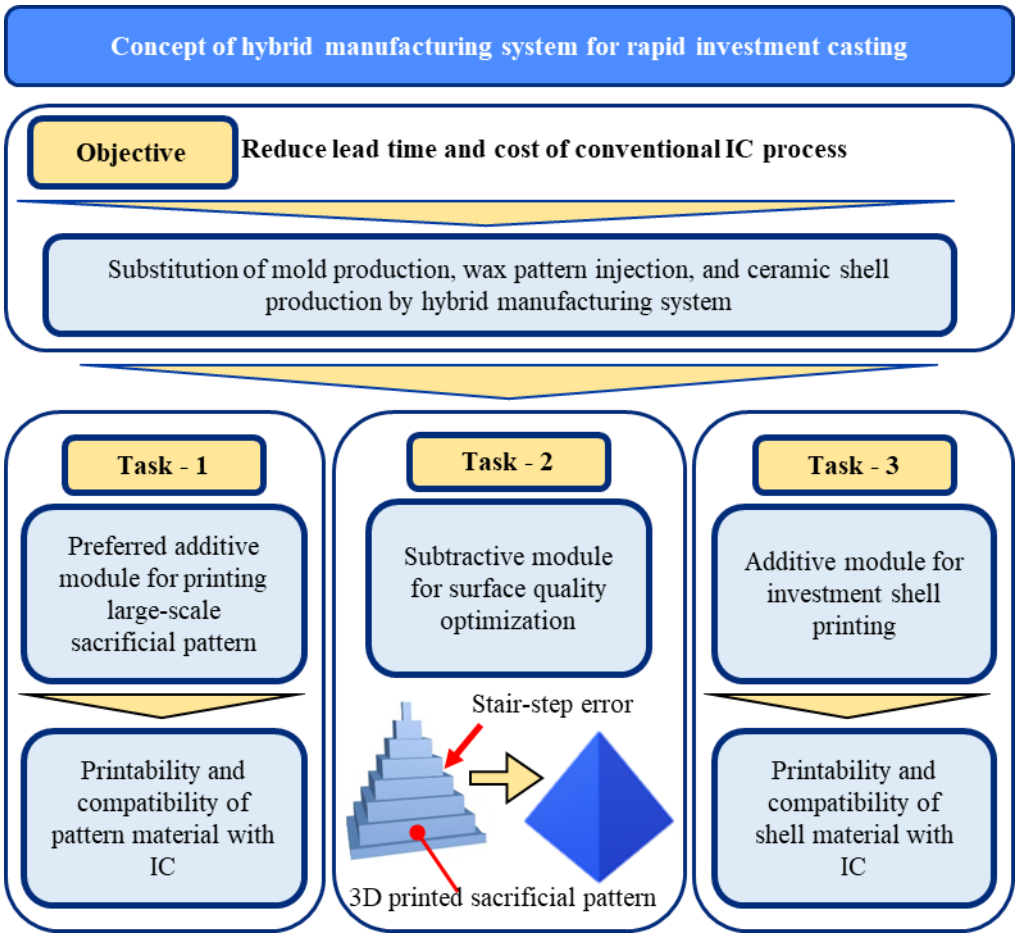


Figure 1-6. Objective of the thesis project

The thesis presents the following research contributions:

- Identification of optimal additive manufacturing techniques for printing sacrificial patterns and investment shells through a literature review that addresses current challenges and drawbacks in the AM techniques for IC applications.
- Choosing commercial additive and subtractive modules using a decision matrix incorporating pre-defined parameters and scenarios.
- Choosing a preferred pattern and shell materials that align with the respective AM techniques for printability and adherence to IC standards.
- Design and construct the in-house large-scale hybrid manufacturing system for experiments to validate the proposed methodology.
- Optimizing and validating key printing process parameters for sacrificial patterns and investment shells through DoE.
- Assessing the industrial utility of the developed system

The simultaneous printing of sacrificial pattern and the investment shell is not included in the scope of this thesis and is mentioned in the future works in the Chapter 6.

### 1.7 Thesis Structure

This section provides a chapter-wise breakdown of the thesis, as outlined below. Figure 1-7 enhances the clarity of the contributions made in this research thesis by presenting a flowchart encapsulating the sequential progression of the thesis.

- **Chapter 1: Introduction and Motivation**

This chapter outlines the limitations of conventional investment casting processes and proposes a solution by introducing a novel manufacturing chain that utilizes a hybrid manufacturing system for rapid investment casting.

- **Chapter 2: Scientometric Analysis and Systematic Literature Review**

This chapter conducts a scientometric analysis of the research domain related to rapid investment casting, aiding in identifying critical keywords, top journals, notable contributors, and investors in this field. It incorporates a systematic literature review on current rapid investment casting additive manufacturing (RIC AM) techniques and their limitations. The chapter concludes by determining the feasible additive manufacturing techniques and fabrication materials for the proposed manufacturing chain.

- **Chapter 3: Design and in-house fabrication of hybrid manufacturing system**

This chapter clarifies the selection process for identifying optimal commercial additive modules for printing sacrificial patterns and the investment shell. A decision matrix with precisely defined parameters facilitated the evaluation, selecting the most suitable print heads. Additionally, it outlines the development and in-house manufacturing of a hybrid manufacturing system used for experimentation throughout the research project.

- **Chapter 4: Fabrication of sacrificial wax patterns through large-scale fused granulated fabrication (FGF – AM) process**

This chapter begins with selecting a preferred commercial sacrificial pattern material and presents an approach for characterizing and optimizing crucial printing parameters. The study integrates in-situ CNC machining to tackle challenges like stair-stepping. Mechanical testing on 3D-printed wax specimens is carried out to assess the impact of

sample location on strength, considering potential alterations in the material's microstructure. Porosity analysis evaluates the system's capability to produce fully dense objects.

- **Chapter 5: Fabrication of investment shell through large-scale direct ink writing (DIW) – Extrusion Additive Manufacturing process**

This chapter highlights the identification of influential printing process parameters and the optimization of the developed system to achieve a fully dense investment shell using a design of experiments approach. The chosen system for fabricating the investment shell comprises two separate sub-systems. Consequently, an analysis was conducted to synchronize the material flow between them for continuous printing.

- **Chapter 6: Conclusion and Future Works**

This chapter concludes by summarizing the achievements of the research project and outlining potential avenues for future work in process optimization.

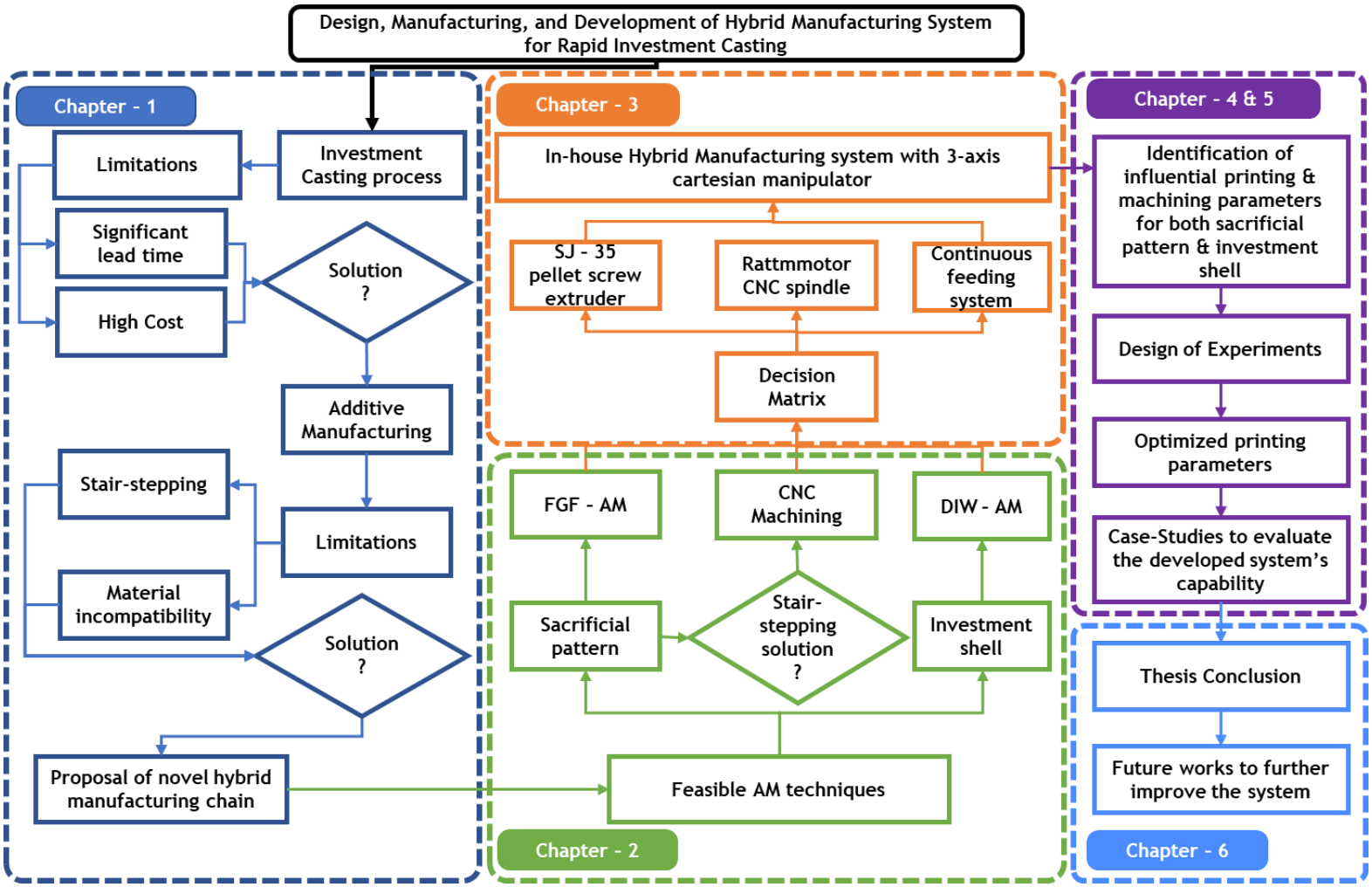


Figure 1-7 . Pictorial representation of the thesis layout

# Chapter 2 Scientometric Analysis and Systematic Literature Review

Since Charles Hull introduced additive manufacturing in 1984 [49], researchers across various disciplines have extensively examined and applied this technology for its user-centric nature and outstanding performance. Rapid Investment Casting (RIC) emerged in 1989 [50] and, over the years, has continuously evolved, driven by advancements in additive manufacturing techniques and materials. This chapter conducts a systematic literature review exploring existing and novel additive manufacturing techniques for fabricating sacrificial patterns and investment shells. Using the PRISMA approach, a structured framework for literature reviews, the chapter extracts relevant information and applies scientometric analysis for insights into research impact, productivity, and quality. It reviews current additive manufacturing techniques in RIC, highlighting limitations and proposing resolutions. The selection of novel additive manufacturing techniques for printing large-scale sacrificial patterns and investment shells is outlined to address scalability and productivity drawbacks. Additionally, a discussion on material selection for the sacrificial pattern and investment shell is conducted based on compatibility with investment casting and additive manufacturing processes.

## 2.1 Literature Review Methodology

In developing a hybrid manufacturing system for rapid investment casting, a comprehensive understanding of diverse domains, including investment casting, additive manufacturing techniques, recent advancements in RIC, hybrid configurations, and materials science, is essential. A systematic approach, including a standardized review protocol, screening criteria, and a scientometric analysis, is followed to address these interdisciplinary aspects and assess the impact of the research topic.

### 2.1.1 Review Protocol

The review protocol is a strategic roadmap for the systematic literature review, outlining an action plan. It includes critical decisions related to the search strategy, formulation of research questions, and establishment of inclusion and exclusion criteria. Various tools and guidelines ensure adherence to the defined procedure, including the Preferred Reporting Items for Systematic Reviews and Meta-Analyses (PRISMA) [51] guideline. PRISMA provides evidence-based, minimal requirements for reporting systematic reviews, ensuring methodical and transparent documentation of the review process.

#### 2.1.1.1 Research Questions

Chapter 1 illustrates the high-level project objective (Figure 1-6) subdivided into tasks. These tasks are formulated as research questions, providing an outline for the systematic review.

(a) Task – 1 Questions:

- What existing AM techniques are used for the direct fabrication of sacrificial patterns?
- What are the limitations of current techniques considering the printing method and materials?
- Are there potential modifications to mitigate limitations in existing AM methods, or are there novel techniques specifically addressing current shortcomings for printing large-scale sacrificial patterns?

(b) Task – 2 Questions:

- What post-processing techniques improve the surface finish and dimensional precision of the 3D-printed sacrificial pattern?

(c) Task – 3 Questions:

- What existing AM techniques are used for the direct fabrication of investment shells?
- Are there potential modifications to mitigate limitations in existing AM methods, or are there novel techniques specifically addressing current shortcomings for printing large-scale investment shells?

#### 2.1.1.2 Data acquisition and eligibility criteria

Data collection significantly influences the quality of a literature review. Scopus, chosen for its extensive collection, serves as the repository for this systematic review. The search equation, based on the research questions, is structured as follows: TITLE-ABS-KEY ("Investment Casting" OR "Lost wax casting" OR "rapid investment casting" OR "hybrid investment casting" OR (("Direct ink writing" OR robocasting) AND (ceramic OR gypsum)) OR ((wax OR ceramic OR gypsum) AND ("3-D printing" OR "3D printing"))). This equation with Boolean operators instructs the database to search for publications with specified terms in titles, abstracts, and keywords. Scopus yielded 7,911 records as of December 2023, with an additional 35 documents added manually, totaling 7,946. Figure 2-1 illustrates the number of studies published each year in this research domain over the last decade, emphasizing the need for comprehensive literature reviews to consolidate the latest information.

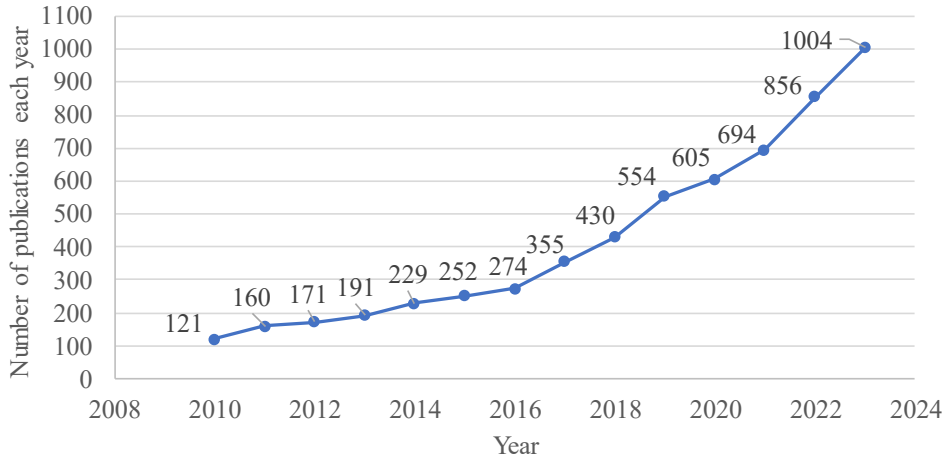


Figure 2-1. Trend of number of records published each year related to investment casting and additive manufacturing

Given the search equation's reliance on specific terms, some retrieved records may be irrelevant due to language barriers, script types, and redundant, obsolete, and trivial records. Establishing predefined eligibility criteria helps filter out these irrelevant records. The criteria for this literature review are:

- Selection is limited to open access and peer-reviewed records for accessibility and academic quality.
- Inclusion of records published from 2010-2023 to cover recent advancements.
- Focus on articles and journal reviews for comprehensive research, excluding conference proceedings.
- Exclusive consideration is given to records published in English due to their universal reach.

After applying the mentioned criteria, 1,502 records were retained from the initial pool of 7,946.

#### 2.1.1.3 Screening Strategies

A multi-step screening process ensures relevance to the literature review's scope and addresses the research questions. The first phase involves title screening, where documents are included or excluded based on titles. Titles suggesting potential relevance are queued for further evaluation, resulting in 933 records progressing to the following screening stage.

Records are included or excluded in the subsequent abstract screening phase based on abstract content, resulting in 591 retained records. Full-text retrieval and examination led to the exclusion of 76 records due to unavailability and 152 records not aligning with the research questions. Including manually added records brings the total to 390 documents for thorough review in the systematic literature analysis. Figure 2-2 provides a detailed PRISMA flowchart illustrating the breakdown of study sources, eligibility criteria, screening strategies, and the overall document count.

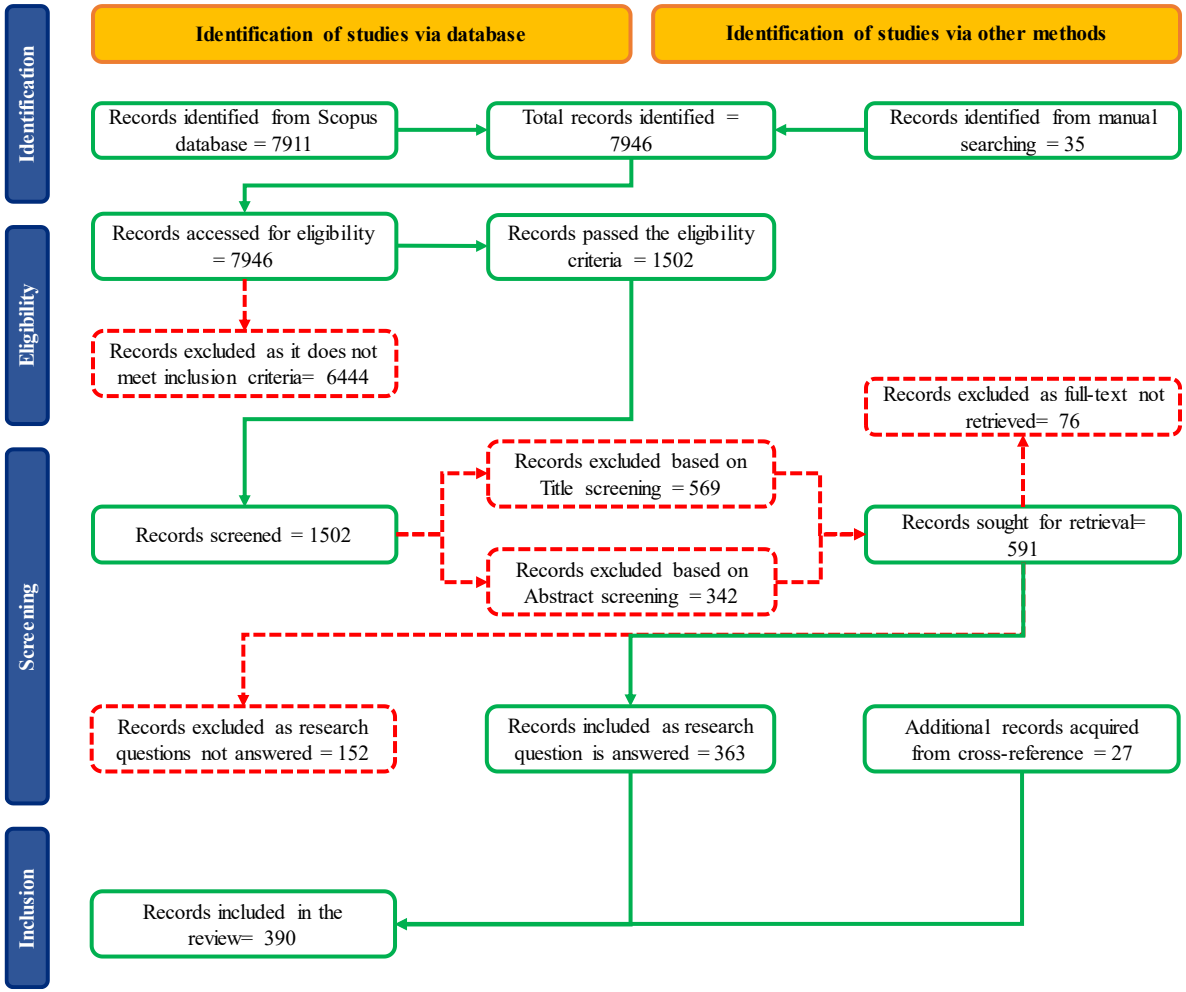


Figure 2-2. PRISMA flowchart showcasing the flow of records through different phases from identification to inclusion along with all the screening strategies applied

### 2.1.2 Scientometric Analysis

Scientometrics, coined in the 1950s, is the "measurement of science," introduced by Nalimova and Mulchenko in 1969 [52–54]. The scientometric analysis supports evidence-based decision-making within academic and research management areas. It quantitatively and qualitatively assesses research impact and is used here as a pivotal tool for bridging interdisciplinary gaps among investment casting, additive manufacturing, and advanced manufacturing [55]. An advanced visualization tool, VOSviewer, addresses that by creating network maps and density graphs, revealing relationships among researchers, institutions, and research topics [56]. The subsequent sections detail specific scientometric analyses conducted in the systematic literature review, presenting results using literature records included following PRISMA guidelines.

#### 2.1.2.1 Literature Coupling Analysis

The literature coupling analysis highlights the global contributions of 179 journals to additive manufacturing technologies and the investment casting process. Table 2-1 summarizes publication counts for the top 16 journals, contributing at least five documents each, representing 40% of the overall documents and 9% of the total journals surveyed. "Materials" led with 28 publications, followed by the "International Journal of Advanced Manufacturing Technology" with 17. The "Journal of the European Ceramic Society"89 had the highest citation count (1359), followed by the "Rapid Prototyping Journal" (875), both exhibiting the highest average citations per article.

Table 2-1. Number of publications from the top journals in the field (contributing at least five publications)

| Journal | Number of relevant articles | Total percentage of publications (%) | Total citations from these articles | Average citation per article |
|---|---|---|---|---|
| Materials | 28 | 7.2 | 411 | 14.7 |
| International Journal of Advanced Manufacturing Technology | 17 | 4.4 | 672 | 39.5 |
| Polymers | 12 | 3.1 | 97 | 8.1 |
| Additive Manufacturing | 10 | 2.6 | 294 | 29.4 |
| Journal of the European Ceramic Society | 10 | 2.6 | 1359 | 135.9 |
| Rapid Prototyping Journal | 10 | 2.6 | 875 | 87.5 |
| Journal of Manufacturing processes | 8 | 2.1 | 300 | 37.5 |
| China Foundry | 8 | 2.1 | 110 | 13.8 |
| Ceramics International | 8 | 2.1 | 51 | 6.4 |
| Archives of Foundry Engineering | 8 | 2.1 | 34 | 4.3 |
| Tezhong Zhuzao Ji Youse Hejin Special Casting and Nonferrous Alloys | 7 | 1.8 | 4 | 0.6 |
| Progress in Additive Manufacturing | 6 | 1.5 | 69 | 11.5 |
| Open Ceramics | 6 | 1.5 | 46 | 7.7 |
| Materials Today Proceedings | 5 | 1.3 | 71 | 14.2 |
| Applied Sciences Switzerland | 5 | 1.3 | 33 | 6.6 |

#### 2.1.2.2 Keyword co-occurrence Analysis

Keywords are essential for research discoverability, and analyzing their interconnectivity reveals the knowledge domain within research topics. In this analysis, 3089 different keywords were identified. Table 2-2 focuses on the top 16 keywords recurring at least 15 times, presenting their occurrences and link strength. "3D printing" leads with 303 occurrences and the highest total link strength of 584. Other vital keywords include "Fused Deposition Modelling" (47) and "Stereolithography" (23), representing prominent AM techniques in RIC. Keywords like "Surface Roughness" (30) and "Dimensional Accuracy" (33) are also present, representing critical features of IC. "Rheology" (15) highlights its role in printability within the AM domain.

Table 2-2. Most frequently used keywords in the specific research domain of RIC along with their relevant network data

| Keywords | Occurrences | Total Link Strength |
|---|---|---|
| 3D printing/ 3d-printing/3-d printing | 303 | 584 |
| Additive Manufacturing | 111 | 492 |
| Investment Casting | 89 | 378 |
| Extrusion | 52 | 237 |
| Fused deposition modelling | 47 | 231 |
| Rapid prototyping | 39 | 180 |
| Rapid Casting | 37 | 173 |
| Dimensional Accuracy | 33 | 140 |
| Surface Roughness | 30 | 181 |
| Ceramic materials | 26 | 139 |
| Mechanical Properties | 24 | 109 |
| Stereolithography | 23 | 98 |

| | | |
|---|---|---|
| Rapid Investment Casting | 21 | 92 |
| Computer aided Design | 19 | 87 |
| Process Parameters | 16 | 84 |
| Rheology | 15 | 58 |

Figure 2-3 provides a concise network visualization with 150 keywords recurring at least six times across diverse documents. Generated using VOSviewer software, it employs a distance-based methodology, where shorter distances signify stronger relational ties. Colored clusters categorize keywords, with the red cluster focusing on rapid investment casting, the blue cluster on ceramic 3D printing, and the violet cluster on large-scale extrusion additive manufacturing. Font size variations indicate keyword frequencies, emphasizing the most frequent terms in this research domain.

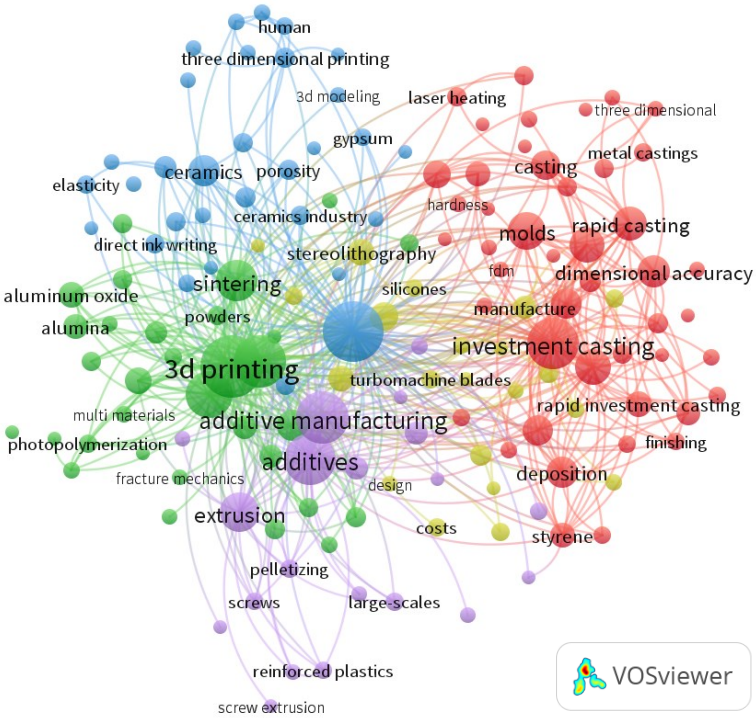


Figure 2-3. Network visualization of most frequently used 150 keywords in RIC, where font size denotes the frequency, distance between keywords denotes the link strength, and the color denotes different clusters

### 2.1.2.3 Authorship Analysis

This study compiles a list of influential researchers in rapid investment casting. Authorship analysis of 1431 authors identifies 11 contributors with a minimum of 5 relevant publications (see Table 2-3). Rupinder Singh is the most contributing scholar with 28 publications and 797 citations, while Chee Kai Chua achieves the highest average citations per publication at 403.6, accumulating 2018 citations.

Table 2-3. Authors contributing in the research field with the highest number of publications along with their citations count

| Author | Number of relevant publications | Citations | Average Citations per publication |
|---|---|---|---|
| Singh, Rupinder | 28 | 797 | 28.5 |
| Kumar, Parlad | 6 | 149 | 24.8 |
| Ahuja, I.P.S. | 5 | 133 | 26.6 |
| Chohan, J. Singh | 5 | 238 | 47.6 |
| Li, Fei | 5 | 397 | 79.4 |
| Wang, Donghong | 5 | 39 | 7.8 |
| Singh, Jaspreet | 5 | 64 | 12.8 |
| Bae, Chang-jun | 5 | 204 | 40.8 |
| Chua, Chee Kai | 5 | 2018 | 403.6 |
| Wang, Zhaogui | 5 | 97 | 19.4 |
| Zhang, Jian | 5 | 12 | 2.4 |

### 2.1.2.4 Countries Activities Analysis

This analysis identifies global research contributions in the specified field from 59 countries. Table 2-4 outlines the top 10 contributors, with China leading in publication volume (77) and total citations (2489), followed by India with 57 publications and 1495

citations. Despite a lower publication count, Singapore stands out with the highest average citations per publication, emphasizing the impact of its research.

Table 2-4. Top contributing Countries by publishing relevant articles in the Rapid Investment Casting research domain

| Country | Number of relevant publications | Citations | Average Citations per publication |
|---|---|---|---|
| China | 77 | 2489 | 32.3 |
| India | 57 | 1495 | 26.2 |
| United States | 49 | 1305 | 26.6 |
| United Kingdom | 24 | 1052 | 43.8 |
| Italy | 23 | 512 | 22.3 |
| Poland | 16 | 139 | 8.7 |
| Germany | 14 | 184 | 13.1 |
| South Korea | 14 | 198 | 14.1 |
| Spain | 12 | 164 | 13.7 |
| Singapore | 11 | 2277 | 207 |

#### 2.1.2.5 Funding Sponsors Analysis

This analysis identifies 161 distinct sponsors supporting research in this field. The top 10 contributors, detailed in Figure 2-4, include the National Natural Science Foundation of China, which sponsored 31 documents. This compilation aids prospective researchers in aligning their objectives with potential funding sources.

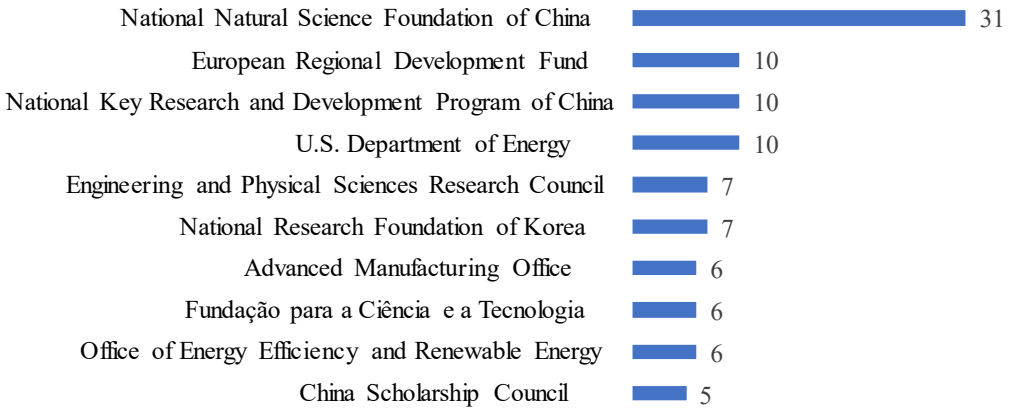


Figure 2-4. Top investors sponsoring in the research domain of Rapid Investment Casting

## 2.2 Comprehensive Literature Survey

This section addresses predefined research questions (subsection 2.1.1.1) through a literature review on additive manufacturing methodologies, 3D printing for sacrificial patterns and investment shells, limitation assessment, modification strategies, and insights into innovative techniques suitable for the research initiative.

### 2.2.1 Additive Manufacturing Techniques

Additive Manufacturing (AM) is a revolutionary methodology that incrementally adds material to fabricate intricate artifacts, contrasting with subtractive manufacturing. Among AM technologies, this literature review explicitly examines 3D printing, which creates objects layer by layer from digital CAD models. While alternative AM technologies enable non-planar orientations (free-form printing), this review concentrates on the 3D printing process [57–61], categorizing techniques based on the printing process and material state (see Figure 2-5).

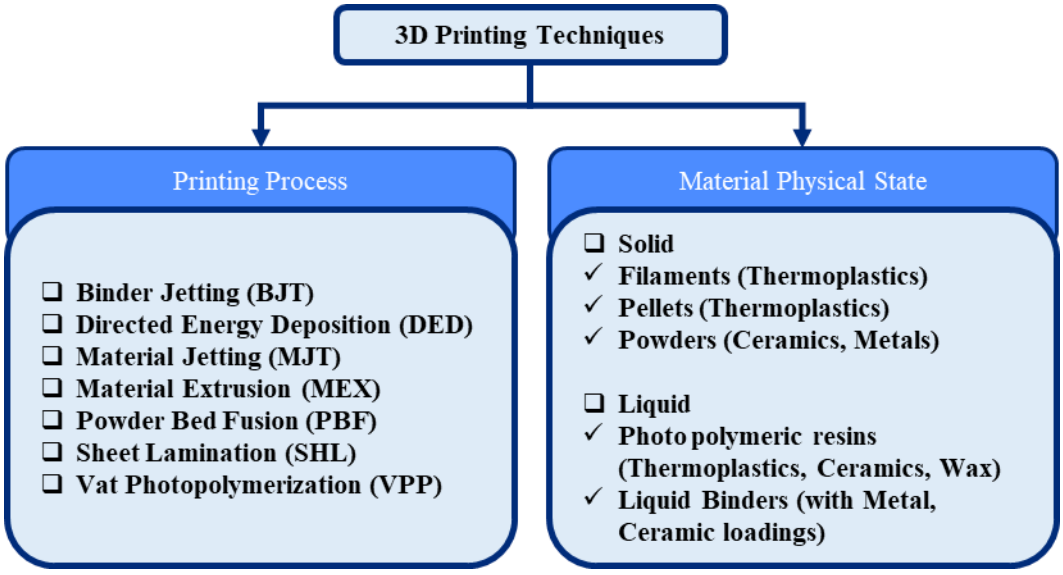


Figure 2-5. Varieties of 3D printing techniques based on the printing process and material's physical state

3D printing based on feedstock's physical state is classified into solids and liquids. In the solid state, materials exist as filaments, wires, pellets, or powders undergoing fusion through melting or sintering. Liquid states include photopolymer resin or particle-filled binders subjected to heat for object construction. Following ISO/ASTM 52900:2021 (en) [62], various 3D printing techniques categorized by processes include Binder Jetting [63–68], Directed Energy Deposition [69–74], Material Extrusion [75–84], Material Jetting [85–90], Powder Bed Fusion [91–97], Sheet Lamination [98–103], and Vat Photopolymerization [104–115]. Table 2-5 provides an overview of these technologies, detailing their printing mechanisms and materials.

Table 2-5. 3D printing techniques with their printing mechanisms and materials used

| 3D printing process | 3D printing technologies | 3D Printing Mechanism | Materials used: Physical State |
|---|---|---|---|
| **Material Extrusion** | Fused Deposition Modelling (FDM) | Filaments are extruded through heated nozzle | Thermoplastics, Engineering grade plastics such as PEEK |
| | Fused Granulated Fabrication (FGF) | Pellets are heated in barrel and extruded through nozzle | Thermoplastics, Continuous/Chopped fiber reinforced plastics |
| | Direct Ink Writing (DIW) | High viscosity slurries (paste) are extruded through nozzle | Ceramic slurry, hydrogels, metal pastes, food pastes, Biopolymers |
| **Vat Photopolymerization** | Stereolithography (SLA) | UV laser selectively cure the photopolymer resin layer-by-layer in a tank | Castable, Biocompatible, Ceramic, Engineering and standard resins |
| | Digital Light Processing (DLP) | Digital light projector cures the entire layer of photopolymer resin in a tank | Castable, Biocompatible, Ceramic, Engineering and standard resins |
| **Powder Bed Fusion** | Selective Laser Sintering (SLS) | High powered laser selectively sinters powered material | Metal powders, Ceramic powder, Nylon, Durable plastics, Biocompatible |
| | Selective Laser Melting (SLM) | High powered laser locally melts the powder to create dense bonded objects | Metals – Stainless steel, Aluminum, Titanium, Nickel, Cobalt-Chromium alloys |
| **Material Jetting** | Poly/Multi-Jet Printing | Multiple print heads precisely jet droplets of liquid photopolymer and UV light cures it layer-by-layer | Photopolymer resin, Wax, Composite materials |

| | | | |
|---|---|---|---|
| | Drop-on-demand Jetting | Particles loaded inks are jetted on the print bed and the object is sintered to remove the binder from ink | UV-curable resins, Wax, Ceramics, Metal powders, Thermoplastics, food materials |
| **Binder Jetting** | Binder Jet 3D printing | Liquid binder is selectively deposited on the powered bed to realize objects | Sandstones, metal powders, ceramics, plaster-based materials, polymer powder |
| **Directed Energy Deposition** | Wire Arc Additive Manufacturing (WAAM) | Electric arc is used as a heat source to melt a wire which is deposited layer-by-layer to build objects | Metal alloys – Stainless steel, Aluminum, Titanium, Nickel, Copper, Inconel |
| | Laser DED | Laser is used as a heat source to melt and fuse wire or powder and is deposited on the substrate | Cobalt chrome alloys, Super alloys, Metal alloys, Invar |
| | Plasma Arc AM | Plasma arc is used as a heat source to melt wire or powder and is deposited on the substrate | Tungsten Carbide, Titanium Carbide, Molybdenum alloy, Colmonoy alloy |
| **Sheet Lamination** | Laminated Object Manufacturing (LOM) | Adhesive coated laminates are bonded together and the laser or knife cut each layer to its desired shape. | Paper, plastic films, metal foils, ceramic sheets, Textiles |

### 2.2.2 3D – Printing techniques used for printing sacrificial patterns

Various 3D printing methods, including SLA, SLS, FFF, RFP, MJP, and Binder Jetting, are used for sacrificial pattern fabrication in RIC [12,15]. Table 2-6 details material compositions, attributes, and any necessary pre/post-processing steps for IC using these AM techniques. Notably, SLA and FDM are favored for their industry accessibility, with SLA achieving high pattern quality and FDM providing a cost-effective option for pattern production [12].

Table 2-6. 3D printing techniques implemented in direct RIC process for printing sacrificial patterns

| AM Technique | Material | Layer height (µm) | Dimensional Tolerance (mm) | Surface roughness (µm) | Residual Ash (%) | Additional pre/post-processing | Reference |
|---|---|---|---|---|---|---|---|
| **SLA** | Castable wax (photopolymer + wax) | 25 | 0.05 | - | 0.1 | Post-curing | [11,116] |
| **FDM** | ABS | 100 - 200 | 0.971 | 0.3 | - | Chemical treatment | [43] |
| **MJP** | Acrylate | 25 | 0.4 | 3.89 | - | N.A. | [117] |
| **RFP** | Water/ice | 150 | 0.94 | 3.2 | - | N.A. | [118][119] |
| **Binder jetting** | Polymethylmethacrylate (PMMA) powder | 300 | 0.43 | 28 | - | Wax and epoxy infiltration | [120] |
| **SLS** | Castform PS (Polystyrene) powder | 150 | | 3 | 0.02 | Wax infiltration | [121] |

#### 2.2.2.1 Limitations in the existing 3D printing techniques used for printing sacrificial patterns

Various 3D printing techniques are used for sacrificial pattern fabrication. However, certain limitations persist which are addressed in the following discussion.

- **Scalability**

Upon examining the layer heights in Table 2-6, it was observed that they ranged from 25-300 μm, posing scalability constraints on the produced artifacts. This limitation increases cycle time, even for smaller sacrificial patterns. Most desktop FDM and SLA printers, widely used in Rapid Investment Casting (RIC), typically have a print bed of around 300 mm × 300 mm and a maximum height of 200 mm. In contrast, traditional investment casting exhibits higher scalability, evident in turbine blades for aircraft. Therefore, the sought-after additive module should be capable of printing patterns with dimensions reaching at least 1 cubic meter.

- **Stair-stepping**

As discussed in section 1.5.1, layer-by-layer printing in 3D techniques creates a stair-stepping effect on sacrificial patterns, affecting surface quality and dimensional precision. Surface quality and dimensional tolerance of metal castings depend directly on sacrificial patterns. Badanova et al. [11] observed stair-stepping even at a 25 μm layer height, impacting cast metal. Chemical processes and sand polishing offer solutions. However, our approach involves in-situ CNC machining on an in-house hybrid manufacturing system to refine sacrificial patterns, improving surface finish and dimensional accuracy to meet investment casting standards.

- **Expensive and complex manufacturing process**

Current sacrificial pattern fabrication AM methods involve complex and costly processes with extended cycle times. For instance, SLA 3D printers require high-powered lasers, intricate designs, and post-curing, significantly increasing overall cycle time. Rapid freeze prototyping demands a consistently controlled environment, leading to high energy consumption. Binder Jetting involves a 24-hour heat treatment, impacting cycle time and production costs. SLS, susceptible to shrinkage, requires post-processing with wax infiltration and utilizes an expensive high-powered laser for material sintering.

- **Material**

For any material to be qualified for the fabrication of the sacrificial pattern, it must exhibit the following characteristics:

i. **Low melting point:** Makes material easy to handle and, at the same time, saves energy due to lower burnout temperature.

ii. **Low viscosity:** Provides high flow characteristics, which ensures efficient escape from the investment shell.

iii. **Exceptional surface finish and structural integrity:** The pattern must exhibit an excellent surface finish to ensure the casting's surface quality. Additionally, it must retain adequate durability to abrasive post-processing required for precise surface quality and dimensional stability.

iv. **No residual ash content:** Mitigate the probable surface defects such as inclusions, porosity, pits, bumps or irregularities, to name a few.

v. **Clean burnout:** Ensures safety from many hazards and minimizes carbon footprint.

vi. **Low coefficient of thermal expansion (CTE):** Pattern material must resemble the CTE of investment shell, minimizing the contrasting shrinkage and expansion during burnout and preventing shell cracking.

vii. **Material reliability and practicality:** Pattern material must demonstrate persistent casting results and balance affordability and performance.

Wax is the preferred material for the traditional IC process [15], meeting specified requirements. Despite attention on 3D printing with thermoplastics like PLA, ABS, and resins, they are unsuitable for IC due to material characteristic issues, leading to challenges such as shell cracking and poor surface finish in RIC [122,123]. Garg et al. [124] and Kumar et al. [22] attempted to improve surface quality and shell cracking by applying a wax coating on FDM-produced 3D-printed thermoplastic patterns. Despite the promise, challenges persisted, including incomplete burnout, residual ash content, and environmentally unsafe constituents released during plastic combustion. Investigative efforts should prioritize printing sacrificial patterns with wax as the primary material.

#### 2.2.2.2 Potential 3D printing technique for printing a sacrificial pattern

Examining constraints in the preceding section reveals three primary challenges associated with the standard 3D printing technique: scalability, complexities, and costliness of standard AM processes. There is also an indirect concern about material compatibility, requiring the selected print head to work with the wax material. While Fused Deposition Modeling (FDM) is a simple and cost-effective process for printing sacrificial patterns with commercially available wax filaments, it lacks scalability for larger print volumes. Therefore, a similar novel extrusion approach of fused granulated fabrication can be explored to fabricate large-scale wax patterns.

**Fused Granulated Fabrication – Additive Manufacturing (FGF – AM) process**

Fused granulated fabrication (FGF) is an innovative large-scale extrusion additive manufacturing process. It eliminates filament fabrication, a key distinction from FDM [125–127]. This omission reduces production costs by over ten times and shortens production time by over 200 times compared to FDM [128–130].

FGF-AM design is simple, using a streamlined process that directly employs plastic pellets, as shown in the schematic diagram in Figure 2-6. A dedicated motor-driven screw mechanism efficiently transports pellets along a stationary barrel with circumferential heaters [131–134]. This setup ensures pellet melting, and the extrudate, at controlled viscosity, is then deposited through a nozzle onto a heated bed [135–138]. FGF-AM can produce up to seven cubic meters of large-scale components, highlighting its industrial utility [139]. The print head's components can be adjusted based on the desired volumetric throughput, and for the current task of printing within a one cubic meter range, the extruder needs a throughput of 2 kg/hour or 500 $mm^3$/sec [140]. This technology will be applied for sacrificial pattern fabrication, optimizing printing parameters for IC applications in Chapter 4.

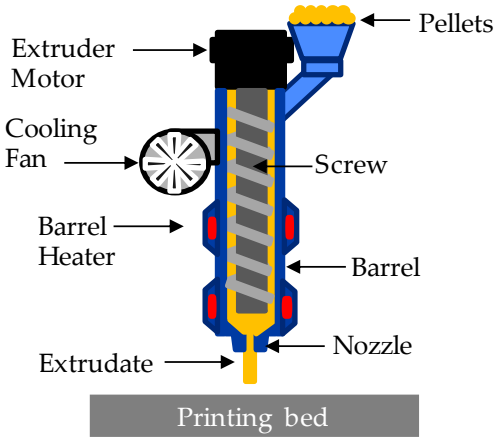


Figure 2-6. Schematic of direct pellet-fed screw extruder

#### 2.2.2.3 Post-processing technique on printed pattern to eliminate stair-stepping

Large-format additive manufacturing, like FGF, operates at a macro-level layer height resolution (1 to 8 mm) [81,141]. The scalability of 3D prints increases the stair-stepping issue, impacting metal casting surface quality. In-situ CNC machining is proposed for post-processing, aiming to eliminate stair-stepping, enhance surface quality, and improve dimensional precision aligned with IC standards.

### 2.2.3 3D – Printing techniques used for printing investment shells

Various 3D printing methods for constructing investment shells are documented in references [142,143]. Table 2-7 summarizes these methodologies, including materials and pre/post-processing procedures. Binder jetting and inkjet 3D printing stand out as preferred methods for ceramic printing among the various techniques.

Table 2-7 3D printing techniques implemented in direct RIC process for printing investment shells/cores

| 3D printing technique | Layer-Height (µm) | Material | Additional pre/post-processing |
|---|---|---|---|
| **Binder Jetting** [64,144–146] | 50-150 | Quartz (Silica), Aluminum oxide, Gypsum | Curing, De-binding and sintering |
| **Inkjet 3D printing** [147,148] | 125 | Calcium Sulphate, Z-Cast 501 powder | Post-curing |
| **DIW** [149–153] | 200-3000 | Alumina-based ceramic slurry, calcium carbonate, Kaolinite clay, Gypsum | Drying, and sintering |
| **SLA** [154–156] | 20-300 | Calcium oxide, Silica ceramic filled photopolymer | Post-curing, De-binding and sintering |
| **SLS** [157–159] | 100-200 | Mullite (Alumina Silicate) powder | De-binding and Sintering |

#### 2.2.3.1 Limitations in the existing 3D printing techniques used for printing investment shells

The standard 3D printing techniques used to produce investment shells possess limitations similar to those identified with the sacrificial patterns, detailed as follows:

- **Scalability**

Like sacrificial pattern fabrication, the 3D printing techniques for investment shell printing are limited to a desktop-scale print volume, constrained by the layer height. Increasing the print volume with a smaller nozzle size would result in impractical time requirements for large-scale objects. The layer height typically ranges from 50 to 300 µm, except for direct ink writing, which can achieve a 3 mm layer height. This scalability aligns with the chosen 3D printing technique for sacrificial pattern fabrication, FGF-AM.

- **Stair-stepping**

Due to the layer-wise additive manufacturing process in 3D printing, investment shells exhibit a stair-stepping effect, which disrupts the surface quality and dimensional precision in metal castings. Unlike sacrificial patterns that can be machined through subtractive methods, the inherent brittleness of ceramics in investment shells poses challenges for machining, leading to cracking. In this context, a shell is printed around the processed sacrificial pattern to mitigate stair-stepping along the interface. The exterior shows stair-stepping, while the inner side remains defect-free.

- **Expensive and complex manufacturing process**

Post-processing, including sintering, is integral to current ceramic 3D printing techniques. However, methods like SLA require additional post-curing, impacting overall cycle time. Sintering in SLA can lead to significant shrinkage and cracks in the final objects. SLS achieves full-density objects, but ceramic fusion challenges require binders and subsequent de-binding processes. The vacuum requirement during SLS printing poses integration challenges with the proposed hybrid manufacturing system. Conversely, DIW offers a simple, cost-effective, large-scale extrusion mechanism seamlessly compatible with other additive and subtractive modules.

#### 2.2.3.2 Potential 3D printing technique for printing investment shells

Among the listed 3D printing methods in Table 2-7, Direct Ink Writing (DIW) [160,161], an extrusion-based additive manufacturing technique, stands out due to its scalability, simplicity, and versatility with a wide range of materials. DIW includes different methods based on the principal components used, as depicted in Figure 2-7, illustrating three primary mechanisms for extruding high-viscosity slurry material through pneumatic pressure, pistons, or positive displacement via a rotating screw.

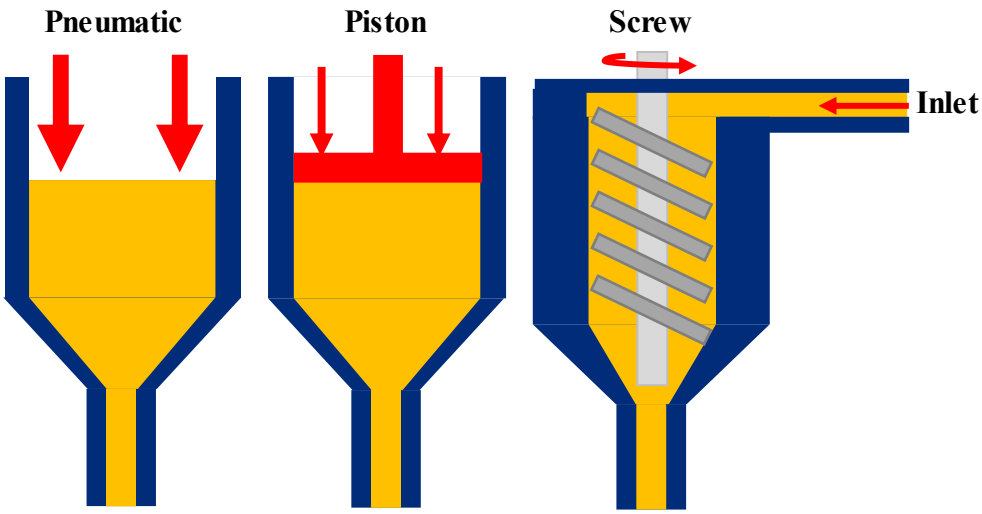


Figure 2-7. Different DIW printing mechanisms (a) Pneumatic-based, (b) Piston-based, and (c) Screw-based

Among the three DIW printing mechanisms, the screw-based approach is the most viable for integration into the hybrid manufacturing system. Unlike pneumatic and piston-based options with scalability limitations, the screw-based print head ensures continuous material supply, enabling uninterrupted, extended printing sessions. Additionally, it usually has a lightweight extruder, maintaining a consistent extrusion rate for 3D printing operations. Hence, the screw-based DIW technique will be used for shell fabrication, with influential printing parameters optimized in Chapter 5.

## 2.3 Conclusion

A scientometric analysis was conducted on the engineering domain of rapid investment casting, providing insights to potential or current stakeholders. This analysis helps identify opportunities and highlights influential countries, institutions, and journals. The chapter includes a systematic literature review, addressing predefined research

questions on optimal 3D printing techniques for fabricating sacrificial patterns and investment shells.

The discussion addresses limitations in existing 3D printing methods and proposes novel techniques. Fused Granulated Fabrication (FGF-AM) is identified as the optimal 3D printing technique for scalable sacrificial patterns, providing up to 10-20 times higher productivity. Implementation of in-situ CNC machining to enhance surface quality and dimensional precision is suggested. Screw-based Direct Ink Writing (DIW) is recommended for large-scale investment shells due to cost-effectiveness and a straightforward mechanism, facilitating integration into the hybrid manufacturing system. The subsequent chapter will focus on designing and manufacturing an in-house hybrid system to validate the proposed rapid investment casting chain, including the selection of commercial additive modules based on predefined criteria.

# Chapter 3 Design and in-house fabrication of hybrid manufacturing system

This chapter focuses on strategically selecting commercial print heads to create large-scale sacrificial patterns and investment shells. A decision matrix was used for the selection process, considering factors like budget, weight, and productivity. The chapter also provides a detailed exploration of the specifications and features of the selected print heads and CNC spindle. It also covers components in the in-house designed robotic manipulator, crucial for executing operations in rapid investment casting. The discussion extends to the motion controller for seamless communication with the hybrid manufacturing system.

## 3.1 Commercial FGF-AM print heads for fabricating sacrificial patterns

Following the literature review in Chapter 2, the fused granulated fabrication extrusion technique is chosen for large-scale sacrificial pattern production for its exceptional material deposition rate. The subsequent sub-sections explore commercially available pellet-fed screw extruders, detailing the selection process based on pre-defined parameters and specifying the chosen print head's specifications.

### 3.1.1 Decision matrix, criterions and weighting scenarios

A decision matrix was established to compare, assess, and select the best suited extruder. Three criteria were identified for the decision matrix: Cost of acquisition (A), print head weight (B), and maximum mass flow rate achievable through extrusion (C). The comparison involved three scenarios. Scenario 1, a balanced approach, assigned equal weightages of 3.33 to each criterion, totaling 10. Scenario 2, prioritizing cost efficiency, assigned the maximum weightage of 8 to cost, while extruder weight and mass flow rate received a weightage of 1 each. Conversely, Scenario 3 prioritized

productivity, allocating the maximum weightage of 8 to mass flow rate, with extruder cost and weight each assigned a weightage of 1.

Table 3-1 compiles commercial Fused Granulated Fabrication (FGF) large-scale extruder models, including manufacturers and critical criteria values such as extruder cost, weight, and maximum mass flow rate. An ideal design criterion, with capped values (CA $10,000 for cost, 15 kg for weight, and 2 kg/hr for mass flow rate), was used to score each extruder on a scale of 10 for each criterion. For instance, an extruder below CA $10,000 received a perfect score of 10. The MDPE 10 extruder by Massive Dimension, priced at CA $22,060, received a score of 5 for exceeding the budget but earned perfect scores for the other two criteria.

A decision matrix, outlined in Table 3-2, utilized three scenarios to score each extruder based on specific criteria. Relative percentages, derived from final scores, were calculated for each extruder within each scenario. The Pulsar extruder by Dyze Design achieved 100% in both balanced and productivity scenarios, while the SJ-35 by Robotdigg scored 100% in the cost-efficiency scenario. Emphasizing cost efficiency, the SJ-35 emerged as the preferred choice for fabricating sacrificial patterns. Notably, even in other scenarios, the SJ-35 consistently ranked high, with percentages ranging from 97 to 99%, reinforcing its suitability compared to alternative print heads.

Table 3-1 Commercial large-scale FGF-AM print heads along with their cost, weight, and maximum flow rate

| **Commercial Systems/Criterions** | | **Cost of acquisition [A]** | **Extruder weight [B]** | **Mass flow rate [C]** |
|---|---|---|---|---|
| **Ideal design criteria** | | Upto CA $ 10,000 | Upto 15 kg | Around 2kg/hr |
| **Dyze Design** | Pulsar | **CA $ 10,330** | **7 kg** | **3kg/hr** |
| | | 9 | 10 | 10 |
| **Massive Dimension** | MDPE 10 | **CA $ 22,060** | **14 kg** | **5.7 kg/hr** |
| | | 5 | 10 | 10 |
| **Massive Dimension** | MDPH 2 | **CA $ 7,500** | **8.4 kg** | **0.9 kg/hr** |
| | | 10 | 10 | 5 |
| **Robotdigg** | SJ-35 | **CA $ 2,518** | **22 kg** | **2 kg/hr** |
| | | 10 | 8 | 10 |
| **Cead Group** | E-25 | **CA $ 35,000** | **29 kg** | **12 kg/hr** |
| | | 1 | 1 | 10 |
| **REV 3RD** | RD-M10+ | **CA $ 21,520** | **9.8 kg** | **12 kg/hr** |
| | | 5 | 10 | 10 |

Table 3-2 Decision Matrix for wax extruders along with relative percent for each scenario

| Commercial Systems/Criterions | | Scenario: Balanced | Scenario: Cost Efficiency | Scenario: Productivity |
|---|---|---|---|---|
| **Dyze Design** | Pulsar | **100 %** | **94 %** | **100 %** |
| **Massive Dimension** | MDPE 10 | **86 %** | **61 %** | **96 %** |
| **Massive Dimension** | MDPH 2 | **86 %** | **97 %** | **61 %** |
| **Robotdigg** | SJ-35 | **97 %** | **100 %** | **99 %** |
| **Cead Group** | E-25 | **41 %** | **19 %** | **83 %** |
| **REV 3RD** | RD-M10+ | **86 %** | **61 %** | **96 %** |

### 3.1.2 Robotdigg SJ-35 Desket-H FGF print head

The SJ-35 Desket-H by Robotdigg in China [162] is a large-scale pellet-fed single-screw extruder weighing 22 kg with dimensions of 840 mm × 170 mm × 170 mm (Figure 3-1). It features a 35 mm inner diameter barrel, a screw with a 13:1 L:D ratio, and a 1:1 compression ratio. The single-phase 250-watt extruder motor reaches up to 1000 RPM, with a 50:1 motor-to-screw gear ratio. A cooling fan near the pellet inlet prevents the material from melting for positive displacement, and two circumferential heaters on the barrel melt the material for extrusion. Three PT-1000 RTD sensors inside the barrel maintain material temperature to extrude within a controlled viscosity range.

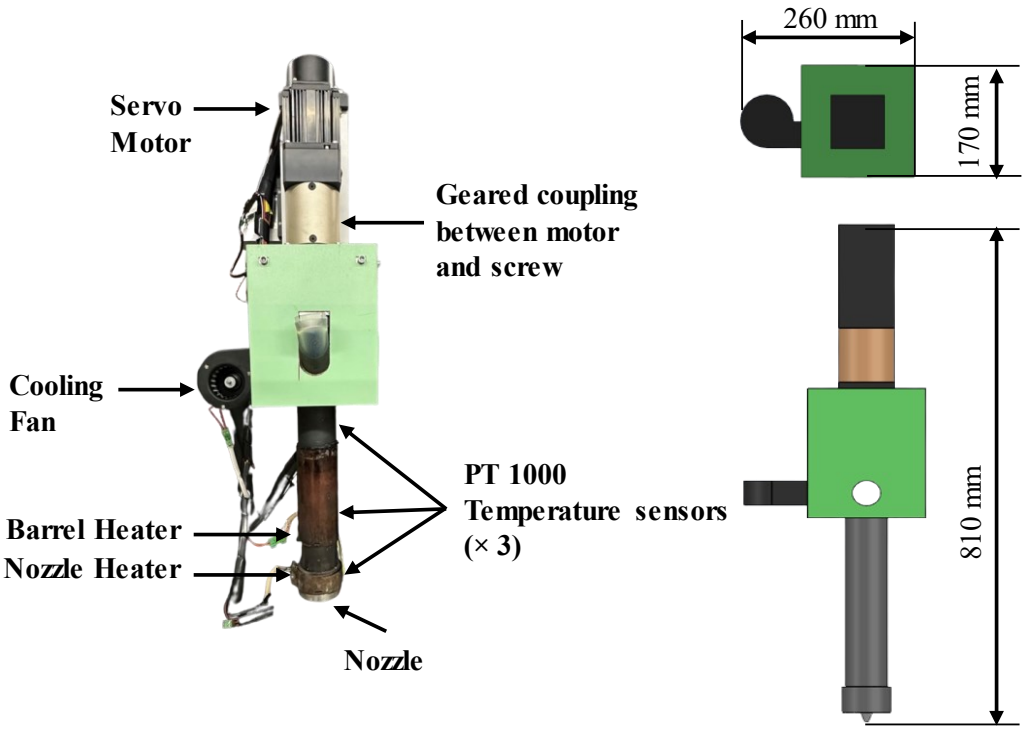


Figure 3-1. SJ-35 FGF pellet-fed print head's components and overall dimensions

## 3.2 Commercial DIW print heads for fabricating investment shells

The Direct Ink Writing (DIW) extrusion 3D printing technique for large-scale investment shell fabrication was also determined through the literature review in

Chapter 2. Similar to section 3.1, this section compares different commercial DIW print heads and selects an optimal one using predetermined criteria and scenarios. The selected print head's specifications and operational details are presented.

### 3.2.1 Decision matrix, criterions and weighting scenarios

The methodology from subsection 3.1.1 for selecting the optimal print head for sacrificial patterns is replicated here for the investment shell print head. Comparison criteria include cost of acquisition (A), extruder weight (B), and reservoir capacity (C), indicating the volume of slurry that can be printed without interruption. The scenarios and weights align with those used for the wax extruder.

Table 3-3 compiles commercial large-scale DIW extrusion print head systems for investment shell fabrication, including manufacturers. Critical decision matrix criteria include a budget of CA $8,000, an extruder weight of up to 5 kg, and a reservoir capacity of approximately 10 liters. Like the FGF print heads scoring, each system is rated out of 10 based on these criteria.

Scores from Table 3-3 were analyzed, and relative percentages in each scenario were computed (Table 3-4). The commercial print head with the highest percentage is deemed optimal in a given scenario. For example, the Continuous Feeding System by Wasp 3D is optimal in both balanced and productivity scenarios but exceeds the budget in cost-efficiency. The 5L Clay Tank with Extruder XL 3.0 by Wasp 3D is the most cost-effective but has less reservoir capacity, and its need for compressed air would make the system complex. Considering these factors, the Continuous Feeding System was chosen as the optimal print head for investment shell fabrication.

Table 3-3 Commercial large-scale DIW print heads along with their cost, weight, and reservoir capacity

| **Commercial Systems/Criterions** | | **Cost of acquisition [A]** | **Extruder weight [B]** | **Reservoir capacity [C]** |
|---|---|---|---|---|
| **Ideal design criteria** | | Upto CA $ 8,000 | Upto 5 kg | Around 10 liters |
| **Stone Flower 3D** | Ram Extruder Big 2.5L with Mortar Print Head | **CA $ 4,400**<br>10 | **12 kg**<br>5 | **2.5 liters**<br>2 |
| **Stone Flower 3D** | Ram Extruder Big 5L with Mortar Print Head | **CA $ 5,410**<br>10 | **15.4 kg**<br>3 | **5 liters**<br>5 |
| **3D Potter** | 4000 ml Linear Actuator Ram | **CA $ 5,250**<br>10 | **13.6 kg**<br>4 | **4 liters**<br>3 |
| **Wasp 3D** | Continuous Feeding system | **CA $ 9,500**<br>8 | **2 kg**<br>10 | **11 liters**<br>10 |
| **Wasp 3D** | 5L clay tank with extruder XL 3.0 | **CA $ 2,500**<br>10 | **2 kg**<br>10 | **5 liters**<br>5 |

Table 3-4 Decision Matrix for ceramic extruders along with relative percent for each scenario

| Commercial Systems/Criterions | | Scenario: Balanced | Scenario: Cost Efficiency | Scenario: Productivity |
|---|---|---|---|---|
| **Stone Flower 3D** | Ram Extruder Big 2.5L With Mortar Print Head | **61 %** | **92 %** | **32 %** |
| **Stone Flower 3D** | Ram Extruder Big 5L WITH Mortar Print Head | **64 %** | **93 %** | **54 %** |
| **3D Potter** | 4000 ml Linear Actuator Ram | **61 %** | **92 %** | **39 %** |
| **Wasp 3D** | Continuous Feeding system | **100 %** | **88 %** | **100 %** |
| **Wasp 3D** | 5L clay tank with extruder XL 3.0 | **89 %** | **100 %** | **61 %** |

### 3.2.2 Continuous feeding system by Wasp 3D

The Continuous Feeding System by Wasp 3D in Italy [163] is a large-scale DIW additive manufacturing system for consistently depositing highly viscous slurries including earthenware, refractory materials and clay. Figure 3-2 illustrates its two primary components: a slurry reservoir and a print head, interconnected by a hose for seamless slurry transfer. A mixing screw in the tank eliminates porosity through degassing. A brushless motor at the reservoir's bottom drives the screw, transferring slurry to the print head. The print head, with a high-torque motor and auger screw, extrudes viscous slurry through the nozzle for direct printing on the bed.

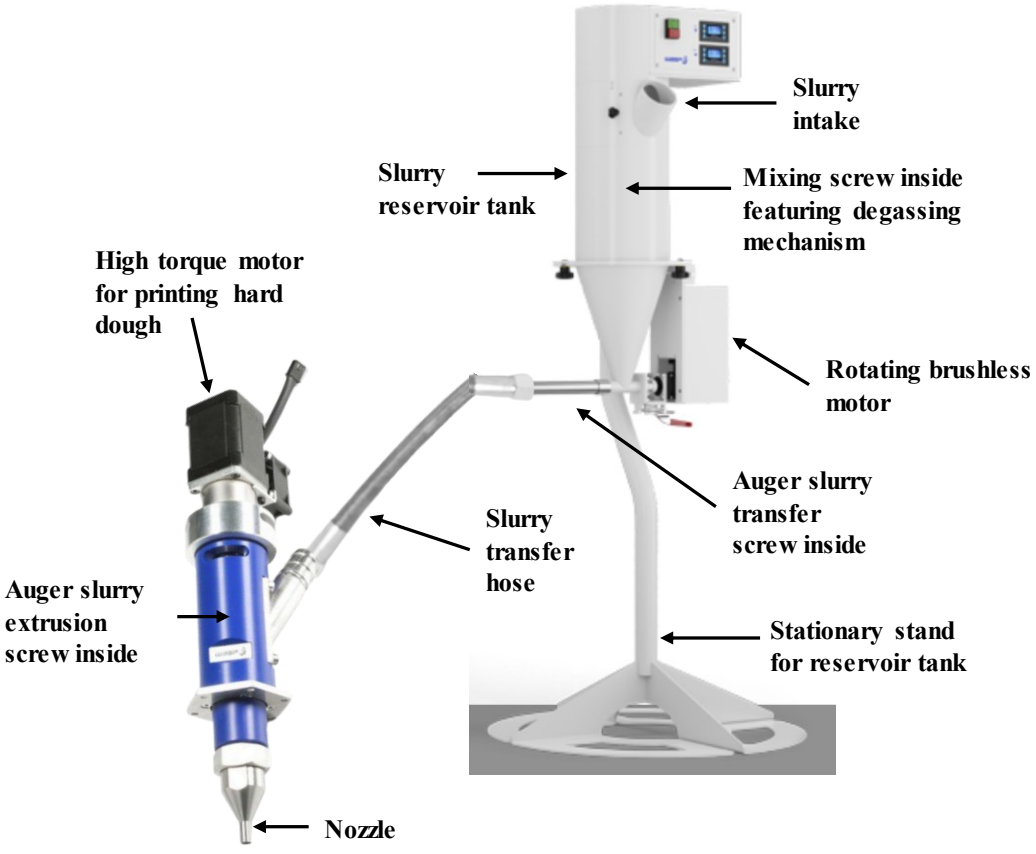


Figure 3-2. Continuous Feeding System by Wasp 3D

### 3.3 CNC spindle for machining the sacrificial pattern

The subtractive module by Rattmmotor [164] features a 500-watt air-cooled CNC spindle motor with an ER-11 collet size, weighing 1.35 kg. Figure 3-3 illustrates spindle components and dimensions. The spindle DC motor achieves a maximum rotational speed of 12,000 RPM with a maximum rated torque of 0.6 Nm.

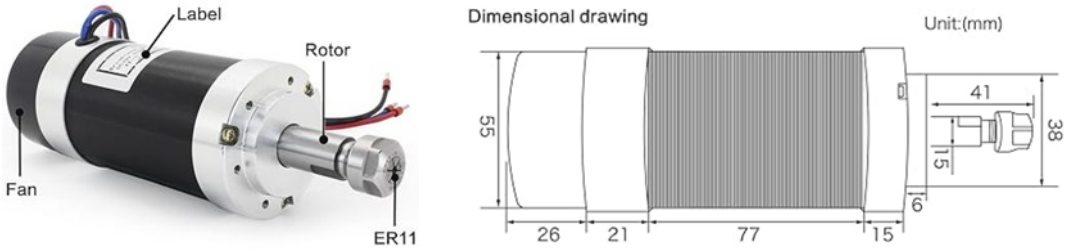


(a) (b)

Figure 3-3. (a) Air-cooled CNC spindle, (b) along with its dimensions

### 3.4 Hybrid Manufacturing System

The identified additive and subtractive modules must integrate into a unified framework for seamless operation. An in-house large-scale hybrid system, including a robotic manipulator and all modules, was designed and developed to address the need. This section details the functionality and specifications of each component in the hybrid manufacturing system.

Figure 3-4 schematically represents the integrated machine. The sequence starts with the SJ-35 pellet-fed screw extruder for sacrificial pattern fabrication, followed by machining to eliminate stair-stepping and enhance surface quality. The continuous feeding system then creates the investment shell around the processed pattern. These operations rely on a robotic manipulator and a controller, detailed in subsequent subsections.

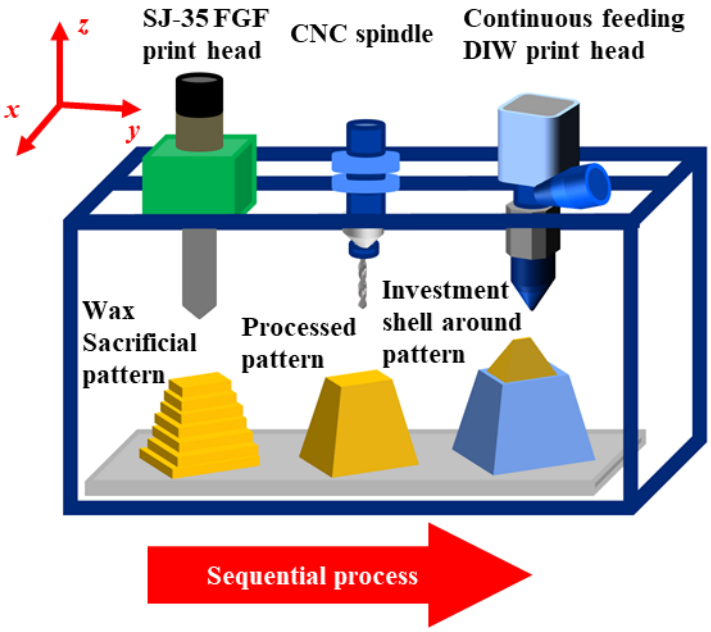


Figure 3-4. Schematic of the hybrid manufacturing system showcasing the sequential process in the proposed novel manufacturing chain

### 3.4.1 Robotic Manipulator

The robotic manipulator is a 3-axis cartesian gantry system with two parallel *x*-axes, a *y*-axis, and independent control over two *z*-axes (*u* and *z*), as shown in Figure 3-5. The linear module is a robust 120 × 76 mm ball screw actuator with a 16 mm diameter, providing support for substantial loads. It is powered by NEMA 34 motors designed for high power and torque in linear motion.

The hybrid manufacturing system's structural framework is built with 3" × 3" aluminum extrusions chosen for their capacity to support substantial moving loads on the gantry. Design and assembly processes utilized SolidWorks software, shown in Figure 3-6. The system has a one cubic meter build volume, with the current print bed intentionally constrained for proof of concept. Induction limit switches facilitate machine homing for repeatability, precisely determining the print head's position in 3D space. Additional gantry specifications are detailed in Figure 3-5.

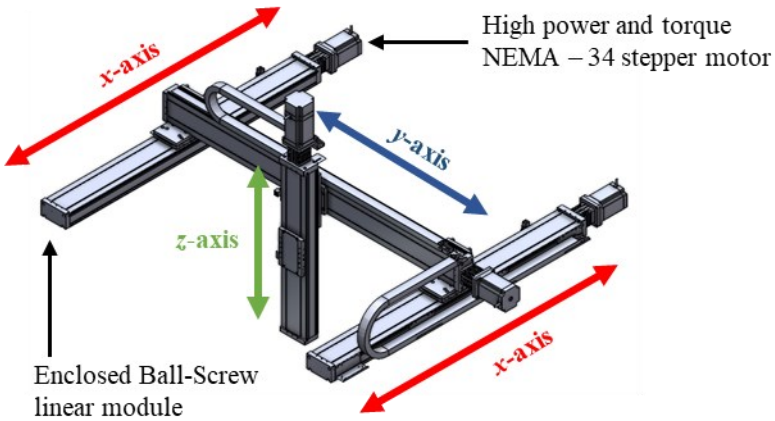


Figure 3-5. The configuration of the gantry used for robotic manipulator

Table 3-5 Other specifications of the hybrid manufacturing system

| Specifications | Value |
|---|---|
| **Build Volume** | 1 $m^3$ |
| **Maximum vertical payload** | 50 kgs |
| **Maximum horizontal payload** | 100 kgs |
| **Precision** | ± 20 µm |
| **Maximum loaded speed** | 380 mm/sec |
| **Maximum acceleration** | 1000 $mm/sec^2$ |
| **Ball screw lead** | 10 mm |

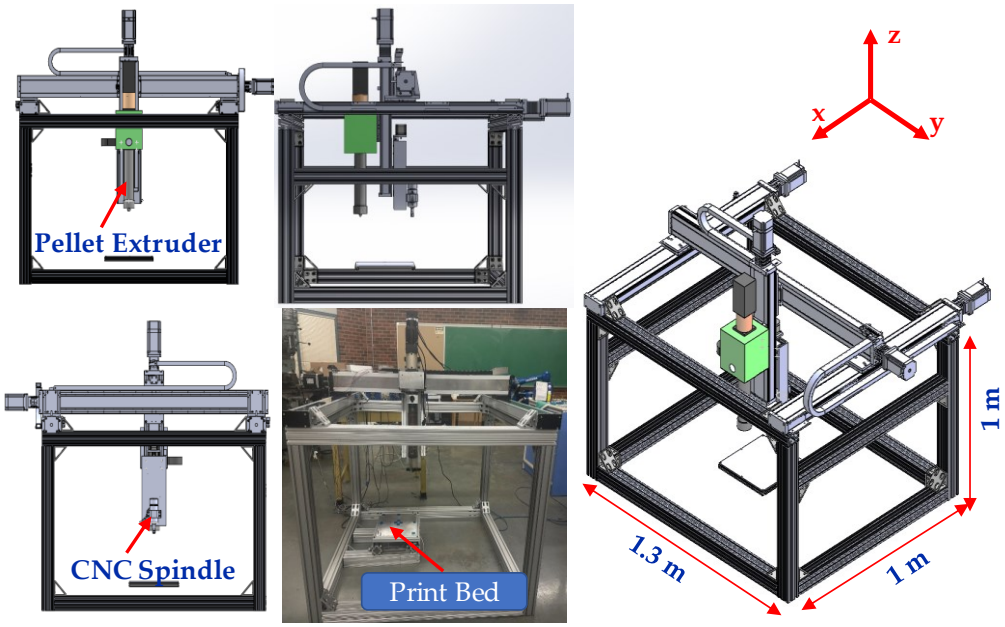


Figure 3-6. In-house designed and developed hybrid manufacturing system

### 3.4.2 Heated Print Bed

A heated print bed is crucial for optimal adherence of deposited wax material from the SJ-35 pellet-fed extruder and to address potential warping. The selected bed material, Aluminum 6061, ensures even heat distribution with a tight-tolerance flatbed measuring 12" × 12" and 8 mm thickness. The underside hosts a 750 W, 120 V Keenovo silicone heater (300 mm×300 mm) affixed with 3M adhesive. The embedded thermistor enables precise temperature control, allowing the bed to reach 180 °C in 10 minutes [165].

Ensuring a leveled print bed is crucial, and the setup incorporates a manual bed leveling mechanism, as shown in Figure 3-7. Supported by compression springs at all four corners, the bed rests on an aluminum extrusion at the base, secured with a centrally positioned screw. Bed leveling is achieved by rotating the screw, adjusting compression, or loosening of the springs. This enables precise leveling along both the *x* and *y* axes.

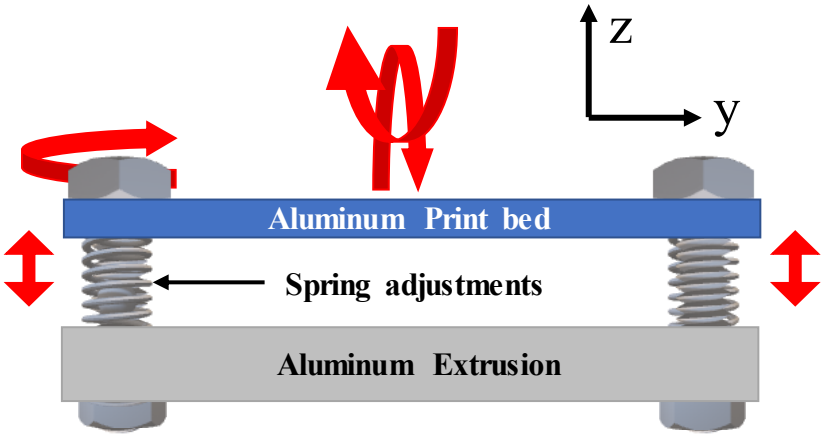


Figure 3-7. Print bed manual levelling mechanism

### 3.4.3 Motion Controller

Centralized coordination is handled by the Duet 3 6XD controller board from Duet3D, Peterborough, UK [166]. This versatile board interfaces seamlessly with multiple motor drivers and temperature control systems, enabling the integration of expansion boards for enhanced operational efficiency and synchronization within the hybrid manufacturing system. RepRap firmware [167] translates G-code [168] instructions into precise electrical signals, facilitating intricate functioning of both additive and subtractive manufacturing. The wiring flowchart is displayed in Figure 3-8.

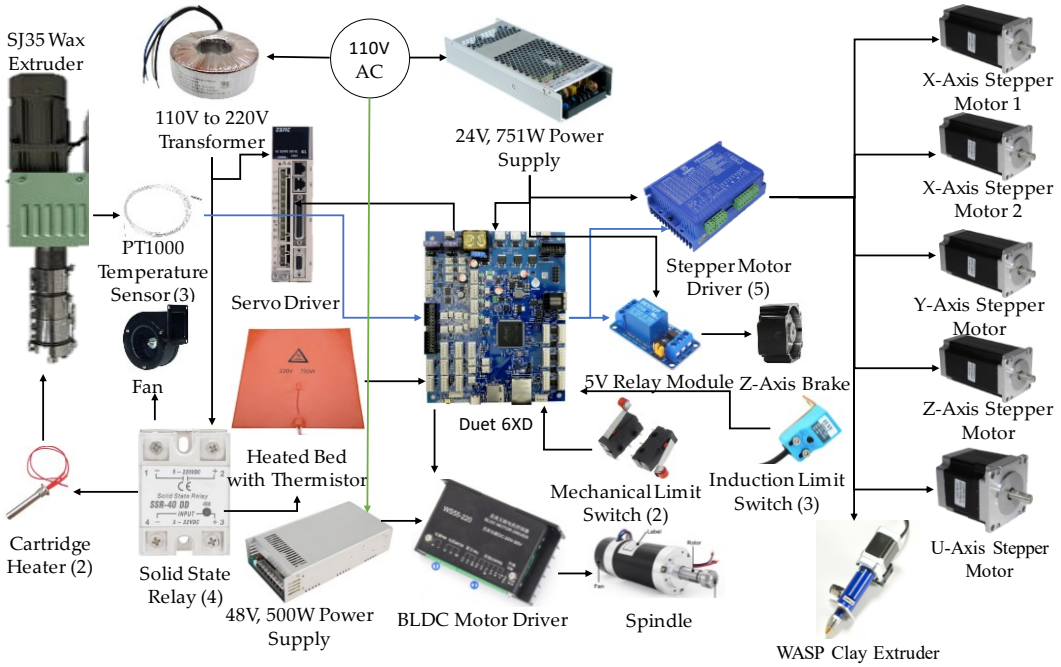


Figure 3-8. Wiring diagram of the hybrid manufacturing system

## 3.5 Conclusion

The decision matrix finalized the selection of commercial print heads, guiding the choice of components. A large-scale hybrid manufacturing system was designed and fabricated in-house, integrating additive and subtractive modules into a unified machine system. The setup facilitates seamless operations for RIC operations. Subsequent chapters optimize printing parameters for additive and subtractive modules, emphasizing sacrificial pattern and investment shell fabrication.

# Chapter 4 Fabrication of sacrificial wax patterns through large-scale fused granulated fabrication (FGF – AM) process

This chapter aims to overcome limitations in traditional and rapid investment casting methods by utilizing large-scale extrusion-based FGF-AM technology for fabricating sacrificial patterns, using wax as the printing material. The study involves developing an experimental approach to characterize and optimize crucial printing parameters through DoE to ensure structural integrity. Additionally, in-situ CNC machining capabilities are integrated into the in-house hybrid manufacturing system to address challenges like stair-stepping, enhance surface quality, and meet dimensional tolerance standards for investment casting. The investigation evaluates the industrial-scale viability of the developed system. Mechanical testing on 3D-printed wax specimens and porosity analysis are conducted to verify mechanical properties' consistency and the system's ability to produce fully-dense objects (near zero porosity).

## 4.1 Methodology

The methodology is shown in Figure 4-1 and is detailed in the following sections.

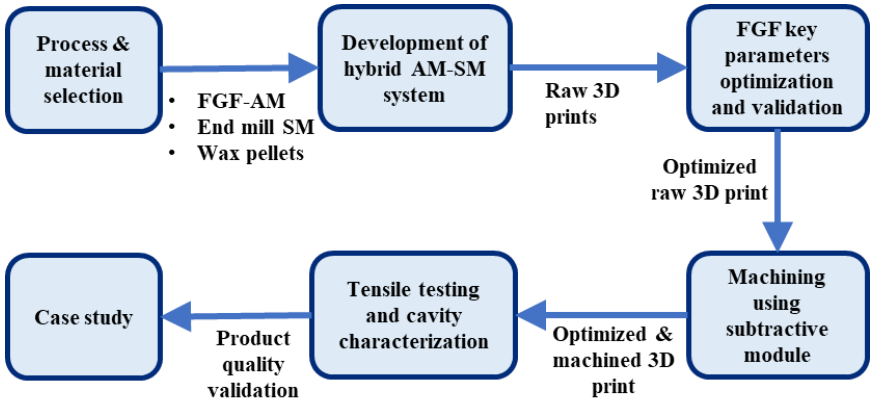


Figure 4-1. Flow chart of the followed methodology

### 4.1.1 Pellets material

Wax is preferred for sacrificial patterns due to its lower melting point, viscosity, coefficient of thermal expansion, and surface roughness compared to other non-wax thermoplastics used in additive manufacturing. These properties ease burnout during pattern removal [169], reducing casting defects, improving metal casting surface quality [170], and supporting environmental sustainability through wax reuse. Additionally, the lower melting point of wax, compared to thermoplastics like PLA, results in significant energy savings during pattern material burnout.

The print head used for pattern fabrication demands the material's physical state to be pellets. This project utilizes proprietary Print-2-Cast (P2C) wax pellets provided by Machinable Wax, USA [171], as showcased in Figure 4-2 (a). Each P2C pellet has a cylindrical geometry with a uniform diameter and height of 3 mm, as shown in the schematic in Figure 4-2 (b). Moreover, it has a precise melting point of 117°C and a specific density (ρ) of 912.38 kg/m$^3$, aligning with the experimental objectives of this research. A few additional material properties, as stated by the manufacturer, are mentioned in Table 4-1.

Table 4-1. Additional properties of the proprietary Print2Cast wax pellets

| Property | Value |
|---|---|
| Hardness (Shore "D" Scale) | 50 |
| Flash point | ~ 302°C |
| Viscosity (η) @ 132°C | 34.4 Pa. s. |
| Residual ash content after burnout | 0.004% |
| Coefficient of thermal expansion | 1.71× 10$^{-4}$ mm/mm °C |
| Volumetric shrinkage | 5 % |

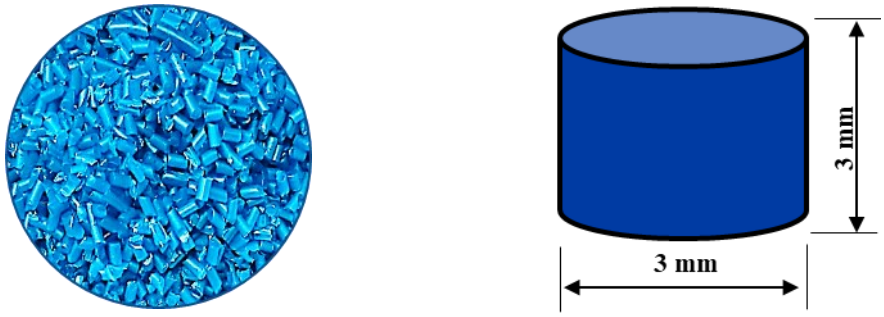


(a) (b)

Figure 4-2. (a) Wax pellets employed for fabricating the sacrificial pattern, and (b) Schematic of the same wax pellet

### 4.1.2 FGF – AM key process parameters

To achieve reliable printability, AM techniques relies on optimizing critical factors like shape retention, inter-layer bonding, bed adhesion, etc. This involves careful examination and adjustment of independent variables (IV), stabilization of fixed variables (FV), and precise control of dependent variables (DV). Table 4-2 characterizes influential printing parameters into these groups.

For this study, the fixed variables are:

- The manufacturer fixes the shape and size of the of wax pellets.
- The bed temperature is maintained at 90 °C per the manufacturer's guidelines [171].
- As shown in Figure 4-3, at 95 °C, die swelling occurred from elevated shear stress, while higher temperatures (~ 110 °C) led to inconsistent diameter and filament breaks due to lower viscosity. At 100 °C, favorable conditions with consistent diameter and continuous flow were observed, prompting the decision to fix the barrel temperature at 100 °C.

Table 4-2. Segregation of influential printing parameters for FGF-AM used in this study

| **Fixed variables (FVs)** | **Independent variables (IVs)** | **Dependent variables (DVs)** |
|---|---|---|
| Type and shape of raw material | Extruder motor speed, $\omega$ (RPM) | Mass flow rate, $\dot{M}$ (kg/hr) |
| Bed temperature (90 °C) | Nozzle size, $d$ (mm) | Extrusion velocity, $V_e$ (mm/sec) |
| Barrel temperature (100 °C) | Layer height, $h$ (mm) | Scanning velocity, $V_{xy}$ (mm/sec) |
| | Overlap percent, $p$ (%) | Bead width, $b$ (mm) |

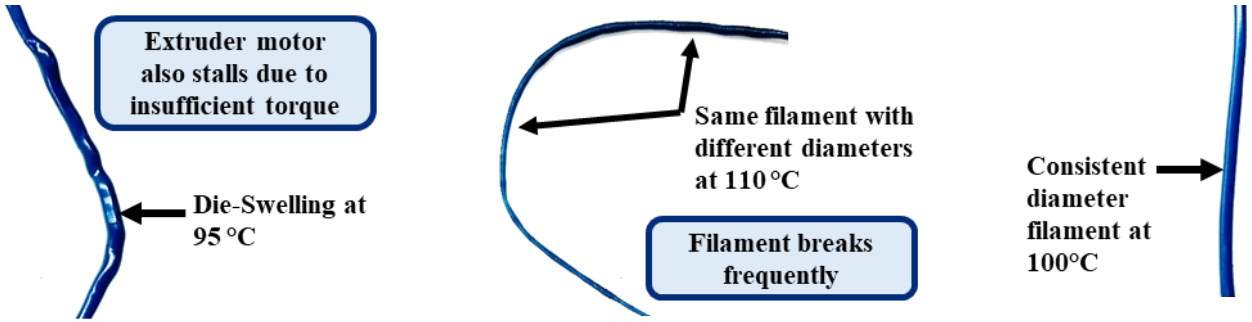


Figure 4-3 (a) Die-swelling due to high viscosity at 95 °C, (b) Inconsistent extrudate due to low viscosity at 110 °C, and (c) Consistent extrudate at 100 °C

Independent variables are the parameters unaffected by other factors. They are varied to observe their impact on dependent or response variables. Independent variables for this study are:

- Extruder motor speed ($\omega$, 0-800 RPM, avoiding >80% capacity).
- Nozzle size ($d$, 3 and 4 mm [128]).
- Layer height ($h$, 2-2.8 mm, proportional to nozzle size).
- Overlap percent ($p$, 0-4% of bead width to prevent inter-bead cavities).

Finally, the dependent variables are:

- The mass flow rate ($\dot{M}$, kg/hr.) of the extrudate relies on extruder motor speed ($\omega$, RPM) (IV), nozzle size ($d$, mm) (IV), and barrel temperature (FV), and its measurement and use are presented in results sections.
- Extrusion velocity ($V_e$, mm/sec) is dependent on the mass flow rate (DV), nozzle size (IV), and the density of the material ($\rho$, kg/m$^3$), as shown in Equation 4.1.
- Scanning velocity is dependent upon layer heights ($h$, mm) (IV), nozzle size (IV), and extrusion velocity (DV) as shown in Equation 4.2 [172] and its calculations and use are shown in results sections.
- Bead width ($b$, mm) depends on independent variables: extruder motor speeds, nozzle sizes, and layer heights. In this study, bead width is measured for all possible combinations of independent variables, as shown in Figure 4-4 and explained in the results section.

$$V_e = \frac{1.112\dot{M}}{\pi d^2 \rho}$$

Equation 4.1. Relation between Extrusion Velocity and Mass flow rate of the extrudate

$$V_{xy} = \frac{V_e}{\left(\frac{4h}{\pi d} + \left(\frac{h}{d}\right)^2\right)}$$

Equation 4.2. Relation between Extrusion and Scanning Velocity

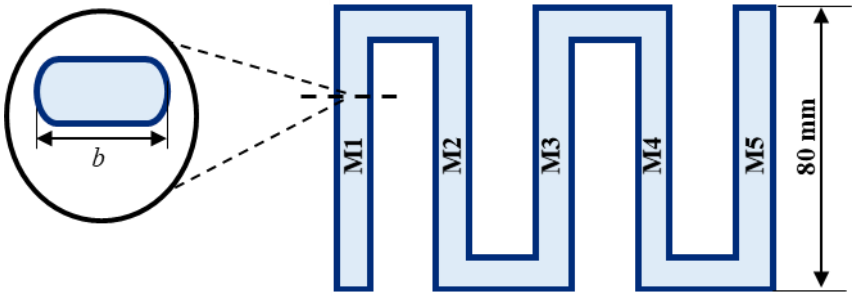


Figure 4-4. Schematic of specimen printed for bead width measurement

### 4.1.3 Design of Experiments (DoE)

In the previous section, four independent variables were selected for this study. To achieve better dimensional tolerance and surface finish and to minimize the need for extensive post-processing, i.e., machining, the selected parameters were optimized using the design of experiments for which the levels and the selected values of these parameters are shown in Table 4-3. The first three continuous parameters allow optimal values anywhere within the specified ranges. At the same time, nozzle size (*d*) is a categorical factor that yields discrete optimal values at the chosen levels. For this study, the objective is to reduce the response variables: stair-stepping depth and the presence of valleys and ridges [44], as shown in Figure 4-5.

Table 4-3. Influential printing parameters with their levels

| Factor Type | Parameters | Level [-1] | Level [0] | Level [+1] |
|---|---|---|---|---|
| **Continuous** | Extruder motor speed ($\omega$, RPM) | 400 | 600 | 800 |
| | Layer height ($h$, mm) | 2.0 | 2.4 | 2.8 |
| | Overlap percent ($p$, %) | 0 | 2 | 4 |
| **Categorial** | | **Level [1]** | | **Level [2]** |
| | Nozzle size ($d$, mm) | 3 | | 4 |

(a) (b)

Figure 4-5. Response variables selected for the DoE (a) Stair-Stepping depth and (b) Valleys & Ridges

The selected specimen for DoE is a cuboid of 60mm in length, with five adjacent beads in four layers, as shown in Figure 4-6. Stair-stepping depth is measured from the sides while valleys and ridges from the top surface using the laser profilometer, (PRO 2 by SICK) [173] with 2 µm resolution. Multiple readings of both response variables were taken at various locations for each specimen to maintain statistical rigor. The central composite design (CCD) DoE approach [174] was chosen as it yields higher-degree polynomial results with fewer experimental runs than other DoE methodologies. Figure

4-7 illustrates the distribution of experimental runs using CCD, which resulted in 34 specimens being printed.

Both response variables were measured for each specimen, and to assess the impact of each individual factor, Analysis of variables (ANOVA) [175] was performed on Minitab software [176]. Printing parameters were optimized using the response optimizer feature. Ultimately, the model was verified by printing multiple specimens using these optimal parameters, measuring their response variables, and comparing them with the Minitab's output.

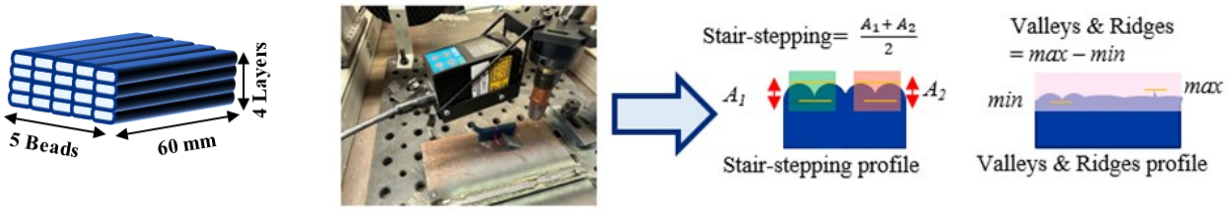


(a) (b)

Figure 4-6. (a) Specimen schematic, and (b) Data collection and acquisition using profilometer

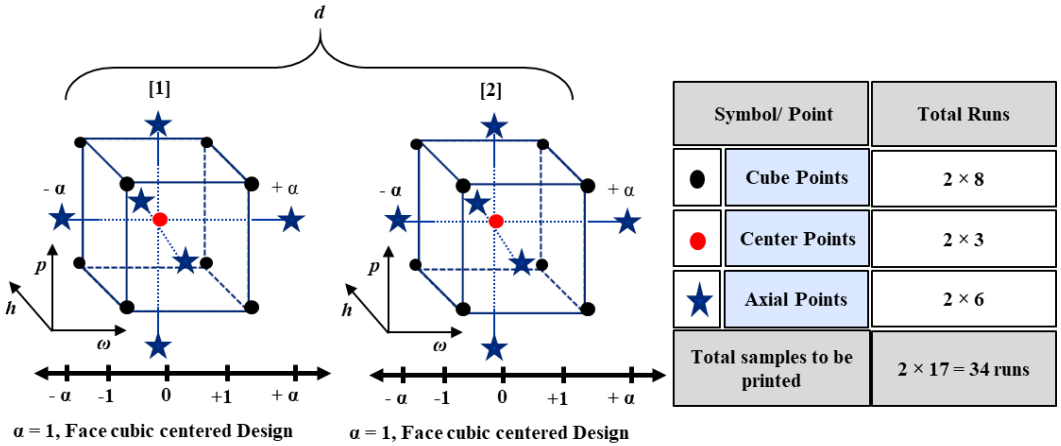


| Symbol/ Point | | Total Runs |
|---|---|---|
| ● | Cube Points | 2 × 8 |
| ● | Center Points | 2 × 3 |
| ★ | Axial Points | 2 × 6 |
| Total samples to be printed | | 2 × 17 = 34 runs |

Figure 4-7. Central Composite Design (CCD) approach applied to the study and the resulted experimental runs

### 4.1.4 Surface roughness and dimensional tolerance measurements

Based on optimal parameters, multiple cuboidal specimens with 40mm × 40mm × 30mm (L × W × H) were printed and machined into smaller cuboids (30mm × 30mm × 25mm) using in-situ end-mill with the process parameters shown in Figure 4-8. These specimens were tested for surface roughness and dimensional tolerance at various locations, and the results were compared with the IC standards. Dimensional measurements were made using a digital caliper with a 0.01 mm resolution and surface roughness was evaluated using a ZEISS CSM-700 confocal laser scanning microscope [177].

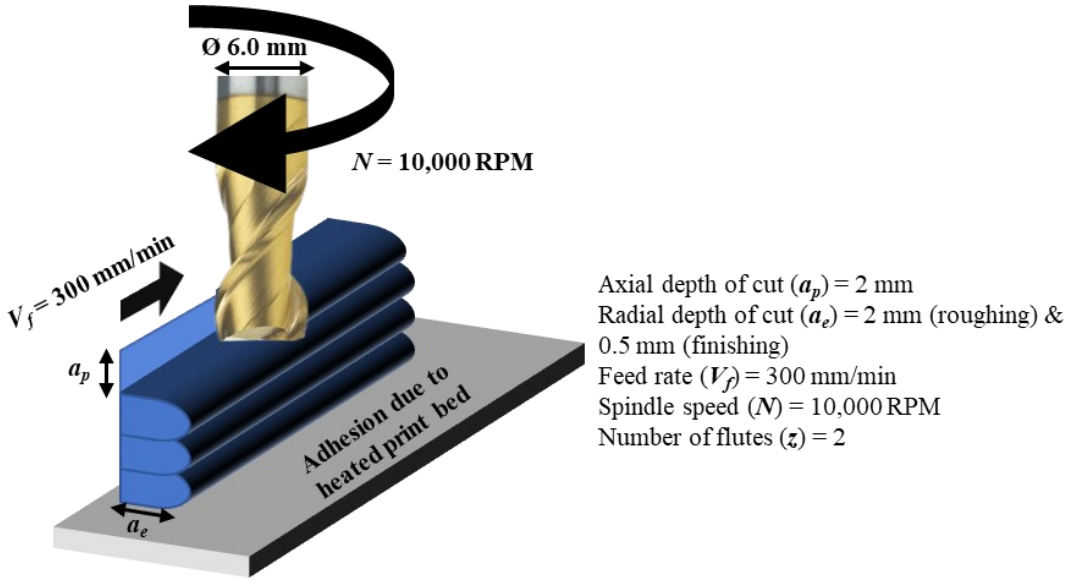


Figure 4-8. CNC machining parameters used for post-processing the 3D printed wax workpiece

### 4.1.5 Tensile testing and cavity characterization

For the strength test, wax dog-bone specimens were produced following ISO 527-2 [178], as shown in Figure 4-9 (a), using optimal parameters. Three plates were printed,

and three specimens were machined from each plate (in workshop) at equidistant locations distributed vertically, as illustrated in Figure 4-9 (b). This design aimed to explore the potential influence of sample location on the mechanical properties, considering microstructure alterations in the wax material. The testing was performed on Instron 3360 series UTS, USA [179]., and the results were assessed. Also, a 10 mm cube was machined from each plate to examine the presence of cavities due to inter-bead voids. The mass and volume of the cubes were measured, and the sample cubes' densities were compared to the material density.

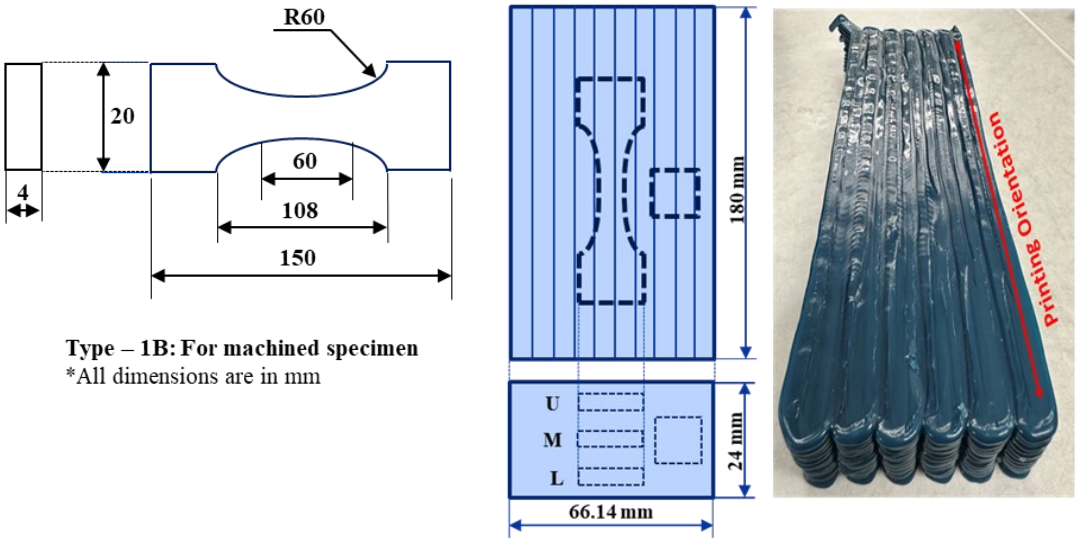


(a) (b)

Figure 4-9. (a) ISO 527-2 dog-bone specimen dimensions and (b) locations of the specimen collected from the printed plate

### 4.2 Results and Discussion

The following subsections present the results obtained from the analyses detailed above.

### 4.2.1 Dependent variables characterization

For printing of the parts, the ratio of scanning and extrusion velocities is an important parameter that influences the quality of the beads. Equation 4.2 gives the required scanning velocity based on the calculated extrusion velocity, which is further dependent upon the mass flow rate, again a dependent variable. For better print quality, the required scanning velocity must be calculated for each combination of independent variables, and it starts with measuring the mass flow rate of the extrudate, which is measured for different RPM and nozzle sizes. For each data point, five measurements were performed for 10 seconds each to establish statistical control and is presented in Figure 4-10 with standard deviations. The results show a linear relationship between mass flow rate and extruder motor speed, indicating reliable results. A significant increase in flow rate is observed with an enlarged nozzle size from 3 to 4 mm, while a peak flow rate of approximately 0.6 kg/hr was achieved at an extruder speed of 800 RPM with a 4 mm nozzle.

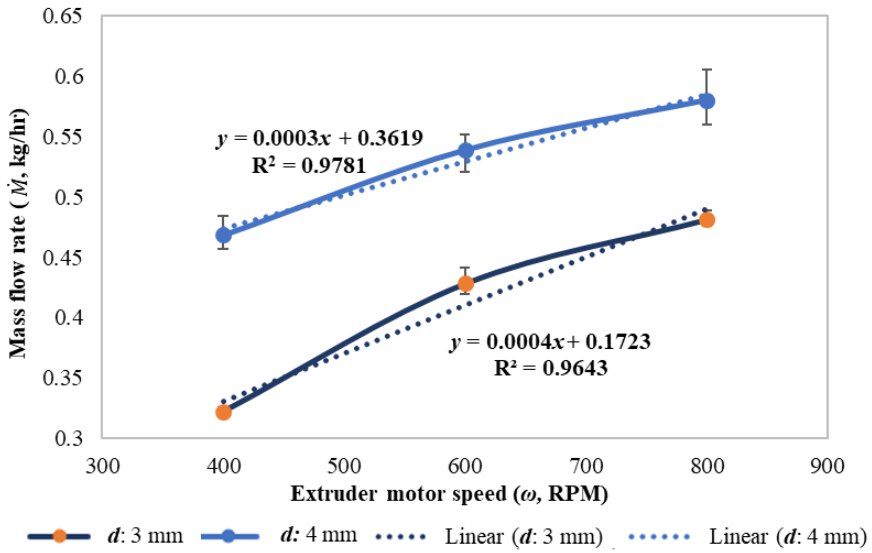


Figure 4-10. Mass flow rate of the extrudate at different motor speed and nozzle sizes with a barrel temperature of 100 °C

Equation 4.1, Equation 4.2, and mass flow rates for each data point were used to calculate the scanning velocity at various combinations of nozzle sizes, layer heights, and extruder motor speeds as shown in Figure 4-11. An upward trend in scanning velocity is observed with increasing layer height and extruder motor speed. The relationship with nozzle size shows distinct behavior, influencing at lower motor speed ranges but diminishing as it approaches higher levels, resulting in near-equivalent scanning velocities.

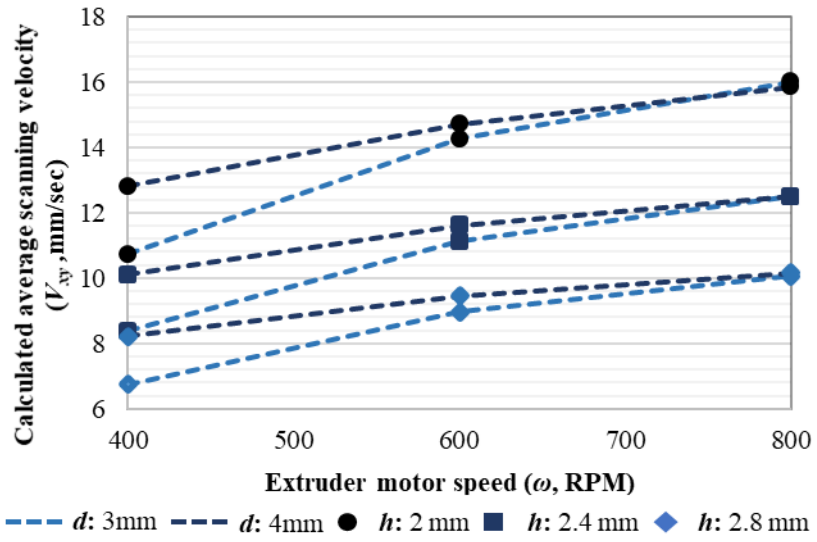


Figure 4-11. Influence of prominent printing parameters on the scanning velocity

Once the respective scanning velocity for all the combinations of independent variables is known, bead width is measured for all possible combinations of independent variables and respective scanning velocity as input. The results are shown in Figure 4-12. Increasing layer height for both nozzle sizes led to wider bead widths, while elevating nozzle size under specific layer heights resulted in reduced bead width. Extruder motor speed, displaying distinctions in average values, showed insignificant differences due to a significant overlap of standard deviations. This trend results from applying the analytical equation for calculating scanning velocity, linked to extrusion velocity (increasing with higher extruder speed) and the *h/d* ratio. This approach mitigates the influence of extruder motor speed on bead width when the *h/d* ratio remains constant.

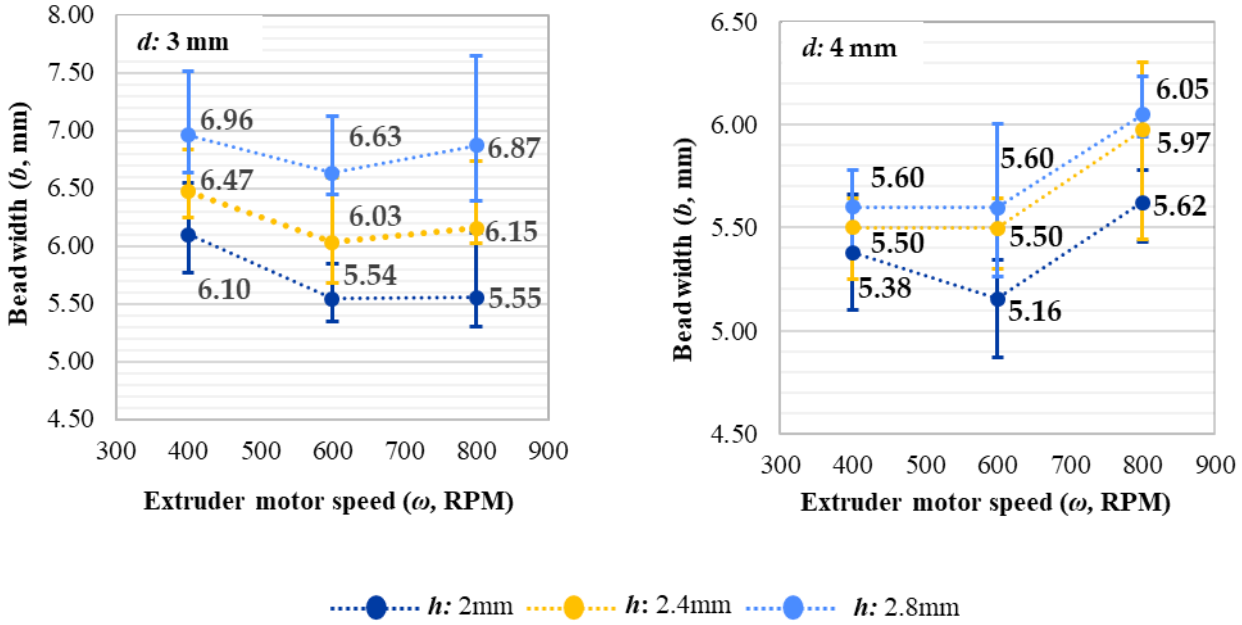


(a) (b)

Figure 4-12. Measured bead widths at pre-defined parameters with nozzle size (a) 3mm, and (b) 4mm

### 4.2.2 Optimization of independent variables

As mentioned earlier, Analysis of variance (ANOVA) was used to investigate the impact of each independent variable on the response variables, shown in Figure 4-13, with the blue solid axis representing the stair-stepping depth and the black dashed axis valleys and ridges. Subplots for continuous factors, like motor speed, reveal a linear relationship with valleys and ridges but a quadratic one with stair-stepping depth. The categorical factor, nozzle size, in the last subplot indicates a decrease in both responses with increased nozzle size, suggesting a preference for a 4 mm nozzle size. The model achieves high R-squared values, reaching 93.39% for stair-stepping depth and 94.25% for valleys and ridges, indicating a substantial attribution of variability to the investigated factors. Figure 4-14 presents Pareto charts for both response variables, visually highlighting the most influential parameters based on the 80/20 rule. Figure 4-14 (a) depicts a chart for stair-stepping depth, where layer height emerges as the most impactful parameter, contributing over 43%. It aligns with findings recommending reduced layer height to mitigate stair-stepping effects [42]. Nozzle size follows, contributing around 20%, and the squared power of extruder motor speed [$\omega^2$] contributes approximately 10%. Referring to Figure 4-14 (b) for valleys and ridges, extruder motor speed holds the most significant influence at 38%, followed by the squared power of overlap percent [$p^2$] at 18%, the interaction between layer height and overlap percent at 16%, and layer height at 14%.

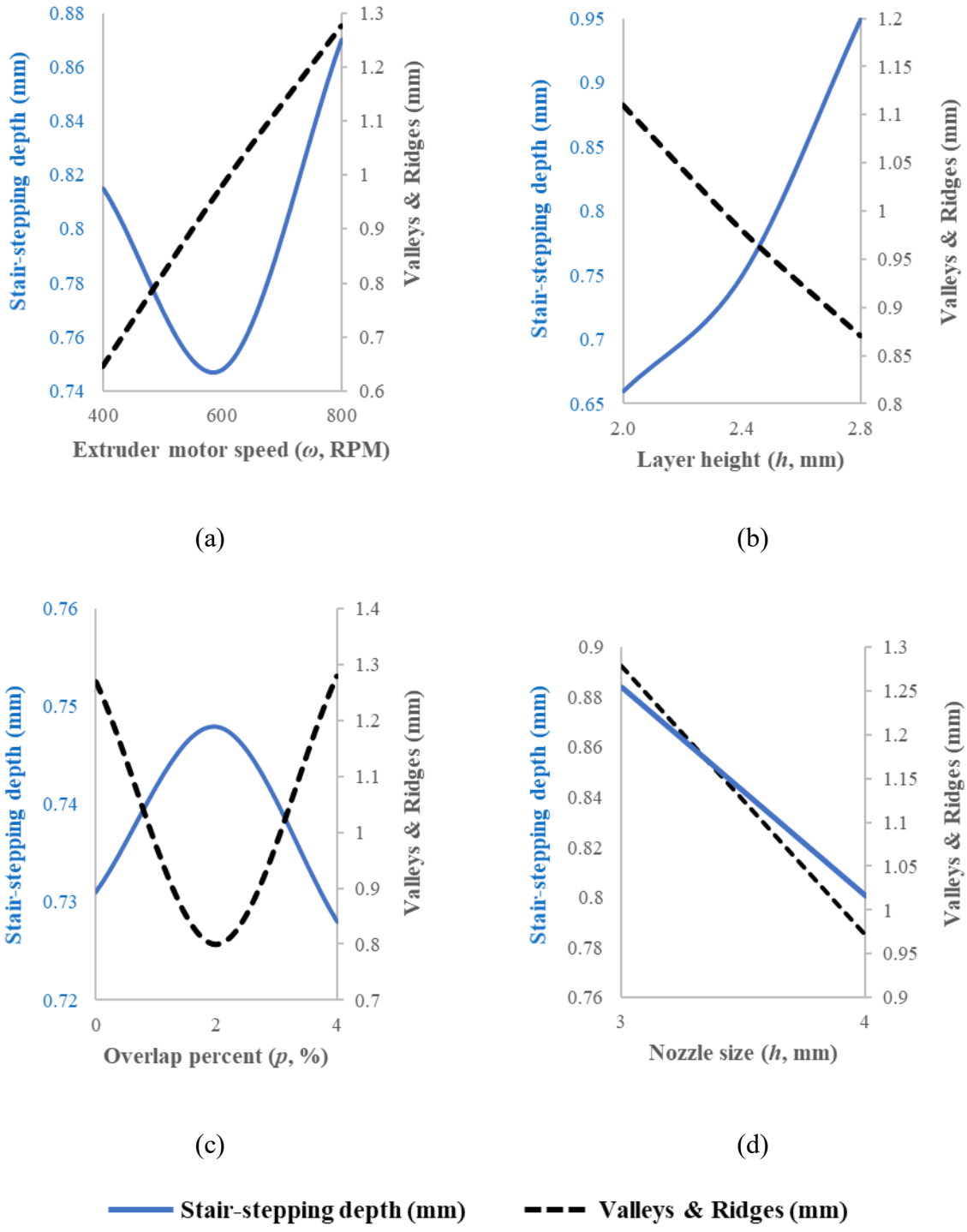


Figure 4-13. Main effect plots for both the response variables with varying (a) Extruder motor speed, (b) Layer height, (c) overlap percent, and (d) Nozzle size

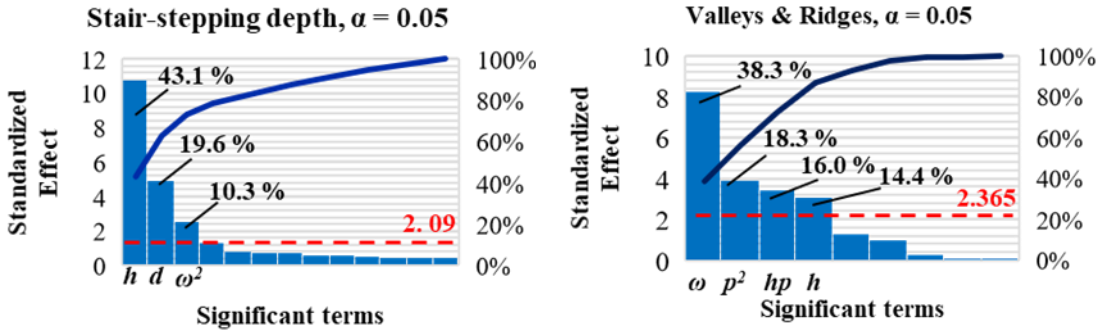


(a) (b)

Figure 4-14. Pareto chart of influential parameters on response variables (a) Stair-Stepping depth, and (b) Ridges and Valleys

The statistical analysis through DOE follows fundamental model assumptions, including normality of residuals and dataset randomization. The former is assessed using a normal probability plot for standardized residuals, shown in Figure 4-15 (a) for stair-stepping depth and Figure 4-16 (a) for valleys and ridges. The absence of residual outliers in both plots validates normality, ensuring robustness for subsequent statistical inferences. The second assumption, regarding random patterns in residuals, is examined through plots of model-fitted values and standardized residuals, illustrated in Figure 4-15 (b) for stair-stepping depth and Figure 4-16 (b) for valleys and ridges. The absence of discernible patterns affirms the model's effective data capture, enhancing overall reliability and robustness. The application of these diagnostic tools significantly strengthens the model's adequacy.

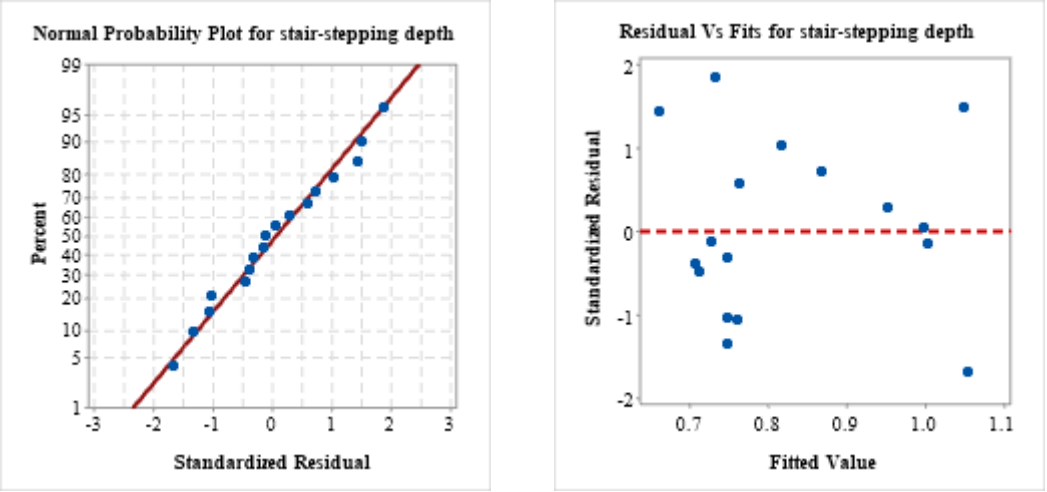


(a) (b)

Figure 4-15. (a) Normal probability plot and (b) residual vs fits plot for the stair-stepping depth

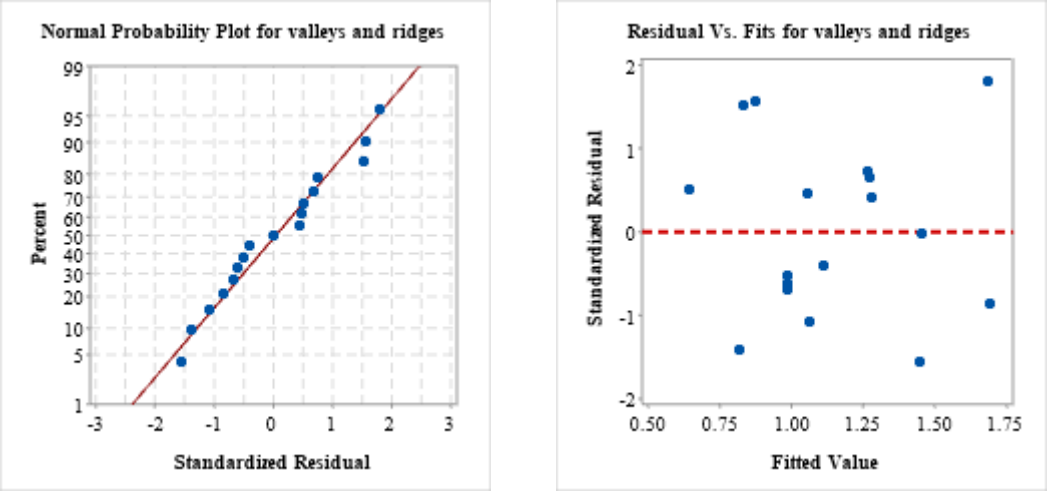


(a) (b)

Figure 4-16. (a) Normal probability plot and (b) residual vs fits for valleys and ridges

The response optimizer feature in Minitab was used to determine optimal printing parameters, minimizing both responses concurrently. The final Optimal parameters are presented in Table 4-4. The model response fit is 0.694 mm for stair-stepping depth and 0.762 mm for valleys and ridges. Three specimens were fabricated with optimal parameters to validate the DoE model, and the collected data showed a mere 3.12% and

0.26% deviation for stair-stepping and valleys and ridges, respectively, when compared to the model-fitted response. The standard deviation range for both observed responses comfortably fell within the 95 percent confidence interval, substantiating the model's validity.

Table 4-4. Optimal printing parameters and model validation.

| **Independent variables** | **Extruder motor speed ($\omega$, RPM)** | **Layer height ($h$, mm)** | **Overlap percent ($p$, %)** | **Nozzle size ($d$, mm)** |
|---|---|---|---|---|
| **Optimal Value** | 420 | 2.0 | 2.8 | 4 |
| **Model Validation** | | | | |
| **Response type** | **Model response fit (mm)** | **Average observed response (mm)** | **Percent deviation (%)** | **95% CI** |
| **Stair-stepping depth** | 0.694 | 0.673 ± 0.011 | 3.12 | (0.597,0.791) |
| **Valleys & Ridges** | 0.762 | 0.760 ± 0.056 | 0.26 | (0.543,0.982) |

### 4.2.3 Dimensional tolerance and surface roughness

Five cuboids were printed at optimal parameters and machined through the developed hybrid system to evaluate the dimensional tolerance and surface roughness, and the results are plotted in Figure 4-17.

For the dimensional tolerance, with a target measurement of 30 mm, each specimen is measured five times in breadth and length, and their mean and standard deviations are calculated and plotted in Figure 4-17 (a). The average reading for all five specimens is

29.96 mm, resulting in an average error of 40 microns. The standard deviation is 170 microns, falling within acceptable IC limits of 50-254 microns [40].

Similarly, the surface roughness of each specimen is measured multiple times at the top and sides, with mean and standard deviation plotted in Figure 4-17 (b). The plot indicates slightly lower surface roughness on the top face than the sides, likely due to different end milling operations—face mill and shoulder mill, respectively. The average surface roughness for the top face is 2.790 ± 0.717 µm Ra and 3.535 ± 0.335 µm Ra for the sides. Both values surpass the 16-20 µm Ra IC range [40], demonstrating geometric compatibility for fabricating wax sacrificial patterns for investment casting.

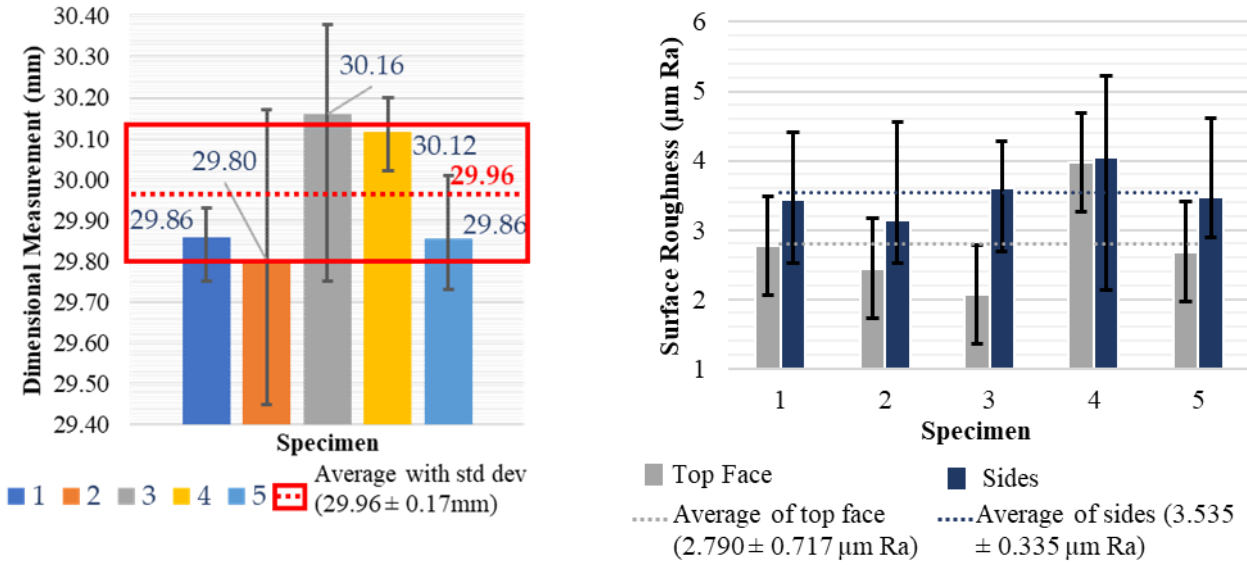


(a) (b)

Figure 4-17. (a) Dimensional tolerance, and (b) Surface roughness of the processed cuboidal specimens

### 4.2.4 Tensile testing and cavity characterization

As explained earlier, the tensile test was performed on nine longitudinal dog-bone specimens extracted from three plates at different vertical heights to assess its potential influence on the material strength due to microstructural changes. Figure 4-18 (a) shows stress-strain curves for all specimens. The first character of the legend indicates specimen location (upper, middle, or lower), and the second denotes the plate number. Analysis of stress-strain plots revealed consistent mechanical behavior and strength across all plate locations.

Young's modulus and ultimate tensile strength were determined following ISO 527 guidelines [178], with the regression method for Young's modulus and considering the maximum stress for ultimate tensile strength. Figure 4-18 (b) shows that upper location specimens exhibited the highest average elastic modulus (405 ± 18 MPa), followed by lower (399 ± 35 MPa) and middle (397 ± 6 MPa). For ultimate tensile strength, the maximum average strength was observed in the lower location specimen (9.31 ± 0.9 MPa), followed by the middle (9.26 ± 0.02 MPa) and upper (9.24 ± 1 MPa). One-way ANOVA ($\alpha$=0.05) revealed no significant difference in mean values among different locations for modulus and strength (p-values of 0.92 and 0.341, respectively). This supports the null hypothesis that all means are equal. Therefore, the overall average modulus for the longitudinally 3D-printed wax specimen is 400 ± 20 MPa, and the overall average tensile strength is 8.9 ± 1 MPa, consistent with findings by Yusof [180].

Porosity in 3D-printed plates was assessed by machining small cubes at random locations (Figure 4-9). Figure 4-19 (a) shows the cube weight and volume details, and were used to compute density. This density was normalized by the wax density, yielding

relative density. Porosity percentage is obtained by subtracting relative density from 100 and is presented in Figure 4-19 (b). The average porosity in the cubes was 0.52% ± 0.1%, indicating the machine's capability to produce objects with total density.

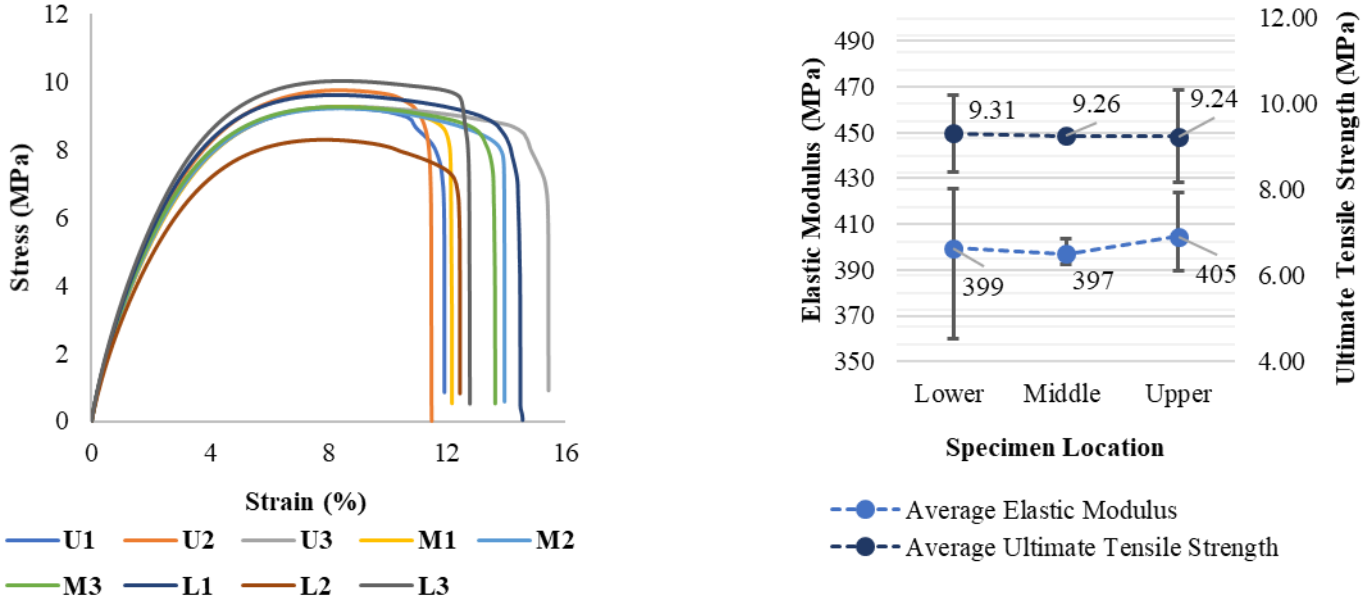


(a) (b)

Figure 4-18. (a) Stress-Strain plots, and (b) Mechanical characterization of dog-bone specimens printed out of wax

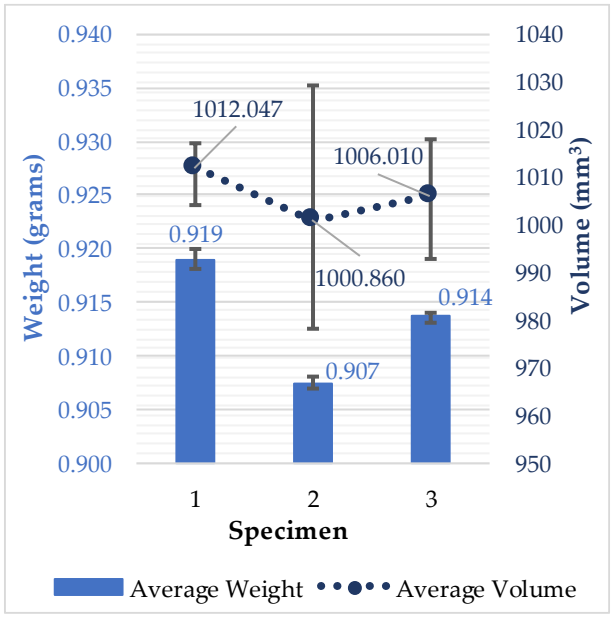


(a)

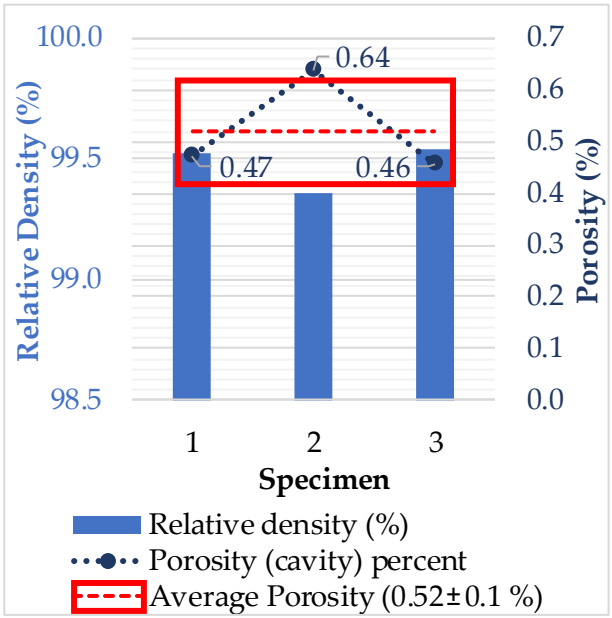


(b)

Figure 4-19. (a) Weight and volume of, and (b) Relative density and porosity observed in the machined and 3D printed cubes

### 4.3 Case-Study – Fabrication of ASME slip-on flange

To assess the industrial and manufacturing capabilities of the developed hybrid manufacturing system (Figure 3-6), a 1½ inch (38.1 mm) slip-on flange was printed using wax, following optimal parameters, and subsequently machined as shown in Figure 4-20. Dimensional tolerance and surface roughness were measured to verify compliance with acceptable limits for IC applications. The 3D scan revealed an average volumetric dimensional deviation of ±170 µm and a surface roughness of 3.7 µm Ra. These values align with those obtained during the experimentation on cubes and fall within the acceptable range for IC applications. The printing process took 35 minutes, with an additional 30 minutes for post-processing. In contrast, producing the same flange with 100% infill through a conventional desktop FDM printer would require 32 hours, emphasizing the substantial reduction in lead time and showcasing the hybrid manufacturing system's effectiveness in producing intricate and precise components for industrial use.

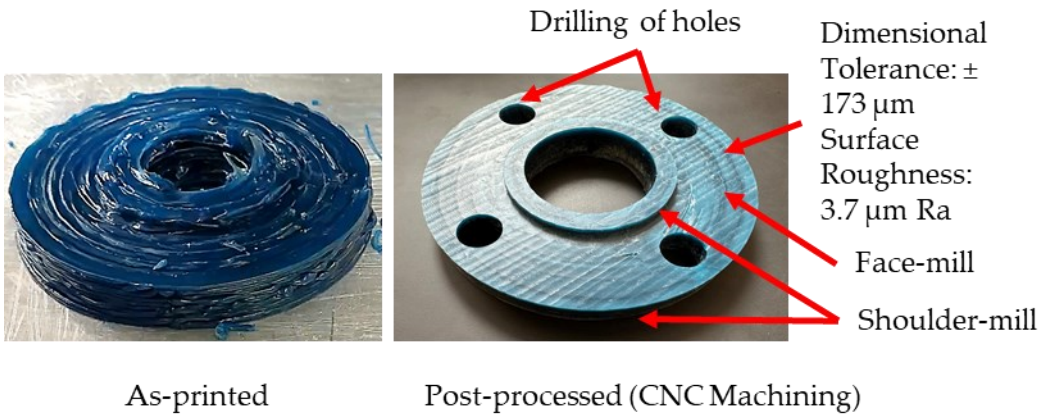


Figure 4-20. Case-Study on the ASME B16.5 Class 150# wax flange fabrication

### 4.4 Results summary and conclusion

To overcome the challenges of scalability, material, and surface quality in existing rapid investment casting, in this work, a large-scale hybrid manufacturing system was built having two modules: an extrusion-based Fused Granular Fabrication-Additive Manufacturing (FGF-AM) module and a CNC machining subtractive module. Wax was selected to be used as a sacrificial pattern material. After optimizing the independent variables, the part was printed on the additive module and machined on the in-situ CNC machining module to enhance the surface quality. The use of hybrid system produced the final product with good results: the pellet screw extruder achieved an optimal throughput of 0.5 kg/hour, DoE minimized the printing defects, and the use on in-situ machining provided an average dimensional accuracy of ±40 µm, precision of ±170 µm, and surface roughness of 3 ± 0.5 µm Ra which are within the IC norms. Printed wax exhibited a tensile strength of 9 MPa and an elastic modulus of 400 MPa in the longitudinal direction with variations in mechanical properties are insignificant along the print volume. Also, the final product exhibited 0.5% porosity, validating the quality of print and ability of the system to produce dense patterns. Finally, the system's hybrid functionality was demonstrated on an industrial-scale case study.

The following are the advantages of the proposed hybrid system over the traditional RIC techniques:

- The novel FGF-AM uses pellets, which eliminates the process of filament fabrication.
- It utilizes wax, which is sustainable and recyclable and has a quicker burnout cycle.

- Pattern production is 10 – 20 times faster than standard AM techniques.
- The total cycle time for investment casting is improved by 50 – 60%.
- In-situ subtractive module enhanced surface quality and dimensional precision.
- It offers digital inventory and twin capabilities, contributing to advanced process monitoring.

# Chapter 5 Fabrication of investment shell through large-scale direct ink writing (DIW) – Extrusion Additive Manufacturing process

This chapter outlines the methodology for fabricating large-scale investment shells using Wasp 3D's continuous feeding system. It integrates direct ink writing, an extrusion additive manufacturing technique, into an in-house developed hybrid manufacturing system (HMS). Similar to the wax methodology in Chapter 4, this chapter focuses on characterizing and optimizing critical printing parameters for red earthenware clay slurry using the design of experiments (DoE). The primary goal is to ensure the buildability and production of large-scale non-porous shells. Material characterization analyzes weight reduction in clay due to water evaporation post-drying (calcination) and its impact on printed specimen metrology.

## 5.1 Material and Methods

This section introduces the slurry material and outlines the methodology for ensuring its printability. It also covers the optimization of printing parameters for fabricating investment shells.

### 5.1.1 Clay material used for printing investment shell

The continuous feeding DIW extrusion system requires high-viscosity slurry as feedstock material. As mentioned in sub-section 2.2.3.1, the choice of investment shell material depends on the casting material, requiring various laboratory tests to avoid undesirable chemical reactions. Since the thesis aims to validate the proposed hybrid manufacturing chain for RIC, the study focuses on using Wasp 3D's proprietary red earthenware clay [181]. Table 5-1 and Table 5-2 detail the material's properties and chemical composition.

Table 5-1 Properties of the proprietary red earthenware clay

| **Property** | **Value** |
|---|---|
| **Density** | 2 g/cm$^3$ |
| **Bisque firing temperature** | 1020 °C |
| **Vitrification temperature** | 920-980 °C |
| **Coefficient of linear expansion** | 78-82 $10^{-7}$ mm/mm |

Table 5-2 Chemical composition of the red earthenware clay

| **Chemical composition** |
|---|
| Aluminum Silicate [clay minerals, kaolinite mixture (1318-47-7), illite (106958-53-6)] |
| Calcium and Magnesium carbonates |
| Quartz [Silica – (14808 – 60 – 7)] |

#### 5.1.1.1 Clay storage

Securing the clay in an air-tight sealed container prevents exposure to air and moisture. Also, the container should be stored in a controlled indoor environment with cool and dry conditions to avoid natural calcination. Failing to do this could affect the slurry's viscosity and cause printing issues, including screw stalling in the print head.

#### 5.1.1.2 Water content in the kneaded clay

A necessary hydration level range should be maintained in the clay to achieve smooth extrusion through the print head and consistent shape retention of the as-printed objects. Deviating from the prescribed hydration range could result in the following challenges:

- Excess moisture reduces the clay's viscosity, leading to issues in shape retention and print failure after a few layers.
- Moisture deficiency increases viscosity, causing resistance in the print head's motor rotation, risking stalling.

An analysis of recently received clay within a perfect hydration level range was performed to measure water absorption. Clay samples were subjected to a 24-hour, 110 °C oven treatment to determine weight percentage loss through calcination. Statistical robustness was ensured by examining five clay samples, measuring each sample's weight before and after calcination using a high-precision digital scale with a $10^{-4}$ grams resolution.

### 5.1.2 Material flow synchronization between the reservoir and print head

The continuous feeding system consists of two subsystems: a reservoir tank and the print head (Figure 3-2). Each subsystem has independent slurry feeding mechanisms. Following the law of conservation of mass, the slurry conveyed to the print head through the reservoir must be extruded at an equivalent deposition rate. Failing to maintain this equilibrium can lead to two scenarios. In the first, excess material may accumulate in the print head if the reservoir's outlet flow exceeds the print head's outlet flow, potentially causing a jam. Conversely, if the print head's deposition rate surpasses a reservoir's, it may lead to starving conditions in the print head, resulting in inconsistent extrudate flow and eventual print failure. In both scenarios, the flow rate from the print head would be reduced compared to the one with the correct synchronization.

An experimental investigation addressed the flow synchronization issue. The print head's mass flow rate was measured at varying screw speeds while maintaining a constant reservoir speed, aiming to find the maximum flow rate. Three different screw speeds were assessed, ensuring that the maximum flow was achieved in the middle level. The extreme levels would tend toward the two scenarios explained above. The screw speed with the maximum flow rate was realized as the synchronized speed for that particular reservoir speed.

### 5.1.3 DIW – AM key process parameters

In Direct Ink Writing (DIW), various printing parameters significantly affect the printed object's material printability and structural integrity. Table 5-3 outlines these critical printing parameters, categorized as independent (IV), fixed (FV), and controlled dependent variables (DV), tailored explicitly for this study's parameters.

Table 5-3 Segregation of influential printing parameters for DIW – AM used in this study

| **Fixed variables (FVs)** | **Independent variables (IVs)** | **Dependent variables (DVs)** |
|---|---|---|
| - Raw material – clay slurry<br>- Layer height, $h$ (2 mm)<br>- Bed temperature (25 °C)<br>- Overlap percent (0 %) | - Print head screw speed in sync. with reservoir speed, $\omega$ (RPM)<br>- Nozzle size, $d$ (mm) | - Mass flow rate, $\dot{M}$ (kg/hr)<br>- Extrusion velocity, $V_e$ (mm/sec)<br>- Scanning velocity, $V_{xy}$ (mm/sec)<br>- Bead width, $b$ (mm) |

For this study, the fixed variables are:

- A propriety clay slurry, used for large-scale shell fabrication.
- The layer height, maintained at 2 mm to match with the optimal layer height for the sacrificial pattern achieved from a separate study in Chapter 4.
- The bed temperature, maintained at 25 °C per the manufacturer's guidelines.
- The overlap percent, maintained at zero percent as it resulted in consistent prints, as shown in Figure 5-1 (a), while a two percent overlap Figure 5-1 (b) resulted in ridges and unevenness. Considering this, zero percent overlap was determined to be optimal and fixed at that value.

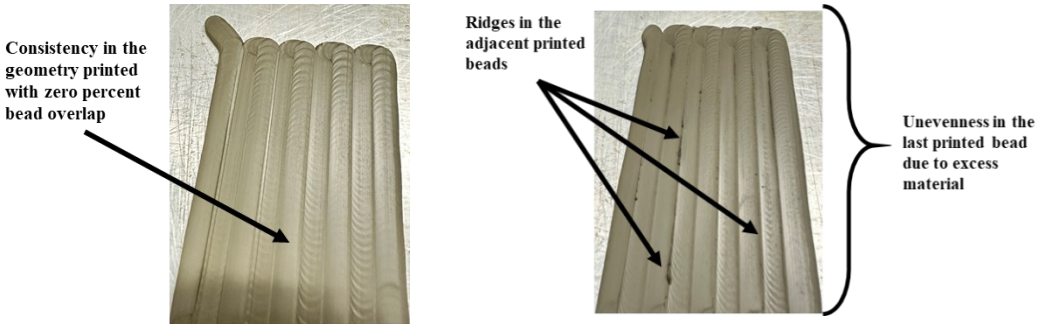


(a) (b)

Figure 5-1. (a) Zero percent overlap, and (b) Two percent overlap with other critical parameters constant for both scenarios.

Independent variables are the parameters unaffected by other factors. They are varied to observe their impact on dependent or response variables. Independent variables for this study are:

- Print head screw speed ranged from 20 – 40 RPM.
- Nozzle size: Two sizes, 6 and 8 mm, were tested as provided by the manufacturer.

The dependent controlled variables for the DIW-AM are same as FGF-AM as showcased in the Chapter 4. Therefore, the same methodology was used here to measure and calculate the dependent variables and are presented in the results section.

### 5.1.4 Design of Experiments (DoE)

In the previous section, two independent variables were selected for this study. Table 5-4 lists both parameters, presenting their respective ranges and levels. The print head screw speed has three equidistant levels, and the nozzle size has two levels, namely 6 and 8 mm. Since the study involves only two parameters, a full-factorial design

approach [182] was used for the DoE as it would have fewer runs. Two replicates were analyzed for each run to reduce the error in the study. Table 5-5 provides an overview of the total number of experimental runs, which resulted in 12 samples being printed.

Table 5-4 Influential printing parameters with their levels for DoE

| **Parameters** | **Level [1]** | **Level [2]** | **Level [3]** |
|---|---|---|---|
| **Print head screw speed (*ω*, RPM)** | 20 | 30 | 40 |
| **Nozzle size (*d*, mm)** | 6 | 8 | N.A. |

Table 5-5 Total DoE runs for the full-factorial design with two replicates

| **Parameters** | **Number of levels** | **Number of replicates** | **Full-factorial total runs** |
|---|---|---|---|
| Print head screw speed (*ω,* RPM) | 3 | 2 | 2 × (3×2) = **12 runs** |
| Nozzle size (*d,* mm) | 2 | | |

Figure 5-2 outlines the DoE methodology, covering sample shape, size, experiment execution, data collection, and analysis. The DoE response variable was the relative density in calcinated specimens, which was aimed to be maximized to acquire fully dense 3D-printed shells. Specimens were printed at all the combinational parameters settings, followed by their weight measurement and 3D scan using the Gen 2 MotionCam – 3D M by Photoneo, Slovakia [183]. After 24-hour calcination at 110 °C, the acquired calcinated samples underwent a second analysis of weight measurements and 3D scans. Relative density was computed using weight and volume data from the CAD model, utilizing the known clay density from manufacturer specifications.

In addition to the DoE analysis, the specimen's post-calcination weight loss and potential shrinkage were documented, which were crucial observations for the investment shell's design phase. Incorporating this data ensures high precision and near-net-shaped metal castings.

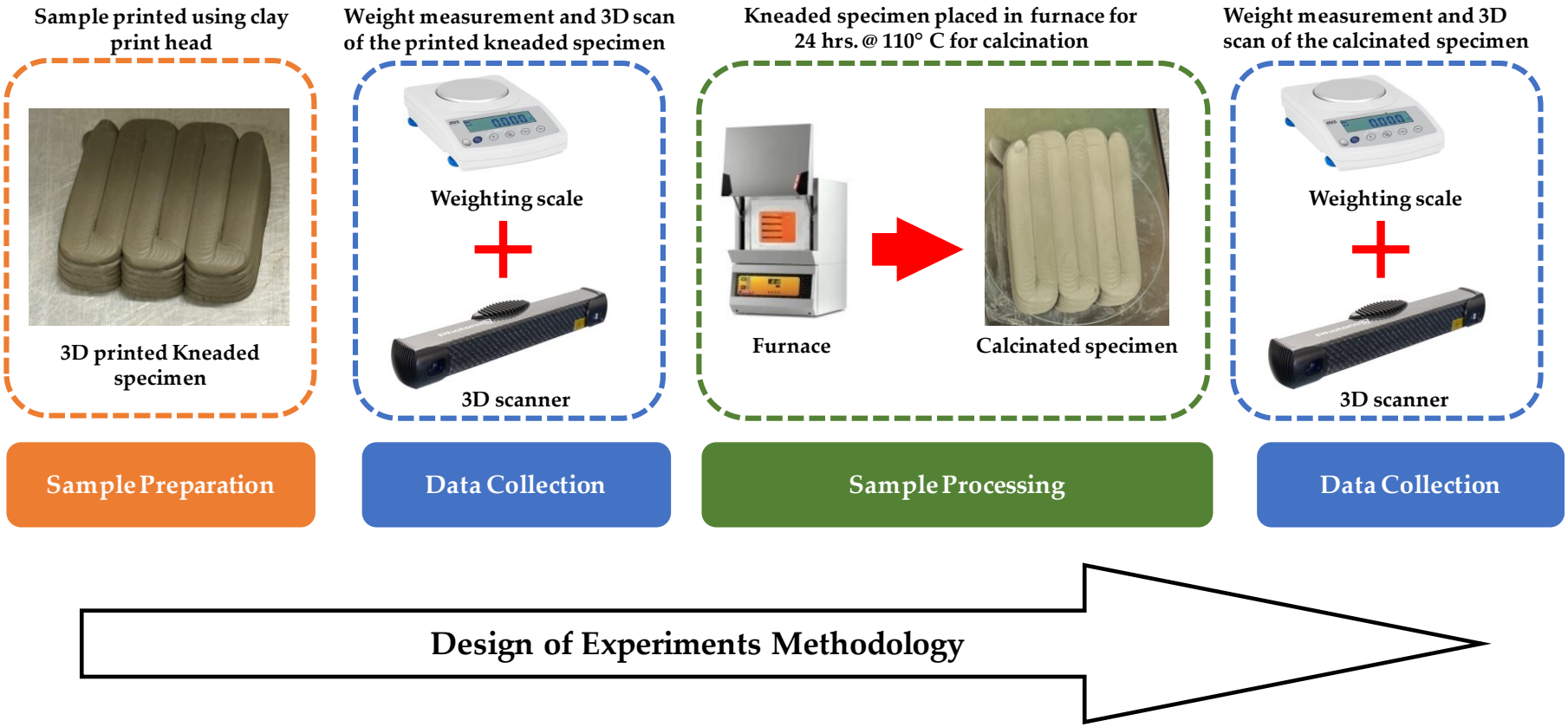


Figure 5-2. Research methodology applied for conducting the design of experiment

## 5.2 Results and Discussion

This section presents the outcomes achieved through the previously explained methodology.

### 5.2.1 Water content in the kneaded clay

Table 5-6 displays clay weight before and after calcination, revealing a 22.9% average reduction in weight with a 1% standard deviation. Reintroducing this water content through re-kneading enables the reuse of the calcinated clay.

Table 5-6 Average weight reduction observed in the red earthenware clay after drying

| | **Weight of Red Earthenware Clay (grams)** | | |
|---|---|---|---|
| **Clay samples** | Before calcination | After calcination | Weight percent reduction (wt.%) |
| **1** | 453 | 351 | 22.43 |
| **2** | 450 | 349 | 22.46 |
| **3** | 456 | 353 | 22.53 |
| **4** | 446 | 347 | 22.20 |
| **5** | 464 | 349 | 24.78 |
| **Average** | 454 | 350 | 22.9 ± 1 % |

### 5.2.2 Material flow synchronization between the reservoir and print head

The analysis determined the maximum flow rate through the print head, synchronizing with a specific reservoir speed. Two reservoir speeds (low and high) were considered with a 4 mm nozzle. Within each reservoir speed, the print head screw speed was varied to achieve the maximum flow rate. Five measurements were taken at each specific setting to maintain statistical robustness. Figure 5-3 (a) illustrates the average flow rates at three print head screw speeds for a lower reservoir speed. A peak flow rate of 1.21 kg/hour was achieved at a print head screw speed of 20 RPM. Deviations from the

optimal 20 RPM confirmed the scenarios in sub-section 5.1.2, resulting in reduced flow rates.

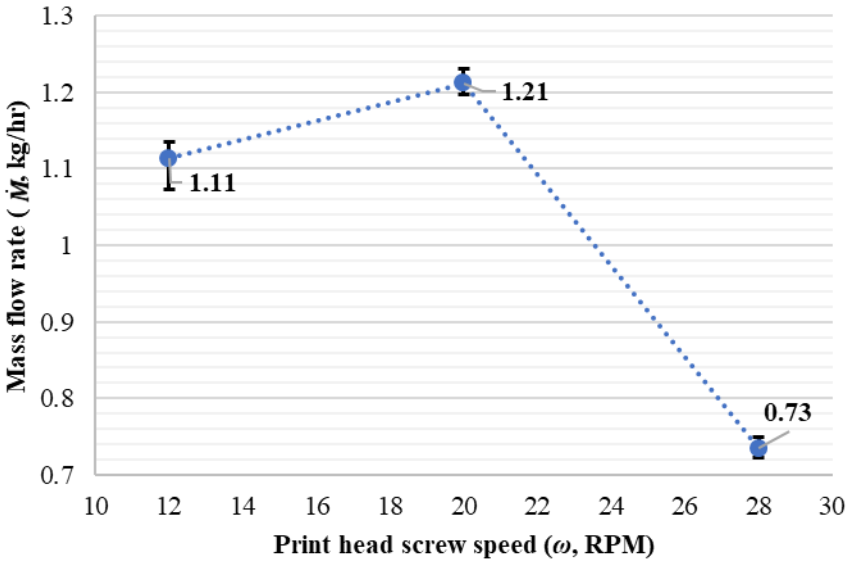


(a)

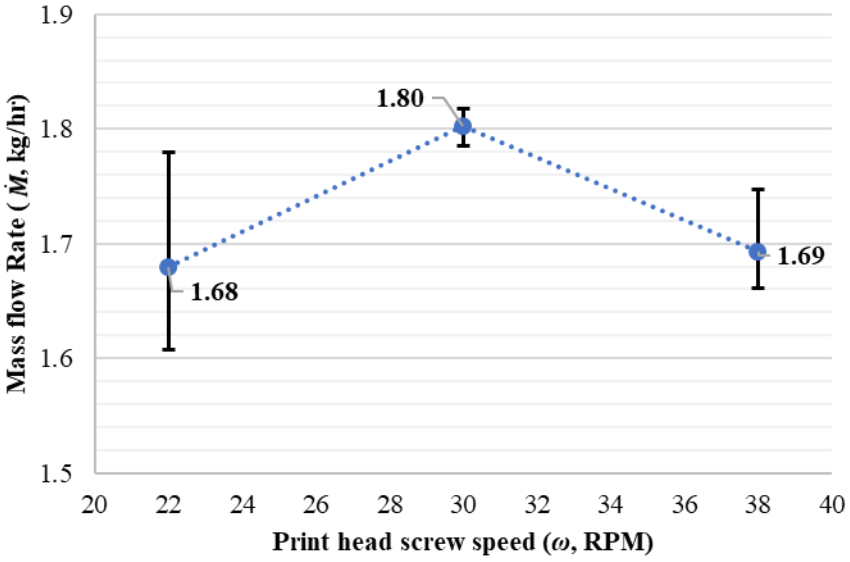


(b)

Figure 5-3. Variation in mass flow rate at different print head screw speed with constant reservoir speed (a) Low reservoir speed, and (b) High reservoir speed

For the higher reservoir speed (1.5 times the low speed), mass flow rates were assessed at 1.5 times the screw speeds used in the lower reservoir speed. The maximum average mass flow rate at high reservoir speed was 1.8 kg/hour at a print head screw speed of 30 RPM, as shown in Figure 5-3 (b). This outcome indicates a linear correlation, suggesting that the flow rate increases with both reservoir and print head screw speeds. In the DoE, where print head screw speed varies from 20-40 RPM, the analysis-derived relation was used to synchronize flow at 40 RPM. Considering that the change in nozzle size would not affect the synchronized speed ratios between the two sub-systems, the same ratios were used for the six and eight-mm nozzles.

### 5.2.3 Dependent variables characterization

Similar to the methodology followed for dependent variable characterization for FGF-AM in Chapter 4, the mass flow rate was measured here by varying the print head screw speed and nozzle sizes, as shown in Figure 5-4. Nozzle size changes (4 to 8 mm) had a negligible impact on the mass flow rate. A significant flow rate increase occurred with an increase in print head screw speed, reaching a maximum average of 2.2 kg/hr with an 8 mm nozzle and 40 RPM print head screw speed.

Scanning velocity was calculated for various nozzle sizes, print head screw speeds, and a 2 mm layer height using Equation 4.1, Equation 4.2, along with mass flow rates from the previous analysis, as shown in Figure 5-5. Increasing print head screw speed requires a corresponding rise in average scanning velocity due to higher mass flow rates. Conversely, a larger nozzle size, at a constant screw speed, reduces the required scanning velocity due to the decrease in extrusion velocity.

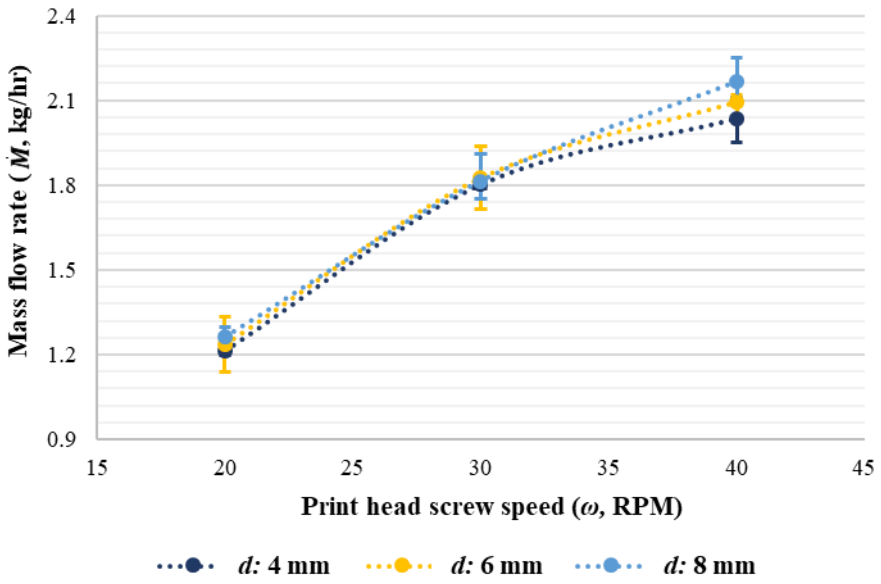


Figure 5-4. Mass flow rate of the extrudate at different print head's screw speed and nozzle sizes

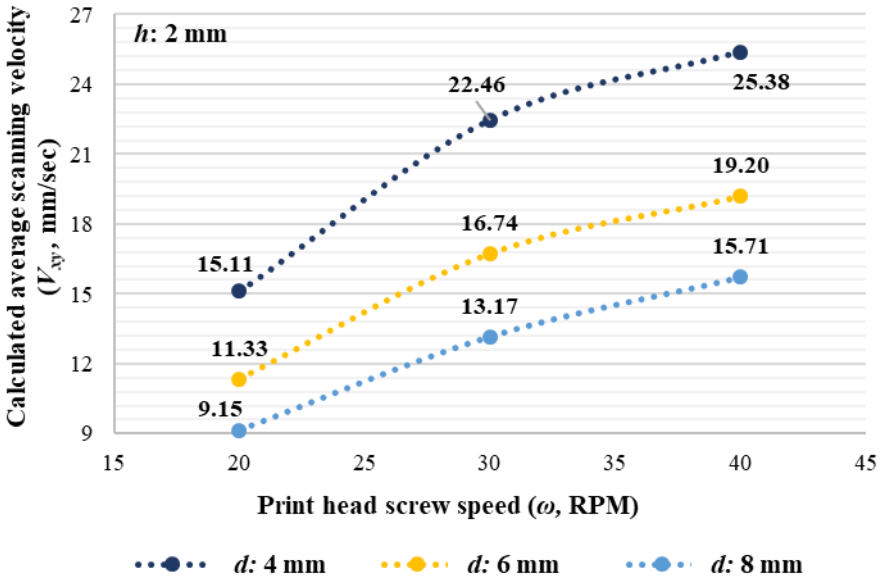


Figure 5-5. Influence of prominent printing parameters on the scanning velocity

After determining the scanning velocity for all independent variable combinations, bead width is measured for each combination, maintaining a 2 mm layer height and

corresponding scanning velocity as input. Figure 5-6 illustrates the trend in bead width variation at print head screw speeds of 20, 30, and 40 RPM and nozzle sizes of 6 and 8 mm. The 4 mm nozzle size was excluded due to poor bed adhesion, likely attributed to a high h/d ratio of 0.5. Observations indicated a positive correlation between print head screw speed and bead width for both nozzle sizes, with larger nozzles resulting in wider beads at constant screw speeds. Five bead width measurements were recorded at each setting to ensure statistical robustness, consistently yielding standard deviations ranging from ±0.03 to ±0.06 mm.

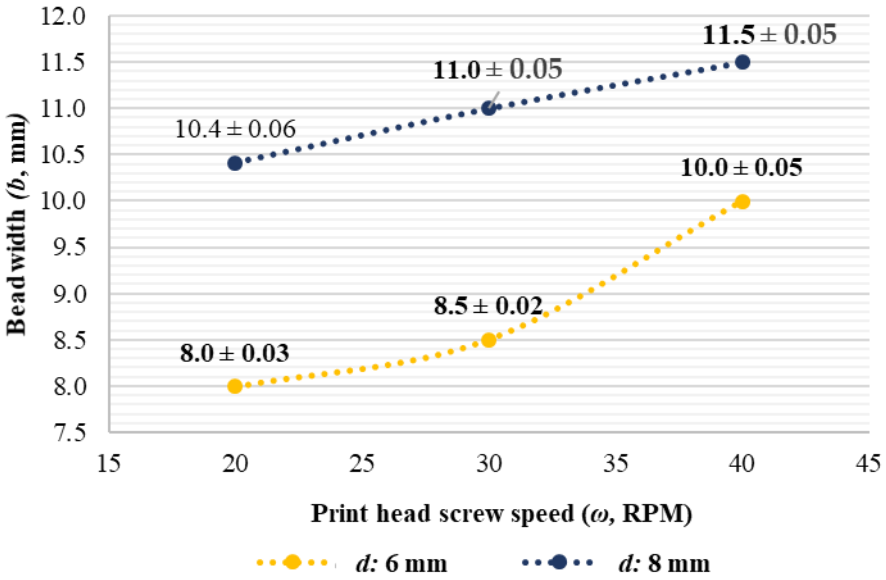


Figure 5-6. Measured bead widths at pre-defined parameters

### 5.2.4 Optimization of independent variables

A full-factorial DoE approach was implemented to optimize printing process parameters, aiming for fully dense investment shells in 3D-printed calcinated clay specimens. Minitab software was used for data analysis. The main effect plots in Figure 5-7 (a) and (b) depict the influence of print head screw speed and nozzle size on relative density. Increasing print head screw speed from 20 to 30 RPM initially increased

relative density, followed by a decline at 40 RPM. No noticeable influence on relative density was observed for nozzle size. The interaction plot in Figure 5-7 (c) highlights the collective impact of both parameters on relative density. Specimens with an 8 mm nozzle exhibited higher relative density up to 30 RPM, followed by a sharp decline. The generated model achieved a high R-squared value of 96.87%, indicating that a large percentage of variability in the response was attributed to the investigated factors.

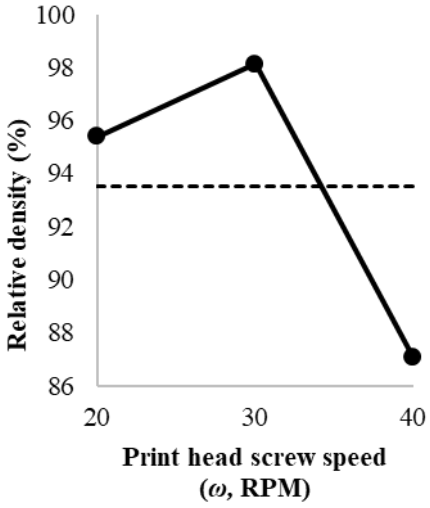


(a)

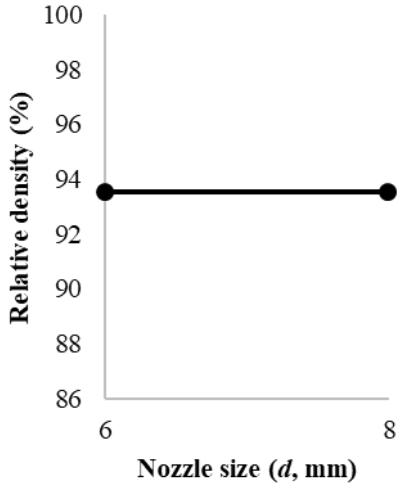


(b)

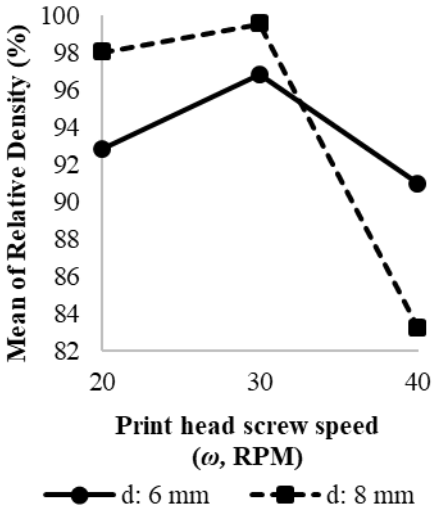


(c)

Figure 5-7. Main effects plot for relative density (%) with varying (a) print head screw speed, (b) Nozzle size, and (c) Interaction plot

Figure 5-8 shows a Pareto chart illustrating the influence of independent variables on relative density. The analysis reveals that print head screw speed has the most substantial impact, contributing 62.6%, followed by the interaction between screw speed and nozzle size at 36.9%. Parameters above the dotted line have a significant influence on the response variable. Notably, nozzle size's 0.5% influence on relative density is insignificant in this context.

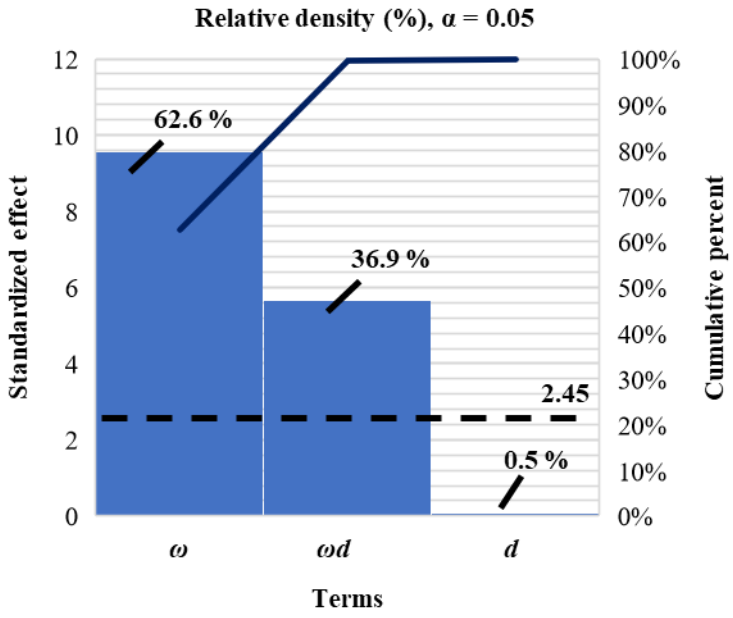


Figure 5-8. Pareto chart of influential parameters on the relative density (%)

The statistical analysis through DOE adheres to fundamental model assumptions, including normality of residuals and randomization within the dataset. Figure 5-9 (a) presents normal probability plots for relative density, confirming the absence of residual outliers and validating the normality assumption. The second assumption, regarding random patterns in residuals, was examined through Figure 5-9 (b), showing

no discernible patterns and affirming the model's effectiveness in capturing data. These diagnostic tools enhance the overall reliability and robustness of the statistical analysis.

Minitab's response optimizer determined optimal printing parameters to maximize relative density within the specified range. Table 5-7 shows that a relative density of 99.5% can be achieved with a print head screw speed of 30 RPM and a nozzle size of 8 mm.

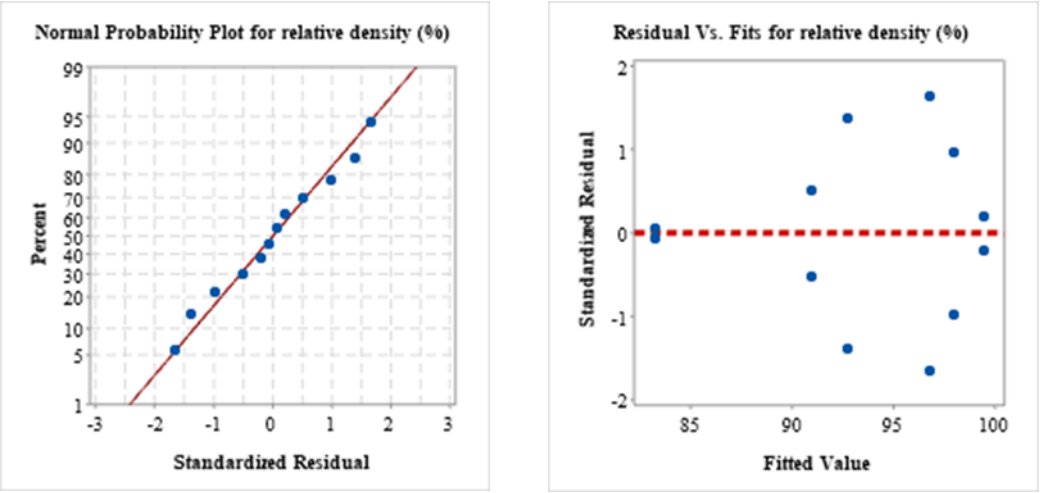


(a) (b)

Figure 5-9. (a) Normal probability plot, and (b) residual vs fits for relative density (%)

Table 5-7. Optimal printing parameters with highest relative density

| **Optimal printing parameters** | **Print head screw speed ($\omega$, RPM)** | **Nozzle size ($d$, mm)** | **Relative density (%) response fit** |
|---|---|---|---|
| **Value** | 30 | 8 | 99.5 |

The research analysis includes determining volumetric shrinkage due to the calcination process. Using 3D scans of the kneaded and calcinated specimens, Table 5-8 displays volumetric shrinkage ranging from 0.64% to 6.06%, with an average of 2.84% in the

optimal parameters. Scaling CAD models up by this percentage enables the production of near-net-shaped investment shells for metal castings.

Table 5-8 Volumetric shrinkage observed in the DoE specimens due to calcination

| **Print head screw speed ($\omega$, RPM)** | **Nozzle size ($d$, mm)** | **Replicate 1 Shrinkage (%)** | **Replicate 2 Shrinkage (%)** | **Average Shrinkage (%)** |
|---|---|---|---|---|
| **20** | **6** | 6.05 | 6.07 | 6.06 |
| **30** | **6** | 6.19 | 5.72 | 5.95 |
| **40** | **6** | 3.06 | 0.55 | 1.81 |
| **20** | **8** | 1.57 | 2.86 | 2.22 |
| **30** | **8** | 2.29 | 3.40 | **2.84** |
| **40** | **8** | 0.61 | 0.67 | 0.64 |

### 5.3 Case-study: Fabrication of large-scale clay complex objects

Figure 5-10 presents a complex clay artifact manufactured using the developed system. The object features intricate twists and turns, affirming the successful execution of slurry extrusion by the print head. The conclusion is that the viscosity of the kneaded clay is adequate for extrusion and layer buildability. Additionally, the object's maintained structural integrity after substantial printed layers suggests that the printed beads exhibit shape retention and sufficient strength to support the weight of subsequent layers.


Figure 5-10. Complex shaped large-scale clay artifact printed at the optimal printing process parameters to check the shape retention

Figure 6 showcases an intricately designed large-scale vase produced to assess the effectiveness of the implemented clay system. The vase's morphology includes challenging overhangs, and it was intentionally printed without support structures to evaluate the material's capacity for shape retention. Successfully printed in the first attempt, the 120 mm-long vase required a total printing time of 15 minutes. Achieving the fabrication of such a complex artifact within this brief duration would be highly challenging through conventional manufacturing processes. This case study effectively demonstrates the competence of the developed in-house DIW–AM system.

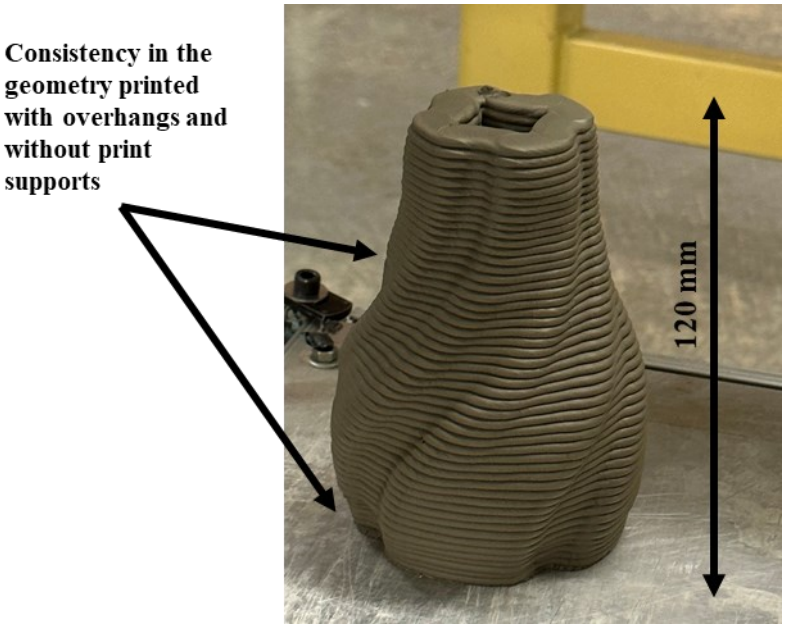


Figure 5-11. 3D printed clay vase with complex geometry and over-hangs printed without needing the support structures

### 5.4 Results summary and conclusion

The research demonstrates the effectiveness of large-scale DIW extrusion-based AM technology in producing investment shells within an in-house hybrid manufacturing system. Successful synchronization of material flow between subsystems enables continuous printing. Red Earthenware clay, chosen as the shell material, undergoes calcination for drying and hardening, with a water content of approximately 22%. Post-calcination volumetric shrinkage is less than 3% under optimal parameters. The primary goal is identifying and optimizing parameters for fully dense shells with a maximum mass flow rate of 2.2 kg/hr. DoE indicates that objects with a relative density of 99.5% can be achieved using the system at optimal parameters.

# Chapter 6 Conclusion and Future Works

This chapter summarizes the conclusive findings of the thesis project, emphasizing potential avenues for future research to enhance the optimization of the developed system and the proposed hybrid manufacturing chain for expedited investment casting processes.

## 6.1 Conclusion

The research project addressed limitations in traditional investment casting, such as prolonged lead times and high costs related to complex tooling for master mold fabrication. A methodology for expediting the process and achieving significant cost savings was proposed by adopting hybrid manufacturing chain for rapid investment casting. This approach eliminates the need for master mold fabrication, streamlining the overall process.

The proposed methodology involves creating a wax sacrificial pattern using a large-scale Fused Granulated Fabrication Additive Manufacturing (FGF – AM) technique. Subsequently, the pattern's surface quality and dimensional tolerance are refined, and stair-stepping effects are eliminated through in-situ CNC machining capabilities. The next phase includes producing the investment shell around the processed sacrificial pattern using a large-scale Direct Ink Writing Additive Manufacturing (DIW-AM) technique. Integrating in-situ capabilities for investment shell fabrication provides a comprehensive solution for manufacturing intricate metal castings with near-net shape properties, offering a cost-effective and time-saving approach.

The following tasks were undertaken to execute the additive-subtractive process:

- A systematic literature review with predefined research questions gathered information on existing additive manufacturing (AM) techniques in investment casting applications, highlighting limitations and potential solutions. It also explored novel AM techniques addressing the research problem.
- A decision matrix with predefined parameters and scenarios was used to select optimal additive modules for producing large-scale sacrificial patterns and investment shells.
- An in-house three-axis hybrid manufacturing system was designed and developed, integrating necessary additive and subtractive modules tailored for investment casting applications.
- Influential printing process parameters for fabricating wax sacrificial patterns and investment shells were identified and optimized using their additive modules.
- Case studies at optimal printing parameters were conducted to assess the capability of the in-house developed hybrid system and estimate potential time and cost savings in investment casting applications.

## 6.2 Future Works

The envisioned future endeavors for the developed hybrid additive-subtractive system include:

- Printing sacrificial pattern and the investment shell together to understand potential limitations and challenges that need to be addressed.
- Establishing in-situ pattern metrology with simultaneous quality control through non-contact metrology techniques.

- Real-time viscosity measurement of the wax material in the pellet-fed screw extruder and vary the barrel temperature accordingly to extrude with consistent viscosity.
- Scaling up the presented work to a robotic system equipped with 8-axis path-planning capabilities, thereby enhancing flexibility and enabling the fabrication of more complex printed objects.

**References**


[1] A. Luo, A.K. Sachdev, B.R. Powell, Advanced casting technologies for lightweight automotive applications, (n.d.). https://www.researchgate.net/publication/287933725 (accessed December 28, 2023).

[2] H. Hu, A. Yu, N. Li, J.E. Allison, Potential Magnesium Alloys for High Temperature Die Cast Automotive Applications: A Review, Materials and Manufacturing Processes 18 (2003) 687–717. https://doi.org/10.1081/AMP-120024970.

[3] K. Haenssgen, A.N. Makanya, V. Djonov, Casting Materials and their Application in Research and Teaching, Microscopy and Microanalysis 20 (2014) 493–513. https://doi.org/10.1017/S1431927613014050.

[4] H. Li, H. Meng, M. Lan, J. Zhou, M. Xu, X. Zhao, B. Xiang, Development of a novel material and casting method for in situ construction on Mars, Powder Technol 390 (2021) 219–229. https://doi.org/10.1016/J.POWTEC.2021.05.054.

[5] Metal Casting Market: Global Industry Trends and Forecast 2023-2028, (n.d.). https://www.imarcgroup.com/metal-casting-market (accessed July 8, 2023).

[6] Casting Process: A Brief Guide by Topgrid - Topgrid, (n.d.). https://www.topgrid.co/casting-process-a-brief-guide-by-topgrid/ (accessed March 5, 2024).

[7] 7 Advantages Of The Metal Casting Process - Faz Foundry, (n.d.). https://fazfoundry.com/advantages-of-metal-casting-process/ (accessed March 5, 2024).

[8] Sheffield Forgemasters announces record-breaking pour, (n.d.). https://www.themanufacturer.com/articles/sheffield-forgemasters-announces-record-breaking-pour/ (accessed November 27, 2023).

[9] Casting Material - an overview | ScienceDirect Topics, (n.d.). https://www.sciencedirect.com/topics/materials-science/casting-material (accessed March 5, 2024).

[10] Minimising Waste In Investment Casting | PI Castings, (n.d.). https://pi-castings.co.uk/minimising-waste-in-investment-casting/ (accessed March 5, 2024).

[11] N. Badanova, A. Perveen, D. Talamona, Study of SLA Printing Parameters Affecting the Dimensional Accuracy of the Pattern and Casting in Rapid Investment Casting, Journal of Manufacturing and Materials Processing 2022, Vol. 6, Page 109 6 (2022) 109. https://doi.org/10.3390/JMMP6050109.

[12] N. Badanova, A. Perveen, D. Talamona, Concise review on Pattern making process in Rapid Investment Casting: Technology, Materials & Numerical modelling aspect, Https://Doi.Org/10.1080/2374068X.2021.1959113 8 (2021) 966–978. https://doi.org/10.1080/2374068X.2021.1959113.

[13] Investment Casting Market Size, Share, Growth, Analysis, 2023-2028, (n.d.). https://www.imarcgroup.com/investment-casting-market (accessed July 8, 2023).

[14] P. Kumar, I.P.S. Ahuja, R. Singh, Application of fusion deposition modelling for rapid investment casting - A review, International Journal of Materials Engineering Innovation 3 (2012) 204–227. https://doi.org/10.1504/IJMATEI.2012.049254.

[15] C.M. Cheah, · C K Chua, · C W Lee, · C Feng, · K Totong, C.W. Lee, K. Totong, Rapid prototyping and tooling techniques: a review of applications for rapid investment casting, (n.d.). https://doi.org/10.1007/s00170-003-1840-6.

[16] S. Ren, K. Bu, S. Mou, R. Zhang, B. Bai, Control of dimensional accuracy of hollow turbine blades during investment casting, J Manuf Process 99 (2023) 548–562. https://doi.org/10.1016/J.JMAPRO.2023.05.077.

[17] S. Norbahiyah, M.M. Haque, Design and development of acrylic die for hip bone joint casting, IFMBE Proc 25 (2009) 207–210. https://doi.org/10.1007/978-3-642-03889-1_56.

[18] M. Koike, T. Okabe, Properties characterization of cast Ti-AI-Cu alloys for dental applications, Medical Device Materials IV: Proceedings of the Materials

and Processes for Medical Devices Conference 2007 (2008) 109–113. https://doi.org/10.1361/CP2007MPMD109.

[19] V. Kumar, S. Mitra, Development in investment casting – A review, Journal of Critical Reviews 7 (2020) 892–897. https://doi.org/10.31838/JCR.07.10.176.

[20] C.K. Chua, C. Feng, C.W. Lee, G.Q. Ang, Rapid investment casting: Direct and indirect approaches via model maker II, International Journal of Advanced Manufacturing Technology 25 (2005) 26–32. https://doi.org/10.1007/S00170-004-1865-5/METRICS.

[21] C. V. Morsiya, S.N. Pandya, Recent Advancements in Hybrid Investment Casting Process—A Review, Lecture Notes in Mechanical Engineering (2022) 817–831. https://doi.org/10.1007/978-981-16-7787-8_65/FIGURES/2.

[22] P. Kumar, I.S. Ahuja, R. Singh, Effect of process parameters on surface roughness of hybrid investment casting, Progress in Additive Manufacturing 1 (2016) 45–53. https://doi.org/10.1007/S40964-016-0004-9/TABLES/6.

[23] P. Jain, A.M. Kuthe, Feasibility Study of Manufacturing Using Rapid Prototyping: FDM Approach, Procedia Eng 63 (2013) 4–11. https://doi.org/10.1016/J.PROENG.2013.08.275.

[24] H.A. Mahrabi, M.R. Jolly, K. Salonitis, Methods of reducing materials' waste and saving energy in investment casting, TMS Annual Meeting 2016-January (2016) 69–76. https://doi.org/10.1007/978-3-319-48166-1_9/COVER.

[25] Refractories - Lung disease, (n.d.). https://www.hse.gov.uk/lung-disease/refractories.htm (accessed March 5, 2024).

[26] K. Kanishka, B. Acherjee, Revolutionizing manufacturing: A comprehensive overview of additive manufacturing processes, materials, developments, and challenges, J Manuf Process 107 (2023) 574–619. https://doi.org/10.1016/j.jmapro.2023.10.024.

[27] K. V Wong, A. Hernandez, A Review of Additive Manufacturing, International Scholarly Research Network ISRN Mechanical Engineering 2012 (2012). https://doi.org/10.5402/2012/208760.

[28] M. Kunovjanek, N. Knofius, G. Reiner, Additive manufacturing and supply chains–a systematic review, Production Planning and Control 33 (2022) 1231–1251. https://doi.org/10.1080/09537287.2020.1857874.

[29] T.D. Ngo, A. Kashani, G. Imbalzano, K.T.Q. Nguyen, D. Hui, Additive manufacturing (3D printing): A review of materials, methods, applications and challenges, Compos B Eng 143 (2018) 172–196. https://doi.org/10.1016/J.COMPOSITESB.2018.02.012.

[30] A. Gisario, M. Kazarian, F. Martina, M. Mehrpouya, Metal additive manufacturing in the commercial aviation industry: A review, J Manuf Syst 53 (2019) 124–149. https://doi.org/10.1016/j.jmsy.2019.08.005.

[31] J. Priyadarshini, R.K. Singh, R. Mishra, M. Dora, Application of additive manufacturing for a sustainable healthcare sector: Mapping current research and establishing future research agenda, Technol Forecast Soc Change 194 (2023) 122686. https://doi.org/10.1016/j.techfore.2023.122686.

[32] V. Mohanavel, K.S. Ashraff Ali, K. Ranganathan, J. Allen Jeffrey, M.M. Ravikumar, S. Rajkumar, The roles and applications of additive manufacturing in the aerospace and automobile sector, Mater Today Proc 47 (2021) 405–409. https://doi.org/10.1016/j.matpr.2021.04.596.

[33] M. Kunovjanek, N. Knofius, G. Reiner, Additive manufacturing and supply chains–a systematic review, Production Planning and Control 33 (2022) 1231–1251. https://doi.org/10.1080/09537287.2020.1857874.

[34] The complete history of 3D printing - UltiMaker, (n.d.). https://ultimaker.com/learn/the-complete-history-of-3d-printing/ (accessed January 31, 2024).

[35] Additive Manufacturing Market Size Report, 2030, (n.d.). https://www.grandviewresearch.com/industry-analysis/additive-manufacturing-market (accessed July 8, 2023).

[36] J. Hengsteler, B. Mandal, C. Van Nisselroy, G.P.S. Lau, T. Schlotter, T. Zambelli, D. Momotenko, Bringing Electrochemical Three-Dimensional

Printing to the Nanoscale, Nano Lett 21 (2021) 9093–9101. https://doi.org/10.1021/ACS.NANOLETT.1C02847.

[37] A. Salandin, A. Quintana-Gallardo, V. Gómez-Lozano, I. Guillén-Guillamón, The First 3D-Printed Building in Spain: A Study on Its Acoustic, Thermal and Environmental Performance, Sustainability (Switzerland) 14 (2022). https://doi.org/10.3390/SU142013204.

[38] A. V. Ripetskiy, G.K. Khotina, O. V. Arkhipova, The role of additive manufacturing in the investment casting process, E3S Web of Conferences 413 (2023) 04015. https://doi.org/10.1051/e3sconf/202341304015.

[39] C.T. Richard, T.H. Kwok, Rapid investment casting: Design and manufacturing technologies, Proceedings of the ASME Design Engineering Technical Conference 1 (2019) 2019. https://doi.org/10.1115/DETC2019-97554.

[40] C.W. Lee, C.K. Chua, C.M. Cheah, L.H. Tan, C. Feng, Rapid investment casting: Direct and indirect approaches via fused deposition modelling, International Journal of Advanced Manufacturing Technology 23 (2004) 93–101. https://doi.org/10.1007/S00170-003-1694-Y/TABLES/7.

[41] A. Nigam, B.L. Tai, Investigation of In-Situ Surface Polishing for Fused Filament Fabrication, ASME 2020 15th International Manufacturing Science and Engineering Conference, MSEC 2020 1 (2021). https://doi.org/10.1115/MSEC2020-8445.

[42] F. Wang, H. Bian, F. Wang, al -, E. Rosenblum, P. Garaud, A. Traxler, A. Mishra, V. Srivastava, N. Kumar Gupta -, R. Dharma Bintara, D. Zakariya Lubis, Y. Rohmat Aji Pradana, The effect of layer height on the surface roughness in 3D Printed Polylactic Acid (PLA) using FDM 3D printing, IOP Conf Ser Mater Sci Eng 1034 (2021) 012096. https://doi.org/10.1088/1757-899X/1034/1/012096.

[43] V.K. Tiwary, P. Arunkumar, A.S. Deshpande, N. Rangaswamy, Surface enhancement of FDM patterns to be used in rapid investment casting for making medical implants, Rapid Prototyp J 25 (2019) 904–914. https://doi.org/10.1108/RPJ-07-2018-0176/FULL/PDF.

[44] A.N.M.A. TOMAL, T. Saleh, Md.R. Khan, COMBINING FUSED DEPOSITION MODELLING WITH ABRASIVE MILLING TO ATTAIN HIGHER DIMENSIONAL ACCURACY AND BETTER SURFACE FINISH ON THE FINISHED PRODUCT, IIUM Engineering Journal 19 (2018) 221–231. https://doi.org/10.31436/iiumej.v19i2.960.

[45] S. Singh, P. Kumar, J. Singh, An approach to eliminate shell cracking problem in fused deposition modeling pattern based investment casting process, IOP Conf Ser Mater Sci Eng 1091 (2021) 012035. https://doi.org/10.1088/1757-899X/1091/1/012035.

[46] W.L. Yao, M.C. Leu, Analysis of shell cracking in investment casting with laser stereolithography patterns, Rapid Prototyp J 5 (1999) 12–20. https://doi.org/10.1108/13552549910251837/FULL/PDF.

[47] M.S. Alsoufi, A.E. Elsayed, Surface Roughness Quality and Dimensional Accuracy—A Comprehensive Analysis of 100% Infill Printed Parts Fabricated by a Personal/Desktop Cost-Effective FDM 3D Printer, Materials Sciences and Applications 09 (2018) 11–40. https://doi.org/10.4236/MSA.2018.91002.

[48] G. Ćwikła, C. Grabowik, K. Kalinowski, I. Paprocka, P. Ociepka, The influence of printing parameters on selected mechanical properties of FDM/FFF 3D-printed parts, IOP Conf Ser Mater Sci Eng 227 (2017) 012033. https://doi.org/10.1088/1757-899X/227/1/012033.

[49] Additive Manufacturing History: From the 1980's to Now, (n.d.). https://markforged.com/resources/blog/additive-manufacturing-history (accessed December 5, 2023).

[50] Greenbaum: Direct investment casting of rapid prototype... - Google Scholar, (n.d.). https://scholar.google.com/scholar_lookup?journal=Proceedings+of+the+2nd+European+Conference+on+Rapid+Prototyping&title=Direct+investment+casting+of+rapid+prototype+parts:+Practical+commercial+experience&author=P.Y.+Greenbaum&author=S.+Khan&pages=77-93& (accessed December 5, 2023).

[51] PRISMA, (n.d.). http://www.prisma-statement.org/ (accessed December 5, 2023).

[52] N. Carl, M.A. Woodley of Menie, A scientometric analysis of controversies in the field of intelligence research, Intelligence 77 (2019) 101397. https://doi.org/10.1016/J.INTELL.2019.101397.

[53] D. Millenaar, T. Fehlmann, S. Scholz, V. Pavlicek, A. Flohr, M. Dillmann, M. Böhm, A. Keller, F. Mahfoud, C. Ukena, Research in Atrial Fibrillation: A Scientometric Analysis Using the Novel Web Application SciPE, JACC Clin Electrophysiol 6 (2020) 1008–1018. https://doi.org/10.1016/J.JACEP.2020.05.010.

[54] Y. V. Granovsky, Is It Possible to Measure Science? V. V. Nalimov's Research in Scientometrics, Scientometrics 52 (2004) 127–150. https://doi.org/10.1023/A:1017991017982.

[55] J.J. Jackson, B.W. Roberts, Conscientiousness, 1 (2015). https://doi.org/10.1093/OXFORDHB/9780199352487.013.18.

[56] O.T. Oladinrin, M. Arif, M.Q. Rana, L. Gyoh, Interrelations between construction ethics and innovation: a bibliometric analysis using VOSviewer, Construction Innovation 23 (2023) 505–523. https://doi.org/10.1108/CI-07-2021-0130/FULL/PDF.

[57] D. Ahlers, F. Wasserfall, N. Hendrich, J. Zhang, 3D printing of nonplanar layers for smooth surface generation, IEEE International Conference on Automation Science and Engineering 2019-August (2019) 1737–1743. https://doi.org/10.1109/COASE.2019.8843116.

[58] S. Chen, W.S. Tan, M.A. Bin Juhari, Q. Shi, X.S. Cheng, W.L. Chan, J. Song, Freeform 3D printing of soft matters: recent advances in technology for biomedical engineering, Biomed Eng Lett 10 (2020) 453–479. https://doi.org/10.1007/S13534-020-00171-8/FIGURES/10.

[59] P. Nayyeri, K. Zareinia, H. Bougherara, Planar and nonplanar slicing algorithms for fused deposition modeling technology: a critical review, International Journal

of Advanced Manufacturing Technology 119 (2022) 2785–2810. https://doi.org/10.1007/S00170-021-08347-X/FIGURES/12.

[60] H. Lee, T.S. Jang, G. Han, H.W. Kim, H. Do Jung, Freeform 3D printing of vascularized tissues: Challenges and strategies, J Tissue Eng 12 (2021). https://doi.org/10.1177/20417314211057236/ASSET/IMAGES/LARGE/10.1177_20417314211057236-FIG9.JPEG.

[61] W.S. Tan, M.A. Bin Juhari, Q. Shi, S. Chen, D. Campolo, J. Song, Development of a new additive manufacturing platform for direct freeform 3D printing of intrinsically curved flexible membranes, Addit Manuf 36 (2020) 101563. https://doi.org/10.1016/J.ADDMA.2020.101563.

[62] ISO - ISO/ASTM 52900:2021 - Additive manufacturing — General principles — Fundamentals and vocabulary, (2021). https://www.iso.org/standard/74514.html (accessed July 7, 2022).

[63] Z. fa Zhang, L. Wang, L. tao Zhang, P. fei Ma, B. heng Lu, C. wei Du, Binder jetting 3D printing process optimization for rapid casting of green parts with high tensile strength, China Foundry 18 (2021) 335–343. https://doi.org/10.1007/S41230-021-1057-Z.

[64] R. Păcurar, P. Berce, O. Nemeş, D.I. Băilă, D.S. Stan, A. Oarcea, F. Popişter, C.M. Borzan, S. Maricic, S. Legutko, A. Păcurar, Cast iron parts obtained in ceramic molds produced by binder jetting 3D printing—morphological and mechanical characterization, Materials 14 (2021). https://doi.org/10.3390/MA14164502.

[65] W. Zhao, W. Liu, J. Chang, Q. Wei, J. Wu, C. Ye, Properties comparison of pure Al2O3 and doped Al2O3 ceramic cores fabricated by binder jetting additive manufacturing, Ceram Int (2023). https://doi.org/10.1016/J.CERAMINT.2023.10.006.

[66] R. Hamano, Y. Nakagawa, V. Irawan, T. Ikoma, Mechanical anisotropy and fracture mode of binder jetting 3D printed calcium sulfate moldings, Appl Mater Today 25 (2021). https://doi.org/10.1016/J.APMT.2021.101160.

[67] R. Shanthar, K. Chen, C. Abeykoon, Powder-Based Additive Manufacturing: A Critical Review of Materials, Methods, Opportunities, and Challenges, Adv Eng Mater 25 (2023). https://doi.org/10.1002/ADEM.202300375.

[68] L. Giorleo, E. Varlik, L. Montesano, A. Pola, Burnout treatment on plaster mould produced with binder jetting technology: effect of process parameters and geometrical complexity, International Journal of Advanced Manufacturing Technology 124 (2023) 2769–2780. https://doi.org/10.1007/S00170-022-10700-7.

[69] D. Svetlizky, B. Zheng, A. Vyatskikh, M. Das, S. Bose, A. Bandyopadhyay, J.M. Schoenung, E.J. Lavernia, N. Eliaz, Laser-based directed energy deposition (DED-LB) of advanced materials, Materials Science and Engineering: A 840 (2022) 142967. https://doi.org/10.1016/j.msea.2022.142967.

[70] T. Feldhausen, L. Heinrich, K. Saleeby, A. Burl, B. Post, E. MacDonald, C. Saldana, L. Love, Review of Computer-Aided Manufacturing (CAM) strategies for hybrid directed energy deposition, Addit Manuf 56 (2022) 102900. https://doi.org/10.1016/j.addma.2022.102900.

[71] A. Shah, R. Aliyev, H. Zeidler, S. Krinke, A Review of the Recent Developments and Challenges in Wire Arc Additive Manufacturing (WAAM) Process, Journal of Manufacturing and Materials Processing 7 (2023) 97. https://doi.org/10.3390/jmmp7030097.

[72] J. Hafenecker, D. Bartels, C.M. Kuball, M. Kreß, R. Rothfelder, M. Schmidt, M. Merklein, Hybrid process chains combining metal additive manufacturing and forming – A review, CIRP J Manuf Sci Technol 46 (2023) 98–115. https://doi.org/10.1016/j.cirpj.2023.08.002.

[73] D. Svetlizky, M. Das, B. Zheng, A.L. Vyatskikh, S. Bose, A. Bandyopadhyay, J.M. Schoenung, E.J. Lavernia, N. Eliaz, Directed energy deposition (DED) additive manufacturing: Physical characteristics, defects, challenges and applications, Materials Today 49 (2021) 271–295. https://doi.org/10.1016/j.mattod.2021.03.020.

[74] D.G. Ahn, Directed Energy Deposition (DED) Process: State of the Art, International Journal of Precision Engineering and Manufacturing - Green Technology 8 (2021) 703–742. https://doi.org/10.1007/s40684-020-00302-7.

[75] S.C. Altıparmak, V.A. Yardley, Z. Shi, J. Lin, Extrusion-based additive manufacturing technologies: State of the art and future perspectives, J Manuf Process 83 (2022) 607–636. https://doi.org/10.1016/J.JMAPRO.2022.09.032.

[76] S.B. Balani, S.H. Ghaffar, M. Chougan, E. Pei, E. Şahin, Processes and materials used for direct writing technologies: A review, Results in Engineering 11 (2021). https://doi.org/10.1016/J.RINENG.2021.100257.

[77] A. Patel, M. Taufik, Extrusion-Based Technology in Additive Manufacturing: A Comprehensive Review, Arab J Sci Eng (2022). https://doi.org/10.1007/S13369-022-07539-1.

[78] C. Tosto, M. Bragaglia, F. Nanni, G. Recca, G. Cicala, Fused Filament Fabrication of Alumina/Polymer Filaments for Obtaining Ceramic Parts after Debinding and Sintering Processes, Materials 15 (2022). https://doi.org/10.3390/MA15207399.

[79] Y. Zhao, J. Zhu, W. He, Y. Liu, X. Sang, R. Liu, 3D printing of unsupported multi-scale and large-span ceramic via near-infrared assisted direct ink writing, Nat Commun 14 (2023). https://doi.org/10.1038/S41467-023-38082-8.

[80] J. Zhang, M. Yarahmadi, L. Cabezas, M. Serra, S. Elizalde, J.M. Cabrera, L. Llanes, G. Fargas, Robocasting of dense 8Y zirconia parts: Rheology, printing, and mechanical properties, J Eur Ceram Soc 43 (2023) 2794–2804. https://doi.org/10.1016/J.JEURCERAMSOC.2022.11.042.

[81] C.M.S. Vicente, M. Sardinha, L. Reis, A. Ribeiro, M. Leite, Large-format additive manufacturing of polymer extrusion-based deposition systems: review and applications, Progress in Additive Manufacturing (2023). https://doi.org/10.1007/S40964-023-00397-9.

[82] D. Labus Zlatanovic, J. Hildebrand, J.P. Bergmann, The study of screw extrusion-based additive manufacturing of eco-friendly aliphatic polyketone,

Journal of Materials Research and Technology 25 (2023) 4125–4138. https://doi.org/10.1016/J.JMRT.2023.06.223.

[83] K. Fedorov, C. Ravindran, K. Fayazbakhsh, Effects of process parameters on friability and surface quality in the rapid investment casting process, International Journal of Advanced Manufacturing Technology 125 (2023) 731–742. https://doi.org/10.1007/S00170-022-10777-0.

[84] F. Clemens, F. Sarraf, A. Borzì, A. Neels, A. Hadian, Material extrusion additive manufacturing of advanced ceramics: Towards the production of large components, J Eur Ceram Soc 43 (2023) 2752–2760. https://doi.org/10.1016/J.JEURCERAMSOC.2022.10.019.

[85] N. Gilani, A. Foerster, N.T. Aboulkhair, Material Jetting, in: Springer Handbooks, Springer Science and Business Media Deutschland GmbH, 2023: pp. 371–387. https://doi.org/10.1007/978-3-031-20752-5_23.

[86] L. Giorleo, M. Ravelli, Laser Polishing of Polymer Parts Produced with Material Jetting Technology: Effect of Laser Scan Speed, Overlapping and Loop Cycles, Journal of The Institution of Engineers (India): Series C 104 (2023) 1065–1077. https://doi.org/10.1007/s40032-023-00979-0.

[87] S. Gangwar, P. Saxena, D. Susana Garcia Morales, T. Biermann, R. Lachmayer, Quality analysis of material jetted silicone material for soft robotics application, Mater Lett 355 (2024) Article 135566. https://doi.org/10.1016/j.matlet.2023.135566.

[88] O.M.F. Marwah, S. Sharif, M. Ibrahim, M.H. Idris, Collapsibility studies of MJM acrylate patterns for investment casting, Applied Mechanics and Materials 330 (2013) 839–842. https://doi.org/10.4028/WWW.SCIENTIFIC.NET/AMM.330.839.

[89] O.M.F. Marwah, S. Sharif, M. Ibrahim, E.J. Mohamad, M.H. Idris, Direct rapid prototyping evaluation on multijet and fused deposition modeling patterns for investment casting, Proceedings of the Institution of Mechanical Engineers, Part L: Journal of Materials: Design and Applications 230 (2016) 949–958. https://doi.org/10.1177/1464420715590602.

[90] P. Turek, G. Budzik, J. Sęp, M. Oleksy, J. Józwik, Ł. Przeszłowski, A. Paszkiewicz, Ł. Kochmański, D. Żelechowski, An analysis of the casting polymer mold wear manufactured using polyjet method based on the measurement of the surface topography, Polymers (Basel) 12 (2020) 1–18. https://doi.org/10.3390/POLYM12123029.

[91] P.M. Gopal, V. Kavimani, K. Gupta, D. Marinkovic, Laser-Based Manufacturing of Ceramics: A Review, Micromachines (Basel) 14 (2023). https://doi.org/10.3390/MI14081564.

[92] S. Wei, J. Zhang, L. Zhang, Y. Zhang, B. Song, X. Wang, J. Fan, Q. Liu, Y. Shi, Laser powder bed fusion additive manufacturing of NiTi shape memory alloys: a review, International Journal of Extreme Manufacturing 5 (2023). https://doi.org/10.1088/2631-7990/ACC7D9.

[93] B. Gao, H. Zhao, L. Peng, Z. Sun, A Review of Research Progress in Selective Laser Melting (SLM), Micromachines (Basel) 14 (2023). https://doi.org/10.3390/MI14010057.

[94] T.C. Dzogbewu, D. de Beer, Powder Bed Fusion of Multimaterials, Journal of Manufacturing and Materials Processing 7 (2023). https://doi.org/10.3390/JMMP7010015.

[95] M. Kuntoğlu, E. Salur, E. Canli, A. Aslan, M.K. Gupta, S. Waqar, G.M. Krolczyk, J. Xu, A state of the art on surface morphology of selective laser-melted metallic alloys, International Journal of Advanced Manufacturing Technology 127 (2023) 1103–1142. https://doi.org/10.1007/S00170-023-11534-7.

[96] M.A. Buhairi, F.M. Foudzi, F.I. Jamhari, A.B. Sulong, N.A.M. Radzuan, N. Muhamad, I.F. Mohamed, A.H. Azman, W.S.W. Harun, M.S.H. Al-Furjan, Review on volumetric energy density: influence on morphology and mechanical properties of Ti6Al4V manufactured via laser powder bed fusion, Progress in Additive Manufacturing 8 (2023) 265–283. https://doi.org/10.1007/S40964-022-00328-0.

[97] D.Y. Pimenov, L.F. Berti, G. Pintaude, G.X. Peres, Y. Chaurasia, N. Khanna, K. Giasin, Influence of selective laser melting process parameters on the surface integrity of difficult-to-cut alloys: comprehensive review and future prospects, International Journal of Advanced Manufacturing Technology 127 (2023) 1071–1102. https://doi.org/10.1007/S00170-023-11541-8.

[98] D. Lee, J. Hong, Development of an Adaptive Slicing Algorithm of Laminated Object Manufacturing Based 3D Printing for Freeform Formwork, Buildings 12 (2022) Article 1335. https://doi.org/10.3390/buildings12091335.

[99] S. Kumar, I. Singh, D. Kumar, M.Y. Yahya, S.S. Rahimian Koloor, Mechanical and Morphological Characterizations of Laminated Object Manufactured 3D Printed Biodegradable Poly(lactic)acid with Various Physical Configurations, J Mar Sci Eng 10 (2022) Article 1954. https://doi.org/10.3390/jmse10121954.

[100] D. Olivier, J.A. Travieso-Rodriguez, S. Borros, G. Reyes, R. Jerez-Mesa, Influence of building orientation on the flexural strength of laminated object manufacturing specimens, Journal of Mechanical Science and Technology 31 (2017) 133–139. https://doi.org/10.1007/s12206-016-1212-4.

[101] Y.S. Liao, Y.Y. Chiu, Adaptive crosshatch approach for the laminated object manufacturing (LOM) process, Int J Prod Res 39 (2001) 3479–3490. https://doi.org/10.1080/00207540110060879.

[102] Y.S. Liao, L.C. Chiu, Y.Y. Chiu, A new approach of online waste removal process for laminated object manufacturing (LOM), J Mater Process Technol 140 (2003) 136–140. https://doi.org/10.1016/S0924-0136(03)00690-3.

[103] Y.S. Liao, H.C. Li, Y.Y. Chiu, Study of laminated object manufacturing with separately applied heating and pressing, International Journal of Advanced Manufacturing Technology 27 (2006) 703–707. https://doi.org/10.1007/s00170-004-2201-9.

[104] V. Truxova, J. Safka, M. Seidl, I. Kovalenko, L. Volesky, M. Ackermann, Ceramic 3d printing: Comparison of SLA and DLP technologies, MM Science Journal 2020 (2020) 3905–3911. https://doi.org/10.17973/MMSJ.2020_06_2020006.

[105] J.H. Sim, B.K. Koo, M. Jung, D.S. Kim, Study on Debinding and Sintering Processes for Ceramics Fabricated Using Digital Light Processing (DLP) 3D Printing, Processes 10 (2022). https://doi.org/10.3390/PR10112467.

[106] S.A. Rasaki, D. Xiong, S. Xiong, F. Su, M. Idrees, Z. Chen, Photopolymerization-based additive manufacturing of ceramics: A systematic review, Journal of Advanced Ceramics 10 (2021) 442–471. https://doi.org/10.1007/S40145-021-0468-Z.

[107] M. Mukhtarkhanov, A. Perveen, D. Talamona, Application of stereolithography based 3D printing technology in investment casting, Micromachines (Basel) 11 (2020). https://doi.org/10.3390/MI11100946.

[108] H. Wu, W. Liu, Y. Xu, L. Lin, Y. Li, S. Wu, Vat photopolymerization-based 3D printing of complex-shaped and high-performance Al2O3 ceramic tool with chip-breaking grooves: Cutting performance and wear mechanism, Journal of Asian Ceramic Societies 11 (2023) 159–169. https://doi.org/10.1080/21870764.2023.2168343.

[109] Y. Lu, L. Wang, A.M.O. Dal Piva, J.P.M. Tribst, I. Nedeljkovic, C.J. Kleverlaan, A.J. Feilzer, Influence of surface finishing and printing layer orientation on surface roughness and flexural strength of stereolithography-manufactured dental zirconia, J Mech Behav Biomed Mater 143 (2023). https://doi.org/10.1016/J.JMBBM.2023.105944.

[110] A. Mukhangaliyeva, D. Dairabayeva, A. Perveen, D. Talamona, Optimization of Dimensional Accuracy and Surface Roughness of SLA Patterns and SLA-Based IC Components, Polymers (Basel) 15 (2023). https://doi.org/10.3390/POLYM15204038.

[111] J. Stampfl, M. Schwentenwein, J. Homa, F.B. Prinz, Lithography-based additive manufacturing of ceramics: Materials, applications and perspectives, MRS Commun 13 (2023) 786–794. https://doi.org/10.1557/S43579-023-00444-0.

[112] S. Negi, P. Bhargava, P. Gandhi, Investigation of processing the alumina slurry through an economic vat photopolymerization process, Open Ceramics 15 (2023). https://doi.org/10.1016/J.OCERAM.2023.100400.

[113] P. Arora, K.G. Mostafa, E. Russell, S. Dehgahi, S.U. Butt, D. Talamona, A.J. Qureshi, Shrinkage Compensation and Effect of Building Orientation on Mechanical Properties of Ceramic Stereolithography Parts, Polymers 2023, Vol. 15, Page 3877 15 (2023) 3877. https://doi.org/10.3390/POLYM15193877.

[114] D.S. Lim, J.K. Chung, J.S. Yun, M.S. Park, Fabrication of 3D Printed Ceramic Part Using Photo-Polymerization Process, Polymers (Basel) 15 (2023). https://doi.org/10.3390/POLYM15071601.

[115] M. De Lisi, C. Shu, U.M. Attia, K. Essa, DLP of Translucent Alumina: In-Depth Investigation on Slurry Development and Debinding Regimes, Machines 11 (2023). https://doi.org/10.3390/MACHINES11030321.

[116] M. Mandolini, M. Sartini, C. Favi, M. Germani, Techno-Economic Analysis for Comparing Stereolithography and Wax Injection for Pattern Manufacturing in Investment Casting, ASME International Mechanical Engineering Congress and Exposition, Proceedings (IMECE) 4 (2023). https://doi.org/10.1115/IMECE2022-96658.

[117] O. Mfm, S. Sharif, M. Busari, Evaluation of Direct Rapid Prototyping Pattern for Investment Casting, (2012). https://doi.org/10.4028/www.scientific.net/AMR.463-464.226.

[118] Q. Liu, G. Sui, M.C. Leu, Experimental study on the ice pattern fabrication for the investment casting by rapid freeze prototyping (RFP), Comput Ind 48 (2002) 181–197. https://doi.org/10.1016/S0166-3615(02)00042-8.

[119] A. Yodice, The Freeze Cast Process, SAE Technical Papers (2000). https://doi.org/10.4271/2000-01-1384.

[120] C. Polzin, S. Spath, H. Seitz, Characterization and evaluation of a PMMA-based 3D printing process, Rapid Prototyp J 19 (2013) 37–43. https://doi.org/10.1108/13552541311292718.

[121] K.D. Dotchev, S.S. Dimov, D.T. Pham, A.I. Ivanov, Accuracy issues in rapid manufacturing CastForm$^{TM}$ patterns, Proc Inst Mech Eng B J Eng Manuf 221 (2007) 53–67. https://doi.org/10.1243/09544054JEM676.

[122] K. Fedorov, K. Fayazbakhsh, C. Ravindran, Surface roughness and dimensional tolerances in A319 alloy samples produced by rapid investment casting process based on fused filament fabrication, International Journal of Advanced Manufacturing Technology 119 (2022) 4423–4437. https://doi.org/10.1007/S00170-021-08644-5/FIGURES/15.

[123] J. Zhu, W. Zhang, X. Gu, On the topology optimization design for the stereolithography based investment casting model, Adv Mat Res 139–141 (2010) 1464–1467. https://doi.org/10.4028/WWW.SCIENTIFIC.NET/AMR.139-141.1464.

[124] P.K. Garg, R. Singh, A. Ips, Multi-objective optimization of dimensional accuracy, surface roughness and hardness of hybrid investment cast components, Rapid Prototyp J 23 (2017) 845–857. https://doi.org/10.1108/RPJ-10-2015-0149/FULL/XML.

[125] Y.P. Shaik, J. Schuster, A. Shaik, Y.P. Shaik, J. Schuster, A. Shaik, A Scientific Review on Various Pellet Extruders Used in 3D Printing FDM Processes, Open Access Library Journal 8 (2021) 1–19. https://doi.org/10.4236/OALIB.1107698.

[126] F. Villano, Exploring Fused Granular Fabrication (FGF) technology : principles, troubleshooting and design considerations, (2023). https://www.politesi.polimi.it/handle/10589/211420 (accessed December 28, 2023).

[127] J.H. Coelho De Brito, F. Jorge, L. Alves, FACULDADE DE ENGENHARIA DA UNIVERSIDADE DO PORTO Design for large-scale additive manufacturing, (n.d.).

[128] J.M. Justino Netto, H.T. Idogava, L.E. Frezzatto Santos, Z. de C. Silveira, P. Romio, J.L. Alves, Screw-assisted 3D printing with granulated materials: a systematic review, International Journal of Advanced Manufacturing Technology 115 (2021) 2711–2727. https://doi.org/10.1007/S00170-021-07365-Z/FIGURES/11.

[129] F. Pignatelli, G. Percoco, An application- and market-oriented review on large format additive manufacturing, focusing on polymer pellet-based 3D printing,

Progress in Additive Manufacturing 7 (2022) 1363–1377. https://doi.org/10.1007/S40964-022-00309-3/FIGURES/10.

[130] L. Fontana, A. Giubilini, R. Arrigo, G. Malucelli, P. Minetola, Characterization of 3D Printed Polylactic Acid by Fused Granular Fabrication through Printing Accuracy, Porosity, Thermal and Mechanical Analyses, Polymers 2022, Vol. 14, Page 3530 14 (2022) 3530. https://doi.org/10.3390/POLYM14173530.

[131] K. Wilczyński, Evaluating Screw Performance in a Single-Screw Extrusion Process, Polym Plast Technol Eng 28 (1989) 671–690. https://doi.org/10.1080/03602558908049822.

[132] A.L. Kelly, E.G. Brown, P.D. Coates, The effect of screw geometry on melt temperature profile in single screw extrusion, Polym Eng Sci 46 (2006) 1706–1714. https://doi.org/10.1002/PEN.20657.

[133] M.F.P. Costa, L. Costa, Optimization of Single Screw Extrusion, (2018) 7–21. http://hdl.handle.net/1822/58517 (accessed May 28, 2022).

[134] F. Previdi, S.M. Savaresi, A. Panarotto, Design of a feedback control system for real-time control of flow in a single-screw extruder, Control Eng Pract 14 (2006) 1111–1121. https://doi.org/10.1016/j.conengprac.2005.06.017.

[135] G.S. Balch, Melting Mechanism in Single Screw Extrusion, n.d.

[136] I.R. Edmondson, R.T. Fenner, Melting of thermoplastics in single screw extruders, Polymer (Guildf) 16 (1975) 49–56. https://doi.org/10.1016/0032-3861(75)90095-6.

[137] A.P.D. Cox, R.T. Fenner, Melting performance in the single screw extrusion of thermoplastics, Polym Eng Sci 20 (1980) 562–571. https://doi.org/10.1002/PEN.760200809.

[138] M. McAfee, G. McNally, Real-time measurement of melt viscosity in single-screw extrusion, Transactions of the Institute of Measurement & Control 28 (2006) 481–497. https://doi.org/10.1177/0142331206069478.

[139] C.M.S. Vicente, M. Sardinha, L. Reis, A. Ribeiro, M. Leite, Large-format additive manufacturing of polymer extrusion-based deposition systems: review and applications, Progress in Additive Manufacturing (2023). https://doi.org/10.1007/S40964-023-00397-9.

[140] J. Kalle, K. Joni, S. Alexander, O. Juhani, Potential and Challenges of Fused Granular Fabrication in Patternmaking, International Journal of Metalcasting 17 (2023) 2469–2476. https://doi.org/10.1007/S40962-023-00989-9/FIGURES/11.

[141] J. Shah, B. Snider, T. Clarke, S. Kozutsky, M. Lacki, A. Hosseini, Large-scale 3D printers for additive manufacturing: design considerations and challenges, International Journal of Advanced Manufacturing Technology 104 (2019) 3679–3693. https://doi.org/10.1007/S00170-019-04074-6.

[142] S. yan Tang, L. Yang, Z. tian Fan, W. ming Jiang, X. wang Liu, A review of additive manufacturing technology and its application to foundry in China, China Foundry 18 (2021) 249–264. https://doi.org/10.1007/s41230-021-1003-0.

[143] Y. sheng Shi, J. liang Zhang, S. feng Wen, B. Song, C. ze Yan, Q. song Wei, J. min Wu, Y. jun Yin, J. xin Zhou, R. Chen, W. Zhou, H. ping Jia, H. qing Yang, H. Nan, Additive manufacturing and foundry innovation, China Foundry 18 (2021) 286–295. https://doi.org/10.1007/s41230-021-1008-8.

[144] W. Zhao, W. Liu, J. Chang, Q. Wei, J. Wu, C. Ye, Properties comparison of pure Al2O3 and doped Al2O3 ceramic cores fabricated by binder jetting additive manufacturing, Ceram Int 49 (2023) 40336–40346. https://doi.org/10.1016/j.ceramint.2023.10.006.

[145] E.M. Sachs, J.S. Haggerty, M.J. Cima, P.A. Williams, Three-dimensional printing techniques, (1989) 10.

[146] L. Giorleo, M. Bonaventi, Casting of complex structures in aluminum using gypsum molds produced via binder jetting, Rapid Prototyp J 27 (2021) 13–23. https://doi.org/10.1108/RPJ-03-2020-0048.

[147] P. Rodríguez-González, P.E.R. Valero, A.I. Fernández-Abia, M.Á. Castro-Sastre, J.B. García, Feasibility of calcium sulfate moulds made by inkjet 3D

printing for rapid casting of aluminium alloys, Metals (Basel) 10 (2020) 1–17. https://doi.org/10.3390/MET10060802.

[148] S.S. Gill, M. Kaplas, Efficacy of powder-based three-dimensional printing (3DP) technologies for rapid casting of light alloys, International Journal of Advanced Manufacturing Technology 52 (2011) 53–64. https://doi.org/10.1007/S00170-010-2716-1/METRICS.

[149] Y. Mu, F. Liu, C. Zhang, Y. Lin, M. Wu, J. Cai, G. Han, Z. Fan, Fabrication of high-strength and anti-hydration water-soluble calcia-based ceramic core modified with nano-ZrO2 via direct ink writing method, Ceram Int 49 (2023) 38623–38634. https://doi.org/10.1016/j.ceramint.2023.09.195.

[150] S. Tang, L. Yang, X. Liu, G. Li, W. Jiang, Z. Fan, Direct ink writing additive manufacturing of porous alumina-based ceramic cores modified with nanosized MgO, (2020). https://doi.org/10.1016/j.jeurceramsoc.2020.07.058.

[151] A. Shahzad, S.A. Khan, A. Paksoy, Ö. Balcı-Çağıran, I. Lazoglu, Negative additive manufacturing of Al2O3-Al cermet material by fused deposition and Direct Ink Writing, Mater Today Commun 33 (2022) 104739. https://doi.org/10.1016/j.mtcomm.2022.104739.

[152] C.F. Revelo, H.A. Colorado, 3D printing of kaolinite clay ceramics using the Direct Ink Writing (DIW) technique, (2017). https://doi.org/10.1016/j.ceramint.2017.12.219.

[153] H. Zhou, Z. Cai, X. Wang, J. Zeng, Y. Feng, C. Peng, R. Wang, Direct Ink Writing of Gypsum: Developing a Printable Gypsum Paste[石膏的直写成型:可打印石膏浆料的研制], Wuji Cailiao Xuebao/Journal of Inorganic Materials 37 (2022) 338–346. https://doi.org/10.15541/jim20210606.

[154] A. Bove, F. Calignano, M. Galati, L. Iuliano, Photopolymerization of Ceramic Resins by Stereolithography Process: A Review, Applied Sciences (Switzerland) 12 (2022). https://doi.org/10.3390/APP12073591.

[155] Q. Yang, W. Zhu, Z. Lu, D. Li, Z. Wang, F. Wang, Rapid fabrication of high-performance CaO-based integral ceramic mould by stereolithography and non-

aqueous gelcasting, Materials 12 (2019) 934. https://doi.org/10.3390/ma12060934.

[156] O. Basar, V.P. Veliyath, F. Tarak, E. Sabet, A Systematic Study on Impact of Binder Formulation on Green Body Strength of Vat-Photopolymerisation 3D Printed Silica Ceramics Used in Investment Casting, Polymers (Basel) 15 (2023). https://doi.org/10.3390/POLYM15143141.

[157] C.H. Li, L. Hu, Y. Zou, J.A. Liu, J.H. Xiao, J.M. Wu, Y.S. Shi, Fabrication of Al2O3-SiO2 ceramics through combined selective laser sintering and SiO2-sol infiltration, Int J Appl Ceram Technol 17 (2020) 255–263. https://doi.org/10.1111/IJAC.13353.

[158] Q. Wei, J. Zhong, Z. Xu, Q. Xu, B. Liu, Microstructure evolution and mechanical properties of ceramic shell moulds for investment casting of turbine blades by selective laser sintering, Ceram Int 44 (2018) 12088–12097. https://doi.org/10.1016/J.CERAMINT.2018.03.227.

[159] Q. WEI, Z. XU, Q. XU, B. LIU, Q. WEI, Z. XU, Q. XU, B. LIU, Effect of sintering temperature on microstructure and mechanical behavior of alumina-based ceramic shell by SLS, Journal of Aeronautical Materials, 2019, Vol. 39, Issue 2, Pages: 10-15 39 (2019) 10–15. https://doi.org/10.11868/J.ISSN.1005-5053.2018.000088.

[160] K.S. Pandya, · Sarang, S. Shindalkar, · Balasubramanian Kandasubramanian, B. Kandasubramanian, Breakthrough to the pragmatic evolution of direct ink writing: progression, challenges, and future, 8 (2023) 1303–1328. https://doi.org/10.1007/s40964-023-00399-7.

[161] S.S. Hossain, K. Lu, Recent progress of alumina ceramics by direct ink writing: Ink design, printing and post-processing, Ceram Int 49 (2023) 10199–10212. https://doi.org/10.1016/j.ceramint.2023.01.143.

[162] Desktop SJ35 extruder, pelletizer, granulating line - RobotDigg, (n.d.). https://robotdigg.com/product/1752/Desktop-SJ35-extruder,-pelletizer,-granulating-line (accessed November 16, 2023).

[163] WASP Continuous Feeding System, (n.d.). https://www.3dwasp.com/en/wasp-continuous-feeding-system/ (accessed December 22, 2023).

[164] RATTMMOTOR 500W CNC Brushless DC Spindle Motor Kit 48V DC Air Cooled Spindle Motor ER11 12000RPM+500 Watt Brushless Driver Controller+600W DC Switching Power Supply+55mm Spindle Mount for CNC Router : Amazon.ca: Tools & Home Improvement, (n.d.). https://www.amazon.ca/RATTMMOTOR-Brushless-12000RPM-Controller-Switching/dp/B0B11R2Q7T/ref=sr_1_26?keywords=spindle+motor&qid=1700502653&sr=8-26&ufe=app_do%3Aamzn1.fos.71722c10-739d-471b-befb-3e4b9bf7d0d6 (accessed December 28, 2023).

[165] Keenovo Standard Square Silicone Heater 3D Printer Build Plate HeatBed – Keenovo Flexible Heaters Store, (n.d.). https://keenovo.store/collections/frontpage/products/keenovo-square-silicone-heater-3d-printer-build-plate-heatbed-heating-pad?variant=8324021092407 (accessed December 23, 2023).

[166] Duet3D, (n.d.). https://www.duet3d.com/duet3mainboard6xd (accessed November 16, 2023).

[167] RepRapFirmware.org, (n.d.). https://www.reprapfirmware.org/ (accessed March 5, 2024).

[168] G-code - Wikipedia, (n.d.). https://en.wikipedia.org/wiki/G-code (accessed March 5, 2024).

[169] J. Yang, Y. Shi, Q. Shen, C. Yan, Selective laser sintering of HIPS and investment casting technology, J Mater Process Technol 209 (2009) 1901–1908. https://doi.org/10.1016/J.JMATPROTEC.2008.04.056.

[170] T.T. Nguyen, V.T. Tran, T.H.N. Pham, V.T. Nguyen, N.C. Thanh, H.M.N. Thi, N.V.A. Duy, D.N. Thanh, V.T.T. Nguyen, Influences of Material Selection, Infill Ratio, and Layer Height in the 3D Printing Cavity Process on the Surface Roughness of Printed Patterns and Casted Products in Investment Casting, Micromachines (Basel) 14 (2023) 395. https://doi.org/10.3390/mi14020395.

[171] 3D Printing Wax - MachinableWax.com, (n.d.). https://machinablewax.com/3d-printing-wax/ (accessed November 16, 2023).

[172] F. Hu, T. Mikolajczyk, D.Y. Pimenov, M.K. Gupta, Extrusion-Based 3D Printing of Ceramic Pastes: Mathematical Modeling and In Situ Shaping Retention Approach, Materials 2021, Vol. 14, Page 1137 14 (2021) 1137. https://doi.org/10.3390/MA14051137.

[173] PRO2-P100B25A1 - Profiler | SICK, (n.d.). https://www.sick.com/at/en/catalog/products/distance-sensors/distance-sensors/profiler/pro2-p100b25a1/p/p356646 (accessed November 16, 2023).

[174] Central Composite Design - an overview | ScienceDirect Topics, (n.d.). https://www.sciencedirect.com/topics/engineering/central-composite-design (accessed March 5, 2024).

[175] ANOVA: Complete guide to Statistical Analysis & Applications, (n.d.). https://www.analyticsvidhya.com/blog/2018/01/anova-analysis-of-variance/ (accessed February 13, 2024).

[176] Data Analysis, Statistical & Process Improvement Tools | Minitab, (n.d.). https://www.minitab.com/en-us/ (accessed November 16, 2023).

[177] Confocal Laser Scanning Microscopes, (n.d.). https://www.zeiss.com/microscopy/en/products/light-microscopes/confocal-microscopes.html?utm_source=google&utm_medium=cpm&utm_campaign=C-00008044&gad_source=1&gclid=CjwKCAiAu9yqBhBmEiwAHTx5p0apn9AJXvjJxaAYD6nho20qauhCMZj9FMpVNTQoM9gEsyCE7R9w0RoClnYQAvD_BwE#lsm (accessed November 16, 2023).

[178] ISO - ISO 527-2:2012 - Plastics — Determination of tensile properties — Part 2: Test conditions for moulding and extrusion plastics, (n.d.). https://www.iso.org/standard/56046.html (accessed May 15, 2022).

[179] Out of Production 3300 Series Universal Testing Systems | Instron, (n.d.). https://www.instron.com/en/products/testing-systems/universal-testing-

systems/low-force-universal-testing-systems/3300-series (accessed November 16, 2023).

[180] M.Y. Zaley, Mechanical Properties Study of Recycled Machinable Wax, (2013).

[181] RED POTTERY Ceramic body | WASP Shop, (n.d.). https://www.3dwasp.shop/prodotto/terraglia-rossa-impasto-ceramico/ (accessed December 24, 2023).

[182] Full Factorial Design - an overview | ScienceDirect Topics, (n.d.). https://www.sciencedirect.com/topics/engineering/full-factorial-design (accessed March 5, 2024).

[183] 3D Camera | MotionCam | Photoneo Focused on 3D, (n.d.). https://www.photoneo.com/motioncam-3d (accessed November 19, 2023).